

# Von Zeipel – Lidov – Kozai cycles in action: *Kepler* triples with eclipse depth variations: KICs 6964043, 5653126, 5731312 and 8023317

T. Borkovits<sup>1,2,3,4,5\*</sup>, S. A. Rappaport<sup>6</sup>, S. Toonen<sup>7</sup>, M. Moe<sup>8</sup>, T. Mitnyan<sup>1,2</sup>, I. Csányi<sup>1</sup>

<sup>1</sup>*Baja Astronomical Observatory of University of Szeged, H-6500 Baja, Szegedi út, Kt. 766, Hungary*

<sup>2</sup>*ELKH-SZTE Stellar Astrophysics Research Group, H-6500 Baja, Szegedi út, Kt. 766, Hungary*

<sup>3</sup>*Konkoly Observatory, Research Centre for Astronomy and Earth Sciences, H-1121 Budapest, Konkoly Thege Miklós út 15-17, Hungary*

<sup>4</sup>*ELTE Gothard Astrophysical Observatory, H-9700 Szombathely, Szent Imre h. u. 112, Hungary*

<sup>5</sup>*MTA-ELTE Exoplanet Research Group, H-9700 Szombathely, Szent Imre h. u. 112, Hungary*

<sup>6</sup>*Department of Physics, Kavli Institute for Astrophysics and Space Research, M.I.T., Cambridge, MA 02139, USA*

<sup>7</sup>*Anton Pannekoek Institute for Astronomy, University of Amsterdam, 1090 GE Amsterdam, The Netherlands*

<sup>8</sup>*University of Arizona, Steward Observatory, 933 N. Cherry Ave., Tucson, AZ 85721, USA*

Accepted XXX. Received YYY; in original form ZZZ

## ABSTRACT

We report the results of the photodynamical analyses of four compact, tight triple stellar systems, KICs 6964043, 5653126, 5731312, 8023317, based largely on *Kepler* and *TESS* data. All systems display remarkable eclipse timing and eclipse depth variations, the latter implying a non-aligned outer orbit. Moreover, KIC 6964043 is also a triply eclipsing system. We combined photometry, ETV curves, and archival spectral energy distribution data to obtain the astrophysical parameters of the constituent stars and the orbital elements with substantial precision. KICs 6964043 and 5653126 were found to be nearly flat with mutual inclinations  $i_{\text{mut}} = 4^\circ.1$  and  $12^\circ.3$ , respectively, while KICs 5731312, 8023317 ( $i_{\text{mut}} = 39^\circ.4$  and  $55^\circ.7$ , respectively) are found to lie in the high  $i_{\text{mut}}$  regime of the von Zeipel-Kozai-Lidov (ZKL) theorem. We show that currently both high inclination triples exhibit observable unusual retrograde apsidal motion. Moreover, the eclipses will disappear in all but one of the four systems within a few decades. Short-term numerical integrations of the dynamical evolution reveal that both high inclination triples are currently subject to ongoing, large amplitude ( $\Delta e \sim 0.3$ ) inner eccentricity variations on centuries-long timescales, in accord with the ZKL theorem. Longer-term integrations predict that two of the four systems may become dynamically unstable on  $\sim$  Gyr timescales, while in the other two triples common envelope phases and stellar mergers may occur. Finally we investigate the dynamical properties of a sample of 71 KIC/TIC triples statistically, and find that the mutual inclinations and outer mass ratios are anti-correlated at the  $4\sigma$  level. We discuss the implications for the formation mechanisms of compact triples.

**Key words:** binaries:eclipsing – binaries:close – stars:individual: KIC 6964043 – stars:individual: KIC 5653126 – stars:individual: KIC 5731312 – stars:individual: KIC 8023317

## 1 INTRODUCTION

The advent of planet-hunter space telescopes such as *CoRoT* (Auvergne et al. 2009), *Kepler* (Borucki et al. 2010), *TESS* (Ricker et al. 2015) has additionally opened up a new window for the detection of exotic multiple stellar systems. This especially includes triple systems and quadruples which are both ‘compact’ and ‘tight’. For simplicity, considering only hierarchical triple systems, by ‘compactness’ we mean that the outer orbital period does not exceed, let’s say  $P_{\text{out}} = 1000$  days, while a triple system is said to be ‘tight’ for an

outer to inner period ratio  $P_{\text{out}}/P_{\text{in}} \leq 100$ .<sup>1</sup> Tightness is important because the magnitude of the gravitational three-body perturbations in a hierarchical triple stellar system, relative to the Keplerian motion, is primarily determined by the ratio of semi-major axes of the inner and outer orbits. This ratio, with the use of Kepler’s third law, can easily be converted to the ratio of the much easier-to-observe orbital periods. On the other hand, compactness, which is closely connected to the physical dimensions of the system, strongly influences the timescale of three- (multiple-) body perturba-

<sup>1</sup> Note, however, that these numerical values were chosen somewhat arbitrarily, and we do not mean to attempt to impose strict limits.

\* E-mail: borko@electra.bajaobs.hu

tions. Moreover, tightness is also important in determining the relations of the magnitudes of other kinds of perturbations, e.g., tidal and relativistic, to the dynamical ones, since these other perturbations primarily scale with the semi-major axis, i.e., the compactness of the system. Finally in this regard, compactness is also an important parameter because, according to our present knowledge, compact multiple systems form and evolve in a different manner than their wider counterparts (see, e.g. Tokovinin 2021, in the sense of their formation, and Toonen et al. 2020, 2022, in regard of their later evolution).

Hierarchical triple systems exhibit periodic gravitational perturbations in three different, well separable timescales. (i) The shortest period ones act on the timescale of the inner orbit ( $P_{\text{in}}$ ), and have a relative amplitude on the order of the ratio  $(P_{\text{in}}/P_{\text{out}})^2$  and thus, this class of perturbations is hardly observable. (ii) The medium timescale class of periodic perturbations have characteristic periods on the order of the period of the outer orbit ( $P_{\text{out}}$ ) and relative magnitude of  $P_{\text{in}}/P_{\text{out}}$  (i.e. longer in period and larger in amplitude than the short-period ones by a factor of  $P_{\text{out}}/P_{\text{in}}$ ). (iii) Finally, the long-period (or, according to another nomenclature, the ‘apse-node’ type) perturbations have a timescale related to  $P_{\text{out}}^2/P_{\text{in}}$  and relative amplitude of unity<sup>2</sup> (i.e., yet longer/larger than the previous perturbations, with a second factor of  $P_{\text{out}}/P_{\text{in}}$ ).

In terms of the formation, evolution, and future fate and stability of hierarchical stellar systems, the largest amplitude, long-period perturbations are by far the most important. It is not surprising, therefore, that theoretical studies of the stellar third-body problem have focused almost exclusively on long-period perturbations (see, e.g. the recent review of Naoz 2016, and further references therein).

Perhaps the most spectacular consequence of these long-period perturbations occurs in the case of highly inclined inner and outer orbital planes. The eccentricity of the inner orbit may then alternate periodically between small values (including zero) and nearly unity and, in parallel with this, the mutual inclination of the orbits also varies substantially in an anticorrelated manner. In recent years these effects are frequently referred as ‘von Zeipel-Lidov-Kozai effects’ (hereafter ZLK) or ‘ZLK oscillations or, cycles’ in the honour of its first investigators (von Zeipel 1910; Lidov 1962; Kozai 1962).<sup>3</sup>

The original ZLK theorem takes into account only the lowest order quadrupole, long-period perturbations, and is strictly valid only if the orbital angular momentum of the triple system is stored exclusively in the outer orbit, which is also circular. This asymptotic quadrupole ZKL theorem has

only one degree of freedom and, hence, is integrable; therefore, the variations of the inner eccentricity ( $e_{\text{in}}$ ), dynamical argument of periastron ( $\omega_{\text{in}}^{\text{dyn}}$ ), and mutual inclination ( $i_{\text{mut}}$ ) can be given in closed form. Based on the analytic form of the perturbation equations, it can readily be shown that the behaviour of the ZKL cycles may be essentially divided into two mutual inclination regimes which are separated by the value of  $|\cos i_{\text{mut}}| = \sqrt{3/5}$ , i.e.  $i_{\text{mut}} \approx 39^\circ.23$  and its retrograde counterpart<sup>4</sup>. Below this mutual inclination (i.e. in the low mutual inclination regime) there may occur only small-amplitude variations in the inner eccentricity and the mutual inclination as well. Furthermore, in the case of an initially circular inner orbit, it remains circular at all times (of course, only insofar as the approximation used remains valid).

In the high mutual inclination case, depending on the initial conditions, (i.e., the value of the inner binary eccentricity, mutual inclination and dynamical argument of pericenter at a given instant), the inner eccentricity and the mutual inclination may oscillate with large amplitudes, while the apsidal line may exhibit either circulation or libration. As an extreme example, an originally circular inner orbit, perturbed by a tertiary orbiting perpendicular to its orbit (i.e.  $i_{\text{mut}} = 90^\circ$ ), may have its eccentricity periodically grow to near unity and then shrink back to zero while, at the same time, the mutual inclination oscillates between  $\cos^2 i_{\text{mut}} = 0$  and  $\cos^2 i_{\text{mut}} = 3/5$ . Taking into consideration the further octupole terms of the perturbation function, and allowing the third body to have any arbitrary eccentricity, e.g., Ford et al. (2000) and Naoz et al. (2013) have shown that the problem will no longer be analytically integrable, and the behaviour of the orbital elements may be more complex. For example, large eccentricity variations may already occur in the case of lower mutual inclination triples, the relative orientations of the orbital planes may show flip-flop phenomena between prograde and retrograde orientations, the semi-major axis of the inner orbit may alternate between libration and circulation, and so forth.

Although the large amplitude ZLK eccentricity cycles are evidently the most important long-period, or secular, effects in the formation and evolution of triple star systems, these are often barely observable in action. The main reason is that, due to their typically long timescale, one cannot expect measurable eccentricity variations from spectroscopic, photometric or, astrometric observations<sup>5</sup> on timescales of years or decades. Fortunately, however, in the case of some other orbital elements, the variations driven by the very same mechanism (i.e., third-body perturbations) may lead to readily observable effects even on ‘astronomer career’ timescales. These long-period perturbations are (i) the third-body forced apsidal motion (in the case of an eccentric inner binary), and (ii) the orbital plane precession (or, nodal regression) in those triple systems where the inner and outer orbital planes are not aligned. (Hence the other name of ‘apse-node timescale perturbations’.)

Eclipsing binaries (EBs) that belong to tight and compact hierarchical triple and multiple stellar systems may be ideal for the detection of both of these effects. In particular, they

<sup>2</sup> Unity is to be meant in that sense, that during the timescale of the long-period perturbations, the numerical value of a given orbital element may take any numerical value within its physical range.

<sup>3</sup> These early authors did not deal with the hierarchical three-body problem in the context of stellar triple systems, but, instead studied the motions of small bodies in triple systems (e.g. perturbations of Jupiter from comets and asteroids orbiting around the Sun – von Zeipel; Kozai; or perturbations of the Moon for Earth-orbiting artificial satellites – Lidov; see the recent monograph of Ito & Ohtsuka 2019). The first analytic works on this theorem, dedicated directly to the stellar three body problem was published by Harrington (1968) and Söderhjelm (1982).

<sup>4</sup> Within the framework of the original ZKL theorem the prograde and retrograde configurations are equivalent.

<sup>5</sup> At least within the accuracy limits of instruments that are commonly available for observing hierarchical triple stellar systems.

can provide important information on the non-alignment of the orbital planes, or, oppositely, the flatness of the given systems. This is the case because the orbital plane precession, in the case of an EB, leads to a variation in the eclipse depths and, even to the disappearance of former eclipses or, in the opposite sense, the occurrence of eclipses in formerly non-eclipsing binaries. The characteristic time-scale of this effect for triples can be estimated by the following simple expression (Söderhjelm 1975):

$$P_{\text{node}} = \frac{4}{3} \frac{1 + q_{\text{out}}}{q_{\text{out}}} \frac{P_{\text{out}}^2}{P_{\text{in}}} (1 - e_{\text{out}}^2)^{3/2} \left| \frac{C}{G_{\text{out}}} \cos i_{\text{mut}} \right|^{-1}, \quad (1)$$

where  $q_{\text{out}}$  represents the outer mass ratio,  $P_{\text{in,out}}$  denote the periods of the inner and outer orbits,  $e_{\text{out}}$  stands for the outer eccentricity,  $C$  is the (constant) total orbital angular momentum of the triple, while  $G_{\text{out}}$  stands for the orbital angular momentum stored in the outer orbit and, finally,  $i_{\text{mut}}$  the mutual (relative) inclination of the two orbital planes.

From an observational point of view, however, the problem is that, although the stability of a hierarchical triple stellar system allows for very tight configurations with  $P_{\text{out}}/P_{\text{in}} \approx 5$  (see, e.g. Mardling & Aarseth 2001), in the vast majority of known triple or multiple systems that contain an EB, this ratio is larger than 100. Moreover, because the periods of the outer stellar components are typically longer than 1 year, the timescale of the precession, and therefore the variation of the eclipse depths, may reach several centuries or, millennia, in most of the systems. Therefore, one might expect eclipse depth variations (EDVs) that occur rapidly enough to be observable during the  $\approx 1.5$  century-long history of EB observations, only in the most compact, tightest, and relatively rare (Tokovinin 2014) triple systems.

Consequently, it is hardly surprising that before the era of the long-duration, ground-based and space-borne photometric surveys, EDVs were (serendipitously) detected in only fewer than a dozen EBs (see the recent review of Borkovits 2022). In contrast to this, Kirk et al. (2016) listed 43 EBs in the original *Kepler* sample which exhibit EDVs. Though some of their systems were probably false positives (for a number of different reasons), on the other hand, they did not list some EBs with evident EDVs (e.g., neither KIC 6964043, nor KIC 5731312, two of our four systems that are analysed in this paper). Therefore, we may confidently state that the number of the EBs with known EDVs had more than tripled by the end of the four-year-long primary mission of the *Kepler* space telescope. The majority of these EDV-exhibiting EBs in the *Kepler*-field also display rapid apsidal motion. Moreover, they have readily detectable medium-period eclipse timing variations (ETV) which are, again, forced by the dynamical effects (DE) of the third body (besides, and instead of, the usual, well-known light-travel time effect – LTTE, Rapaport et al. 2013; Borkovits et al. 2015, 2016). Therefore, these systems offer excellent opportunities to determine their complete geometric and dynamical configurations with unexpectedly high precision through complex, photodynamical analyses. In this manner, these triple stellar systems may serve as actual case studies for later, in-depth investigations of the formation, as well as past, present and future evolutions of hierarchical triple star systems.

In Sect. 2 we introduce the four triples selected for our present investigations, and we discuss the prior results on these systems that are relevant in the context of the present

study. Then the description of the observational data and their preparation can be found in Sect. 3, while the applied photodynamical method is summarized in Sect. 4. In Sect. 5 we discuss the results of the photodynamical analyses, and study the future dynamical and astrophysical evolutions of each system based on these results. Moreover, the implications of our present and former findings about compact triple star systems for the formation processes of multiple star systems are also discussed on a statistical basis. Finally, general concluding remarks are made in Sect. 6.

## 2 SELECTED SYSTEMS

In a previous work Borkovits et al. (2015) analysed 26 such eccentric EBs in the original *Kepler*-field for which perturbations by a close tertiary star dominated the eclipse timing variations (ETV). Amongst these triples, 17 were found to exhibit EDVs to differing degrees, indicating that the tertiary star has an inclined orbit relative to the plane of the inner binary. We have selected four targets of these 17 systems for a detailed analysis. According to the previous analytic ETV analysis of Borkovits et al. (2015), two of the four systems belong to the low mutual inclination regime and, hence, one can expect rapid, but small amplitude medium and long period variations in the orbital elements. By contrast the other two systems belong to the rare class of highly inclined close triples, with  $i_{\text{mut}}$  close to the inclination limit of the asymptotic, quadrupole ZKL theory. Therefore, they may be ideal for direct observational detections of such exotic perturbation effects, as, e.g. rapid, strong eccentricity variations and/or retrograde (or, librating) apsidal motion. The main cataloged parameters of the systems are tabulated in Table 1, while their four-year-long *Kepler* lightcurves are plotted in Fig. 1. Below we summarize the main properties found from their prior results for these four systems individually. Because we are mainly interested in the consequences of the inclined inner and outer orbital planes, we list the systems throughout this paper in the order of increasing value of the mutual inclination ( $i_{\text{mut}}$ ) parameter as it is obtained from the present study.

*KIC 6964043 = KOI-1351* ( $P_1 = 10.73$  d;  $P_2 = 239$  d;  $P_2/P_1 = 22.3$ ) was observed by *Kepler* in long cadence (LC) mode only from the fourth quarter (Q4) of the primary mission to its end (Q17). Moreover, it was also observed in 1-min short cadence (SC) mode in Q12. It is the only triply eclipsing triple system in our sample. These extra, third-body eclipses are the largest amplitude, longest duration features of the lightcurve (see upper left panel of Fig. 1 and Figs. 2, 3). The regular inner eclipses are quite shallow (with depths of  $\sim 1 - 2\%$ ). The inner EB exhibits growing eclipse depths during the first few quarters and then, after a short period of constancy, the eclipse depths continuously decrease. This is the most compact and tightest triple in our sample. Borkovits et al. (2015) have investigated the ETV of the EB and pointed out that it is clearly dominated by DE, i.e., third-body perturbations over the LTTE. Therefore, besides the orbital elements and mass ratio of the outer orbit, they were able to determine the full spatial configuration of the triple and, hence, the mutual inclination and got  $i_{\text{mut}} = 19^\circ \pm 2^\circ$ <sup>6</sup> Moreover,

<sup>6</sup> Note, that in contrast to the other three systems where our new

**Table 1.** Main properties of the three systems from different catalogs

Parameter	6964043	5653126	5731312	8023317
RA (J2000)	19 : 44 : 03.474	19 : 58 : 48.479	19 : 53 : 00.434	19 : 19 : 52.879
Dec (J2000)	+42 : 25 : 20.09	+40 : 53 : 46.51	+40 : 54 : 12.77	+43 : 49 : 13.84
$G^b$	15.5868 ± 0.0003	13.1434 ± 0.0001	13.8246 ± 0.0001	12.8453 ± 0.0002
$G_{BP}^b$	16.0472 ± 0.0029	13.5364 ± 0.0007	14.3641 ± 0.0008	13.2064 ± 0.0005
$G_{RP}^b$	14.9591 ± 0.0014	12.5802 ± 0.0004	13.1272 ± 0.0005	12.3194 ± 0.0005
$B^a$	16.307 ± 0.068	14.159 ± 0.026	15.030 ± 0.066	13.819 ± 0.036
$V^a$	16.007 ± 0.137	13.225 ± 0.069	14.035 ± 0.103	12.990 ± 0.069
$g'$	16.007 ± 0.071 <sup>c</sup>	13.709 ± 0.014 <sup>d</sup>	14.584 ± 0.001 <sup>e</sup>	13.329 ± 0.031 <sup>d</sup>
$r'$	15.533 ± 0.048 <sup>c</sup>	13.139 ± 0.035 <sup>d</sup>	13.659 ± 0.001 <sup>e</sup>	12.810 ± 0.045 <sup>d</sup>
$i'$	15.276 ± 0.083 <sup>c</sup>	13.028 ± 0.093 <sup>d</sup>	13.069 ± 0.001 <sup>e</sup>	12.702 ± 0.028 <sup>d</sup>
$J^f$	14.231 ± 0.027	11.957 ± 0.021	12.242 ± 0.022	11.682 ± 0.023
$H^f$	13.758 ± 0.026	11.710 ± 0.022	11.729 ± 0.023	11.395 ± 0.020
$K^f$	13.705 ± 0.043	11.632 ± 0.020	11.598 ± 0.018	11.340 ± 0.011
$W1^g$	13.658 ± 0.025	11.543 ± 0.023	11.559 ± 0.024	11.310 ± 0.023
$W2^g$	13.680 ± 0.031	11.572 ± 0.021	11.611 ± 0.023	11.359 ± 0.021
$W3^g$	13.061	11.595 ± 0.122	12.926	11.163 ± 0.094
$W4^g$	9.614	8.897	9.458	9.442
$T_{\text{eff}}$ (K) <sup>a</sup>	5445 ± 122	6980 ± 118	4885 ± 60	5638 ± 103
Distance (pc) <sup>h</sup>	2162 ± 142	1296 ± 32	351 ± 3	753 ± 7
$[M/H]^a$	–	0.435 ± 0.111	–0.372 ± 0.057	0.224 ± 0.016
$E(B - V)^a$	0.130 ± 0.008	0.213 ± 0.014	0.073 ± 0.024	0.035 ± 0.002
$\mu_\alpha$ (mas yr <sup>-1</sup> ) <sup>b</sup>	–2.95 ± 0.03	0.38 ± 0.02	1.69 ± 0.03	–4.25 ± 0.01
$\mu_\delta$ (mas yr <sup>-1</sup> ) <sup>b</sup>	–1.69 ± 0.04	–1.12 ± 0.02	5.58 ± 0.03	–1.09 ± 0.01

*Notes.* (a) TESS Input Catalog (TIC v8.2) (Paegert et al. 2021). (b) Gaia EDR3 (Gaia collaboration 2021). (c) AAVSO Photometric All Sky Survey (APASS) DR10, (Henden 2019), <https://www.aavso.org/download-apass-data>. (d) AAVSO Photometric All Sky Survey (APASS) DR9, (Henden et al. 2015), <http://vizier.u-strasbg.fr/viz-bin/VizieR?-source=II/336/apass9>. (e) The Kepler-INT survey (Greiss et al. 2012). (f) 2MASS catalog (Skrutskie et al. 2006). (g) WISE point source catalog (Cutri et al. 2013). (h) Bailer-Jones et al. (2021).

Note also, that for the SED analysis in Sect. 4 the uncertainties of the passband magnitudes were set to  $\sigma_{\text{mag}} = \max(\sigma_{\text{catalog}}, 0.030)$  to avoid the strong overdominance of the extremely accurate Gaia magnitudes over the other measurements.

they estimated the periods of both the apsidal motion and the nodal regression to be about 26-27 yr. KIC 6964043 was also observed with *TESS* in full-frame image (FFI) mode in Sectors 14 and 15, but these observations exhibit neither regular inner eclipses, nor third-body eclipses, which is in accord with our photodynamical model, as will be discussed below, in Sect. 5.

*KIC 5653126 = KOI-6612* ( $P_1 = 38.51$  d;  $P_2 = 968$  d;  $P_2/P_1 = 25.1$ ) has by far the longest inner period of all the triples in our sample. It was observed throughout the original *Kepler*-mission ( $Q0 - Q17$ ) in LC mode, while SC data are also available for quarters  $Q9 - Q17$ . The EB exhibits continuously increasing eclipse depths. In the first seven quarters only primary eclipses were observable. The first, very shallow, grazing secondary eclipse with a depth of  $\sim 0.002\%$  can be identified at BJD 2 455 539.7 (near the end of  $Q7$ ). During the second half of the data train both kinds of eclipses can be clearly detected (see upper right panel of Fig. 1 and left panel of Fig. 4). Borkovits et al. (2015) found a mutual inclination of  $i_{\text{mut}} = 11^\circ \pm 1^\circ$  and apsidal motion and nodal periods on the order of 2-3 centuries. The system was observed also by the *TESS* spacecraft in FFI-mode during Sectors 14, 15

results confirm the mutual inclinations obtained from the prior pure ETV analysis of Borkovits et al. (2015), in the case of this triple the present, more complex study (see later in Sect. 4) resulted in a much lower value of  $i_{\text{mut}} = 4^\circ 1 \pm 0^\circ 1$ .

and 41, where the observations led to the detection of one additional primary, and three secondary eclipses. The 2019 summer (S14,15) observations show flat-bottomed eclipses, while the somewhat shallower 2021 (S41) secondary eclipse is again V-shaped, indicating that the eclipse depths are now decreasing after an interval of total eclipses (right panel of Fig. 4).

*KIC 5731312 = KOI-6621* ( $P_1 = 7.95$  d;  $P_2 = 911$  d;  $P_2/P_1 = 114.6$ ) is the shortest inner period triple in our sample. Similar to *KIC 5653126*, it was observed throughout the original *Kepler*-mission ( $Q0 - Q17$ ) in LC mode. One quarter ( $Q10$ ) of SC data are available as well. During the *Kepler* observations this system exhibited the deepest primary eclipses amongst the four systems. During the first half of the observations, only a small smooth decrease in the amplitude of the eclipses can be observed (which is nearly obscured by a wave-like pattern which, however, is only a beating effect between the data sampling and the eclipsing periods). Then, between BJDs 2 455 700 and 800 a sudden decrease in eclipse depths occurred, which was then again followed by a slow smooth decrease. The much shallower secondary eclipses followed the same trend (see lower left panel of Fig. 1 and left panel of Fig. 5). At the same time, the primary and secondary ETV curves also exhibited dramatic peaked variations, clearly indicating periastron passage of the eccentric third body. Note, despite the fact that the outer to inner period ratio exceeds one hundred, the ETV curves of this EB are clearly dominated by the DE over the LTTE. Borkovits et al. (2015)

and, in their slightly revised ETV-analysis Borkovits et al. (2016), also found that this triple system is probably quite inclined with a mutual inclination of  $i_{\text{mut}} = 37^\circ.8 \pm 0^\circ.4$ . In addition, their analytical model fit resulted in a currently retrograde apsidal motion. The EB was also observed with *TESS* in Sectors 14, 15 and 41. By this time the secondary eclipses had disappeared, which is again in accord with our photodynamical results to be presented below. Moreover, in between the 2019 and 2021 space telescope observations, two additional primary eclipses were also observed at Baja Observatory, Hungary, within the framework of our photometric *Kepler* and *TESS* EB follow-up programme.

*KIC 8023317 = KOI-6049* ( $P_1 = 16.58$  d;  $P_2 = 611$  d;  $P_2/P_1 = 36.9$ ) displays slowly and continuously increasing primary eclipse depths throughout the *Q0 – Q17 Kepler* LC data. (SC data were also gathered during quarters *Q5.2* and *Q17.1*.) The very shallow secondary eclipses, however, have constant depths during the 4-year-long data set (see lower right panel of Fig. 1 and right panel of Fig. 5). This is due to the fact that the flat bottom of the secondary eclipses clearly indicates that during these events, the smaller fainter and colder secondary star was totally eclipsed. The EDV for the first time was reported by Rappaport et al. (2013) who also made the first ETV analysis of the system. The system was also included in the more sophisticated ETV analyses of Borkovits et al. (2015, 2016). All three investigations led to similar results indicating that *KIC 8023317* is one of the most inclined triple systems with  $i_{\text{mut}} = 49^\circ.5 \pm 0^\circ.6$  amongst the EBs observed with *Kepler*. Moreover, similar to *KIC 5731312*, the analytic solutions of Borkovits et al. (2015, 2016) led to the conclusion that the apsidal motion of this EB is, again, retrograde. This triple was reobserved with *TESS* during Sectors 14, 40 and 41. These data exhibit five additional, U-shaped primary eclipses, however, the much smaller SNR of the *TESS* lightcurves does not allow for a secure detection of the very low-amplitude secondary eclipses.

### 3 OBSERVATIONAL DATA AND ITS PREPARATION

Our analysis is primarily based on the photometric data gathered by the *Kepler* spacecraft during its four-year-long primary mission. We use exclusively the same LC (time resolution of 29.4 min) data sets, that were used in our previous work on the comprehensive ETV analyses of hundreds of *Kepler* EBs (Borkovits et al. 2016). The majority of these lightcurves were downloaded from the Villanova website<sup>7</sup> of the third revision of the Kepler Eclipsing Binary Catalog (Kirk et al. 2016; Abdul-Masih et al. 2016) while, in the case of *KIC 5731312*, the missing quarters 12 and 13 were downloaded directly from the MAST database<sup>8</sup>.

Regarding the more recent *TESS* observations, as mentioned above, all four systems were measured in 30-min cadence mode during Year 2 observations. Additionally, three of the systems (with the exception being *KIC 6964043*) were also observed in the 10-min cadence mode during the first sectors of Year 4 observations. We processed the original

*TESS* FFIs using a convolution-based differential photometric pipeline implemented in the FITSH package (Pál 2012). These raw lightcurves, however, exhibited large amounts of scattered light and, moreover, due to the large pixel size of *TESS*, the signal of *KIC 5653126* was blended with that of the 4.81-day-period EB *KIC 5738698* and, therefore, needed disentanglement. This disentanglement was carried out with a principal component analysis (PCA) as follows.

We used the built-in routines from the LIGHTKURVE Python package (Lightkurve collaboration 2018). First, differential images centered on our targets were constructed by the previously mentioned FITSH pipeline subtracting a median image from the raw images. These differential images were then read in as a  $60 \times 60$  pixel-sized *TargetPixelFile* object and the raw differential lightcurve was calculated by summing up the residual fluxes in a  $3 \times 3$  pixel-sized aperture around the target. After that, assuming that all of the signal originated from our target is located inside the chosen aperture, all the other pixels outside this aperture were used to constrain a *DesignMatrix* object with the vectors that contain information about scattered light, spacecraft motion and other leftover extrinsic light variabilities (e.g. the signal of a close variable star partly measured in the aperture). From this *DesignMatrix*, we supplied the first 5-7 principal components to LIGHTKURVE's *RegressionCorrector* in order to construct the noise model and remove the underlying systematic noise from the raw lightcurves, and, in the case of *KIC 5653126*, also to deblend the signal of *KIC 5738698* from the lightcurve. As a final step, the relative fluxes of the detrended lightcurves were referenced to the zero-point values calculated from the  $G_{\text{RP}}$  magnitudes<sup>9</sup> and were normalized to unity.

Moreover, in the case of *KIC 5731312* we included in the analysis two additional primary eclipses that were observed by us at Baja Astronomical Observatory (Hungary) between the Year 2 and Year 4 *TESS* observations.

In preparing these datasets for the photodynamical analyses, first we determined accurate eclipse times from the *TESS* and ground-based follow up observations in the same manner as the *Kepler*-observed eclipse times were determined earlier for our previous analytic ETV analyses in Borkovits et al. (2016). Thus, we obtained 4 (1 primary and 3 secondary) new mid-eclipse times for *KIC 5653126* and, moreover, 11 and 5 primary eclipse times for *KICs 5731312* and *8023317*, respectively. In the case of *KIC 6964043* no further eclipses were detected in the *TESS* data. We list all of these eclipse times together with the former *Kepler* data in the tables of Appendix B. Moreover, the ETV curves, together with the best photodynamical fits (see below, in Sect. 4) are plotted in Fig. 6.

For the photodynamical analysis we took some additional preparatory steps with the lightcurves. First, to obtain a more uniform sampling, we converted the Year 4 10-min cadence *TESS* data into 30-min bins. Second, in order to save computational time and also to give the eclipses themselves (which carry the vast bulk of both the relevant astrophysical and dynamical information) a higher statistical weight we kept only small sections of the lightcurves around the primary and

<sup>7</sup> <http://keplerebs.villanova.edu/>

<sup>8</sup> <https://archive.stsci.edu/missions-and-data/kepler>

<sup>9</sup> This is a rather good approximation due to the significant overlap between the passbands of *TESS* and Gaia. (Ricker et al. 2015; Jordi et al. 2010)

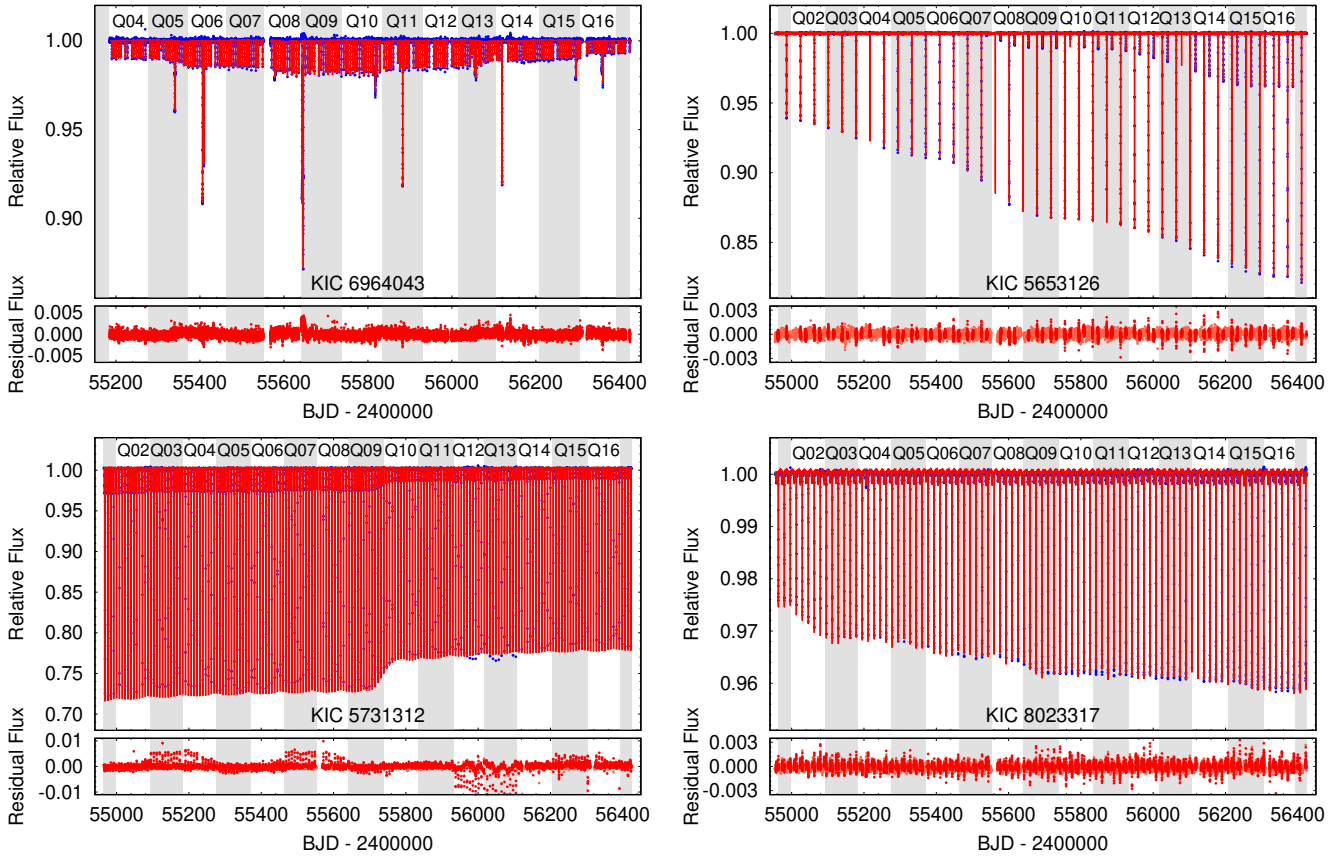


**Figure 1.** Four-year long *Kepler* long cadence lightcurves of the four investigated systems with the photodynamical model solution. Small blue circles are the data points while the continuous red curves are the photodynamical models. Note, the alternating gray-white stripes help to distinguish the observing quarters.

secondary eclipses of the inner binaries. (Note, more strictly speaking, we kept the small sections of the lightcurves around the minima of the sky-projected distances of the stellar disks of the inner binaries, irrespective of whether eclipses have actually occurred or not.) Moreover, in the case of KIC 6964043 we kept some additional few-day-long sections around the third-body eclipses, as well.

Finally we note that the lightcurves also exhibit some low-level systematics, which might have either an instrumental origin or be caused by stellar variability. Due to their very low amplitude we did not attempt to remove these effects. However, in the future, analyses using a simultaneous fit of Gaussian Processes or wavelet-based (Csizmadia et al. 2021) noise models can remove some of these systematic behaviours and thereby slightly improve the fit and error estimations.

#### 4 PHOTODYNAMICAL MODELING

For the four triple systems, we have carried out a photodynamical analysis with the software package LIGHTCURVEFACTORY (see, e.g. Borkovits et al. 2019a, 2020a, and references therein). As described in these earlier papers, the code contains (i) a built-in numerical integrator to calculate the gravitationally (three- or four-body effects), tidally, and (optionally) relativistically perturbed coordinates and velocities of

the three (four) stars in the system; (ii) emulators for multi-band light curves (allowing multiple eclipses), ETV curves, and radial velocity (RV) curves (if available), (iii) built-in, tabulated PARSEC grids (Bressan et al. 2012) for interpolating fundamental stellar parameters (e.g. radii and effective temperatures) as well as composite spectral energy distribution (SED) model for the three (four) stars, and (iv) an MCMC-based search routine for fitting the parameters. The latter utilizes an implementation of the generic Metropolis-Hastings algorithm (see e.g. Ford 2005). The use of this software package and the consecutive steps of the entire analysis process have been previously explained in detail as the code was applied to a variety of multiple stellar systems (Borkovits et al. 2018, 2019a,b, 2020a,b, 2021, 2022; Mitnyan et al. 2020; Rappaport et al. 2022).

For the four current systems, in the absence of RV data, we combined a composite SED analysis and the use of pre-calculated PARSEC grids as proxies to determine the masses of the constituent stars. As a consequence, such a photodynamical model solution is no longer astrophysically model-independent. Nonetheless, in our previous work (Borkovits et al. 2022) we have shown that for compact, strongly dynamically interacting triples (as is the case for the currently investigated systems), such a solution (which we call ‘MDN’ - astrophysical model-dependent solution without RV data) results in fundamental stellar parameters (masses, radii)

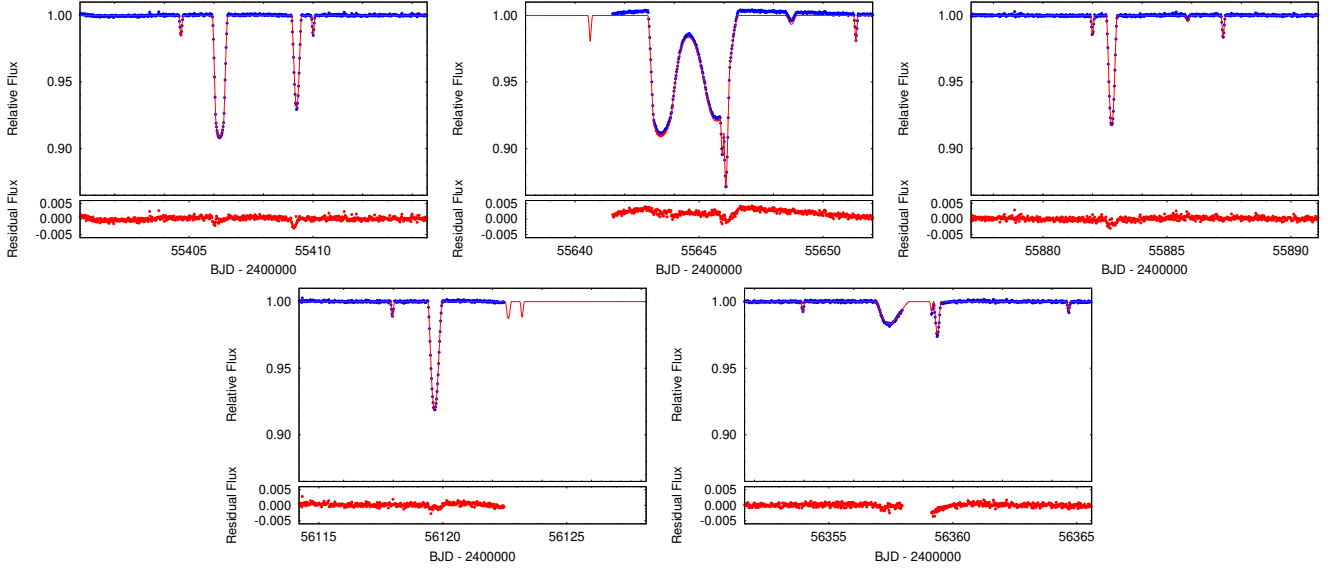


**Figure 2.** The ‘primary’ third-body, or outer eclipses of KIC 6964043 observed with *Kepler*. During these events the two red dwarfs of the inner binary transit (either partially or, totally) in front of the disk of the outer, most massive, G-star component. Blue dots represent the observed LC fluxes, while red lines represent the best-fitting photodynamical model.

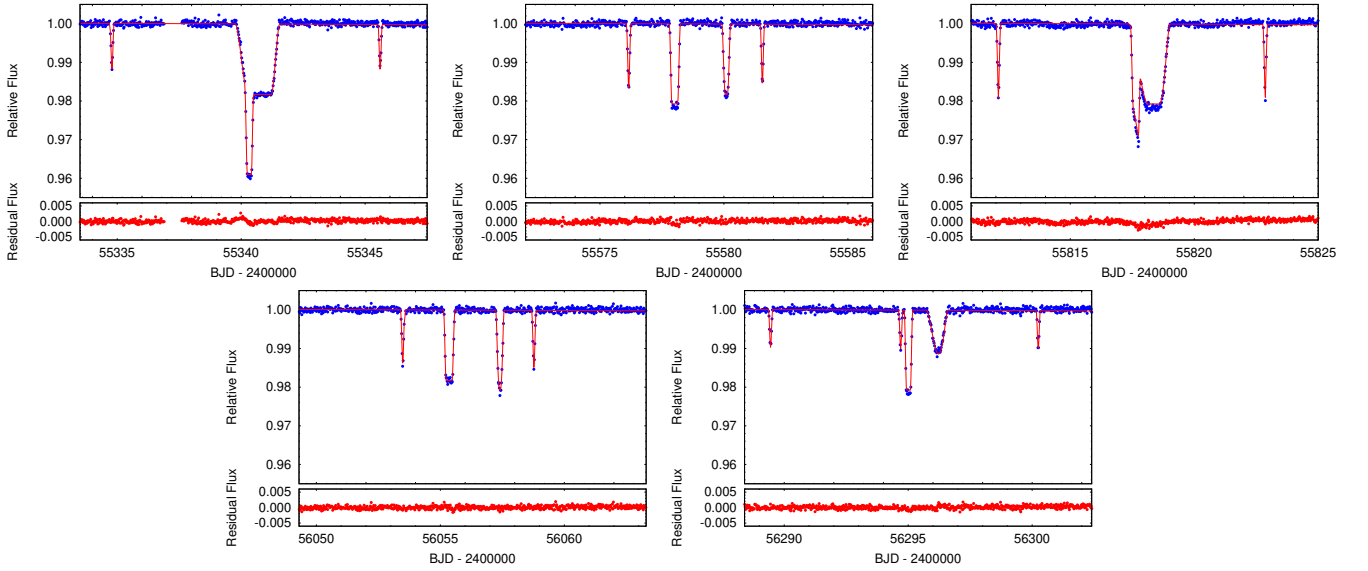


**Figure 3.** The ‘secondary’ third-body, or outer eclipses of KIC 6964043 observed with *Kepler*. During these events the two red dwarfs of the inner binary are eclipsed (either partially or, totally) by the outer, most massive, G-star component. Blue dots represent the observed LC fluxes, while red lines represent the best-fitting photodynamical model.

within 5-10% to the results of an ‘MIR’ (astrophysical model-independent solution with RV data) solution. The geometric and dynamical parameters (i.e. the orbital elements and, also the mass ratios), as well as dimensionless quantities like the fractional radii and temperature ratios of the stars remain practically unchanged between the MDN and MIR solutions.

In the case of these ‘MDN’ runs the adjusted parameters were as follows:

(i) Orbits: Three of six orbital-element related parameters of the inner, and six parameters of the outer orbits, i.e., the components of the eccentricity vectors of both orbits ( $e \sin \omega$ )<sub>in,out</sub>, ( $e \cos \omega$ )<sub>in,out</sub>, the inclinations relative to the

plane of the sky ( $i_{in,out}$ ), and moreover, three other parameters for the outer orbit, including the period ( $P_{out}$ ), the longitude of the node relative to the inner binary’s node ( $\Omega_{out}$ ), and, in the case of the triply eclipsing system KIC 6964043, the sixth parameter was the time of the first (inferior) conjunction of the tertiary star observed in the *Kepler* data ( $\mathcal{T}_{out}^{inf}$ ) (which corresponds to the first observed third-body eclipse), while for the other three systems the periastron passage times ( $\tau_{out}$ ) were adjusted.

(ii) Stars: Three stellar mass related parameters: the mass of the most massive component (being either  $m_{Aa}$ , the primary of the inner pair or,  $m_B$ , the tertiary star), and the inner

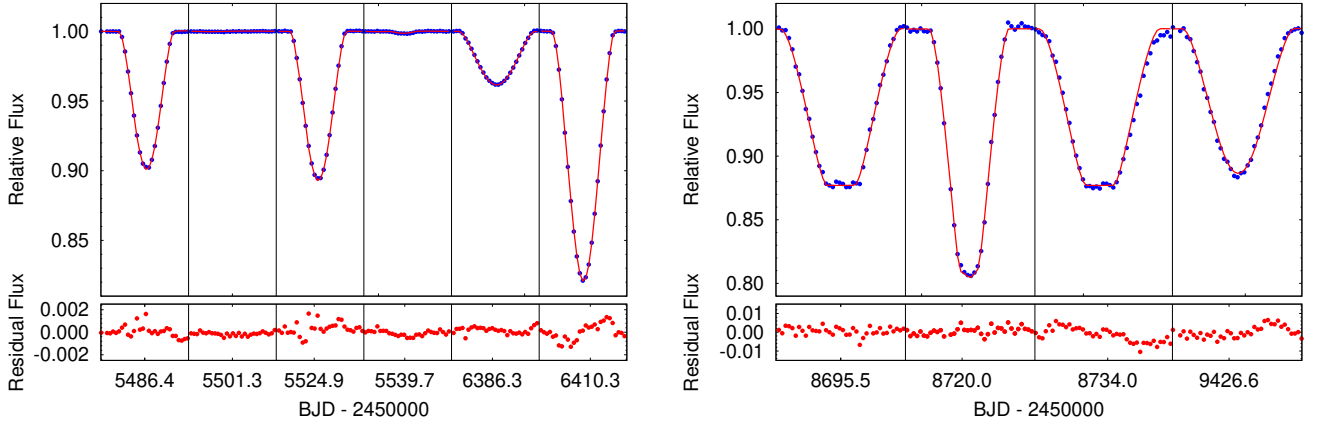


**Figure 4.** Some characteristic primary and secondary eclipses of KIC 5653126 in the *Kepler* (left) and *TESS* lightcurves (right) overplotted with the photodynamical model solution. All the strips have durations of 0.6 and 0.8 days in the left and right panels, respectively. The left panel shows that between the two consecutive primary eclipses around BJDs 2 455 486.3 and 2 455 524.9 no secondary eclipse can be detected, but just one orbital period later, the very first extremely shallow secondary eclipse occurs at  $\sim 2\,455\,539.7$ . The last secondary and primary eclipses observed by *Kepler* are also plotted in the last two segments of the left panel. As one can see, by that time, the durations of the secondary eclipses exceeded that of the primary ones, which is a consequence of the slower orbital motion closer to apastron. In the right panel all the eclipses (three secondary and one primary minima) observed with *TESS* are plotted. Note, the secondary eclipses in sectors 14 and 15 are clearly flat-bottomed, implying total eclipses, while the S41 secondary eclipse was, again, V-shaped, i.e., a partial eclipse.

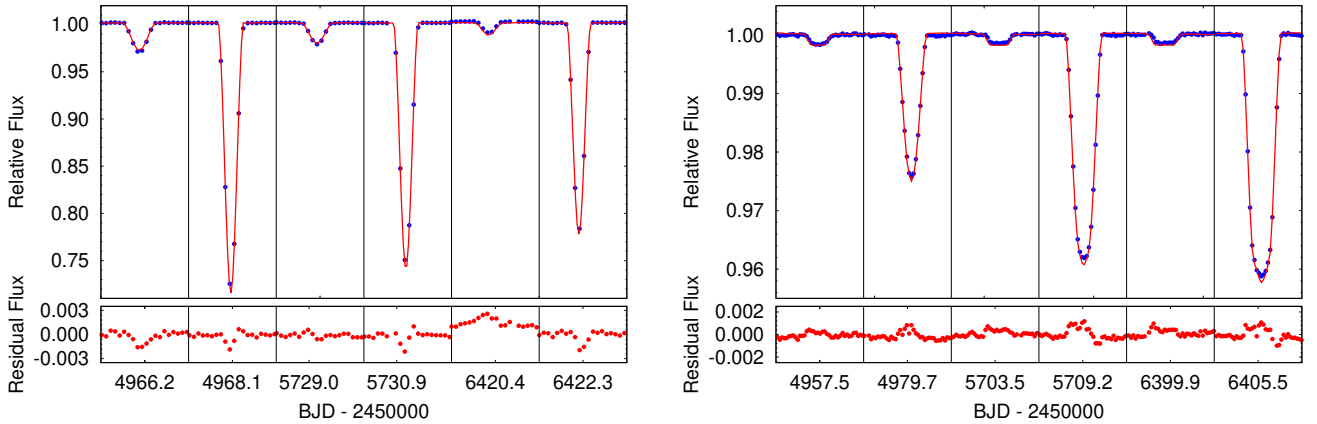


**Figure 5.** Secondary and primary eclipses of KICs 5731312 (left) and 8023317 (right) at the beginning, middle and end of the four-year-long *Kepler* observations. The lengths of the lightcurve sections are 0.4 and 0.8 days in the left and right panels, respectively.

and outer mass ratios ( $q_{\text{in,out}}$ ). Additionally, the metallicity of the system ( $[M/H]$ ), the (logarithmic) age of the three coeval stars ( $\log \tau$ ), and the interstellar reddening  $E(B - V)$  toward the given triple were also varied. Moreover, due to the strong contamination of the *TESS* lightcurve of KIC 8023317, for this lightcurve only, the ‘extra light’ contamination,  $\ell_4$  parameter was also freely adjusted.

A couple of other parameters were *constrained* instead of being adjusted or held constant during our analyses, as follows:

(i) Orbits: The orbital period of the inner binary ( $P_{\text{in}}$ ) and its orbital phase (through the time of an arbitrary primary eclipse or, more strictly, the time of the inferior conjunction of the secondary star –  $T_{\text{in}}^{\text{inf}}$ ) were constrained internally through the ETV curves.

(ii) Stars: The radii and temperatures of the three stars were calculated with the use of three-linear interpolations from the precomputed 3D (metallicity; logarithmic age; stellar mass) PARSEC grids. Additionally, the distance of the system (which is necessary for the SED fitting) were calculated a posteriori at the end of each trial step, by minimizing the value of  $\chi_{\text{SED}}^2$ .

(iii) Atmospheric parameters of the stars: we handled them in a similar manner as in our previous photodynamical studies. We utilized a logarithmic limb-darkening law (Klinglesmith & Sobieski 1970) for which the passband-dependent linear and non-linear coefficients were interpolated in each trial step via the tables from the original version of the *Phoebe* software (Prša & Zwitter 2005). We set the gravity darkening exponents for all late type stars to  $\beta = 0.32$  in accordance with the classic model of Lucy (1967) valid for convective stars and held them constant. Note, however, that the choice of

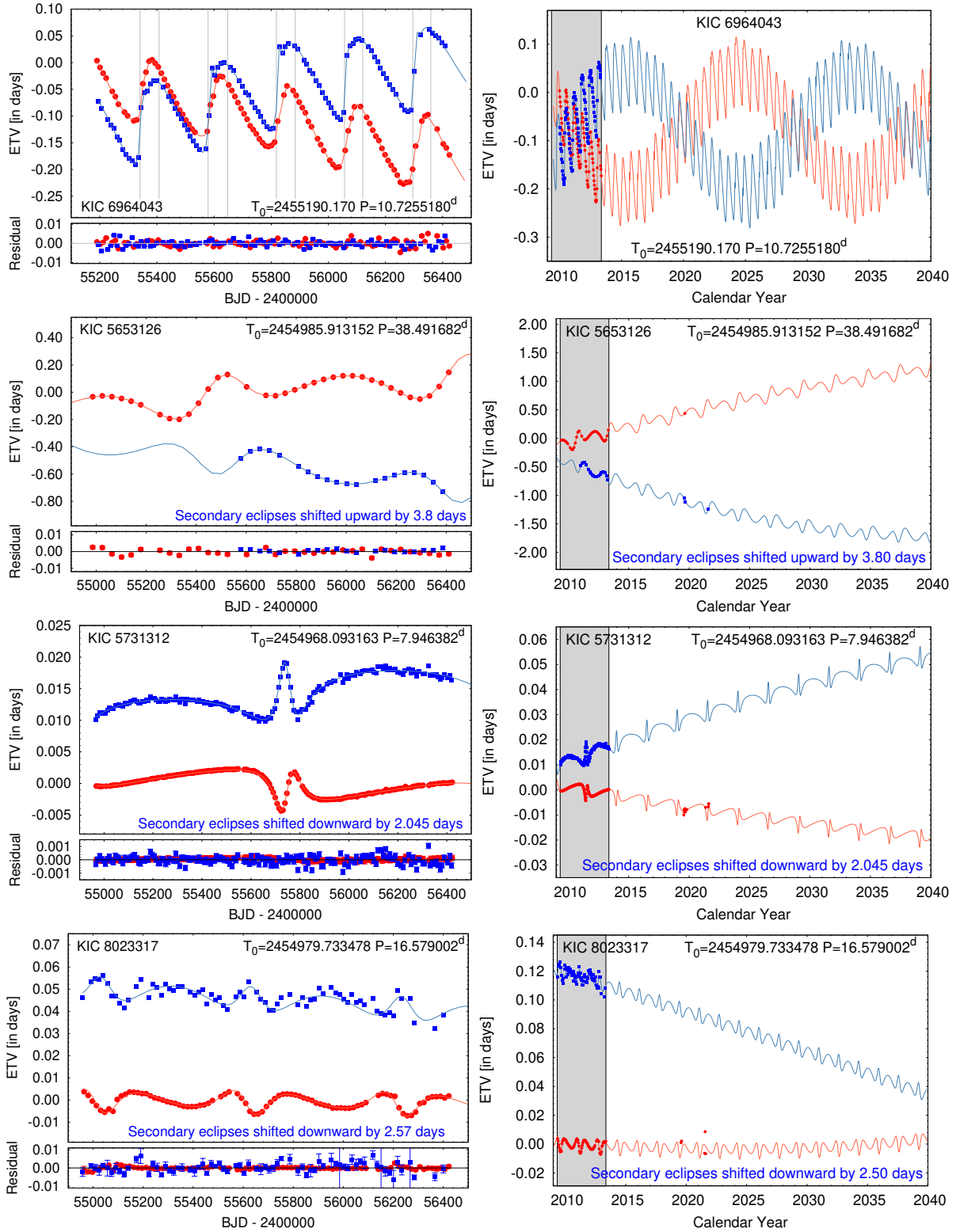


**Figure 6.** Eclipse timing variations of KICs 6964043 (upper), 5653126 (2nd row), 5731312 (3rd row) and 8023317 (bottom). Left panels represent the timing variations during the *Kepler* observations, while right panels exhibit longer time intervals up to 2040. In these panels gray shaded area shows the nominal interval of the original *Kepler* mission. (Note, in those parts of the curves, where no eclipses would be observed due to the low orbital inclinations, the times of the minimal sky-projected distances of the stellar disks were calculated.) Red and blue dots represent the primary and secondary binary eclipses, respectively, while the correspondingly colored curves connect the best-fitting photodynamical model ETV points. In the upper left panel the solid vertical gray lines indicate the times of the third-body eclipses detected by *Kepler* in the triple system KIC 6964043. The lower parts of the left panels show the residuals from the model fit.

this parameter has only minor consequences, since the stars in the present study are close to spheroids.

The median values of the orbital and physical parameters, as well as some derived quantities, of the four triple systems, computed from the MCMC posteriors and their  $1\sigma$  uncertainties are tabulated in Tables 2 and 3. Furthermore, the observed vs. model lightcurves are plotted in Figs. 1–5, while the observed vs. model ETV curves are shown in Fig. 6.

## 5 DISCUSSION

In this section, first we briefly describe the photodynamical results for each individual system, and then we study the short and longer term dynamical evolutions of our triples. For the investigation of the short- and long-term dynamical evolutions we integrate the future motion of the triple star systems with two different numerical integrators. For the short-term ( $\leq 1$  Myr-long) integration we use the very same integrator which is built into LIGHTCURVEFACTORY, and described in Borkovits et al. (2019a,b). Here we note that this integrator works directly with the equations of the orbital motions, including point-mass, tidal and relativistic contributions, and the Eulerian equations of uni-axial stellar rotations. Its main advantage is that it returns at every integration step the spatial coordinates and velocities of each star and, therefore, can be used directly to generate the system lightcurve. It also gives the osculating orbital elements at each instant and, hence, the observational consequences of the motions can be easily studied. The disadvantages are, however, that neither stellar evolution nor tidal dissipation are built in and, therefore, it cannot be used for realistic simulations on much longer timescales. Moreover, another disadvantage is that it is much slower than the method we use for the investigations of the long-term (up to several Gyrs) dynamical evolution of the systems. For this latter approach we use the triple stellar evolution code *TRES* (Toonen et al. 2016) which incorporates secular dynamical evolution including the quadrupole & octupole level interactions, stellar evolution including stellar winds & stellar interaction processes such as mass transfer, common-envelope evolution, mergers, tidal forces, and gravitational wave emission.<sup>10</sup>

Finally, we discuss the implications of our findings on the system parameters for the formation processes of multiple stellar systems in general.

### 5.1 KIC 69640403

This is the only triply eclipsing triple among our sample, and the system is found to be nearly flat. In contrast to the previous findings of Borkovits et al. (2015, 2016), here we find the mutual inclination of the inner and outer orbital planes to be  $i_{\text{mut}} = 4.14 \pm 0.09^\circ$ . This is also the only system in the present study for which the outer stellar component was found to be the most massive one. This tertiary is a slightly evolved twin

of our Sun ( $m_B = 1.00 \pm 0.08 M_\odot$ ;  $R_B = 1.98 \pm 0.09 R_\odot$ ;  $T_{\text{eff},B} = 5500 \pm 50$  K), and it emits more than 96% of the total flux of the system (at least in the *Kepler* photometric band). The inner binary consists of two very similar red dwarf stars ( $m_{Aa} = 0.59 \pm 0.04 M_\odot$ ;  $R_{Aa} = 0.59 \pm 0.03 R_\odot$ ;  $T_{\text{eff},Aa} = 4130 \pm 50$  K and  $m_{Ab} = 0.57 \pm 0.04 M_\odot$ ;  $R_{Ab} = 0.57 \pm 0.03 R_\odot$ ;  $T_{\text{eff},Ab} = 4040 \pm 40$  K, respectively). This triple was found to be the oldest ( $\tau = 9_{-2}^{+1}$  Gyr) and most distant ( $d = 2450 \pm 120$  pc) among the set of studied systems. The distance is greater by  $\approx 2\sigma$  than the Gaia EDR3 distance, but such an inconsistency, in the case of a triple system with an outer period near 2/3 of a year, might be expected. Both the inner and outer mass ratios are relatively close to unity ( $q_{\text{in}} = 0.97 \pm 0.01$  and  $q_{\text{out}} = 0.87 \pm 0.01$ ) which, together with the flatness and compact nature of the system, imply that this system might have formed through a sequential disk instability mechanism (Tokovinin & Moe 2020; Tokovinin 2021) which may lead to compact triple systems with both the inner and outer mass ratios close to unity (double twins, Tokovinin 2018).

Regarding the orbital parameters, while the inner orbit is only slightly eccentric ( $e_{\text{in}} = 0.0037 \pm 0.0005$ ), the eccentricity of the outer orbit is moderately high ( $e_{\text{out}} = 0.4781 \pm 0.0006$ ). As a consequence, the periastron distance of the outer orbit is  $a_{\text{out}}(1 - e_{\text{out}}) \approx 5.1 a_{\text{in}}$ , which places the system quite close to the dynamical stability limit; however, the system is definitely within the dynamically stable region. This is clearly illustrated in the upper panels of Fig. 7 which show the variations of the inner eccentricity and the mutual inclination over the first 250 years of our one million year-long numerical integration. This short-term stability is mainly guaranteed by the nearly perfect flatness of the system, which leads to the suppression of any long-term or secular perturbations in the semi-major axes, as well as to the almost complete disappearance of the quadrupole order long-term perturbations in the eccentricities and the mutual inclination. Moreover, due to the nearly equal masses of the inner binary, the octupole-order terms also remain very small.

In the middle and bottom panels of Fig. 7 we show decades-long (left) and centuries-long (right) variations of some further orbital elements which have readily detectable observational consequences. In the middle panels the time evolution of the observational and dynamical arguments of periastrons ( $\omega_{\text{in,out}}$  and  $\omega_{\text{in,out}}^{\text{dyn}}$ , respectively) are shown. Similar to the other three triples, the apsidal advances of both the inner and outer orbits are clearly dominated by third-body perturbations over the relativistic and tidal effects (see the corresponding rows in Table 2). Due to the flatness of the system, again the apsidal motion is practically linear in time, apart from the small amplitude  $P_{\text{out}}$ -medium period timescale variations. The theoretical<sup>11</sup> inner and outer apsidal motion periods in the dynamical frame are  $P_{\text{apse}}^{\text{dyn}} = 13$  and 199 years, respectively. Naturally, in the observational frame a much longer apsidal motion period will be observed due to the counterbalancing effect of the nodal regression.<sup>12</sup> Thus,

<sup>11</sup> For the calculations we used the formulae described in Borkovits et al. (2015), Appendix C.

<sup>12</sup> It can be readily shown that the observable and dynamical apsidal motion rates relate each other as  $\Delta\omega = \Delta\omega^{\text{dyn}} + \Delta\Omega^{\text{dyn}} \cos i_{\text{dyn}} - \Delta\Omega \cos i$  (see, e.g. Borkovits et al. 2007, 2015). For eclipsing binaries  $\cos i \ll 1$  hence, the last term is negligible

<sup>10</sup> Note, we have also numerically integrated the dynamical evolution of the systems with *TRES* on the shorter timescales and obtained similar (dynamical) results to those found with the built in integrator of LIGHTCURVEFACTORY for all four systems considered in this paper.

**Table 2.** Orbital and astrophysical parameters of the low mutual inclination triples KICs 6964043 and 5653126 from the joint photodynamical lightcurve, ETV, SED and PARSEC isochrone solution. Note, besides the usual angular orbital elements (given in both the observational and dynamical frame of references),  $i_{\text{inv}}$  and  $\Omega_{\text{inv}}$  give the position of the invariable plane with respect to the tangential plane of the sky. The osculating orbital elements are given for epochs  $t_0$ , given in the first row.

	KIC 6964043			KIC 5653126		
	orbital elements					
	Aa–Ab		A–B	Aa–Ab		A–B
$t_0$ [BJD - 2400000]	55182.0			54953.0		
$P$ [days]	10.69787 <sup>+0.00012</sup> <sub>-0.00015</sub>		239.2519 <sup>+0.0076</sup> <sub>-0.0083</sub>	38.44825 <sup>+0.00028</sup> <sub>-0.00028</sub>		971.39 <sup>+0.25</sup> <sub>-0.25</sub>
$a$ [ $R_\odot$ ]	21.47 <sup>+0.47</sup> <sub>-0.34</sub>		209.8 <sup>+4.9</sup> <sub>-3.6</sub>	69.77 <sup>+0.26</sup> <sub>-0.35</sub>		675.8 <sup>+3.0</sup> <sub>-3.8</sub>
$e$	0.03687 <sup>+0.00025</sup> <sub>-0.00052</sub>		0.47806 <sup>+0.00056</sup> <sub>-0.00053</sub>	0.2935 <sup>+0.0015</sup> <sub>-0.0021</sub>		0.1787 <sup>+0.0011</sup> <sub>-0.0011</sub>
$\omega$ [deg]	75.46 <sup>+0.15</sup> <sub>-0.15</sub>		311.41 <sup>+0.09</sup> <sub>-0.10</sub>	304.36 <sup>+0.32</sup> <sub>-0.22</sub>		323.90 <sup>+0.36</sup> <sub>-0.32</sub>
$i$ [deg]	88.797 <sup>+0.111</sup> <sub>-0.087</sub>		89.811 <sup>+0.013</sup> <sub>-0.015</sub>	87.128 <sup>+0.018</sup> <sub>-0.018</sub>		87.608 <sup>+0.526</sup> <sub>-0.463</sub>
$\mathcal{T}_0^{\text{inf}}$ [BJD - 2400000]	55190.1678 <sup>+0.0004</sup> <sub>-0.0043</sub>		55340.658 <sup>+0.018</sup> <sub>-0.015</sub>	54985.8390.1678 <sup>+0.0007</sup> <sub>-0.0007</sub>		...
$\tau$ [BJD - 2400000]	55184.3510 <sup>+0.0043</sup> <sub>-0.0044</sub>		55110.444 <sup>+0.047</sup> <sub>-0.050</sub>	54949.355 <sup>+0.030</sup> <sub>-0.020</sub>		55481.39 <sup>+0.65</sup> <sub>-0.63</sub>
$\Omega$ [deg]	0.0		-4.023 <sup>+0.089</sup> <sub>-0.086</sub>	0.0		-12.344 <sup>+0.163</sup> <sub>-0.175</sub>
$i_{\text{mut}}$ [deg]		4.138 <sup>+0.087</sup> <sub>-0.061</sub>			12.348 <sup>+0.168</sup> <sub>-0.152</sub>	
$\omega^{\text{dyn}}$ [deg]	331.3 <sup>+1.7</sup> <sub>-1.3</sub>		27.2 <sup>+1.8</sup> <sub>-1.4</sub>	212.4 <sup>+2.0</sup> <sub>-2.1</sub>		51.3 <sup>+2.1</sup> <sub>-2.1</sub>
$i^{\text{dyn}}$ [deg]	3.620 <sup>+0.076</sup> <sub>-0.055</sub>		0.519 <sup>+0.009</sup> <sub>-0.008</sub>	10.152 <sup>+0.129</sup> <sub>-0.119</sub>		2.197 <sup>+0.041</sup> <sub>-0.036</sub>
$\Omega^{\text{dyn}}$ [deg]	284.2 <sup>+1.3</sup> <sub>-1.8</sub>		104.2 <sup>+1.3</sup> <sub>-1.8</sub>	272.4 <sup>+2.4</sup> <sub>-2.1</sub>		92.4 <sup>+2.4</sup> <sub>-2.1</sub>
$i_{\text{inv}}$ [deg]		89.685 <sup>+0.015</sup> <sub>-0.017</sub>		87.514 <sup>+0.437</sup> <sub>-0.383</sub>		
$\Omega_{\text{inv}}$ [deg]		-3.506 <sup>+0.045</sup> <sub>-0.062</sub>		-10.149 <sup>+0.127</sup> <sub>-0.135</sub>		
mass ratio [ $q = m_{\text{sec}}/m_{\text{pri}}$ ]	0.972 <sup>+0.008</sup> <sub>-0.009</sub>		0.866 <sup>+0.009</sup> <sub>-0.007</sub>	0.736 <sup>+0.006</sup> <sub>-0.006</sub>		0.418 <sup>+0.004</sup> <sub>-0.004</sub>
$K_{\text{pri}}$ [ $\text{km s}^{-1}$ ]	50.06 <sup>+1.10</sup> <sub>-0.77</sub>		23.41 <sup>+0.74</sup> <sub>-0.44</sub>	40.69 <sup>+0.22</sup> <sub>-0.28</sub>		10.52 <sup>+0.11</sup> <sub>-0.11</sub>
$K_{\text{sec}}$ [ $\text{km s}^{-1}$ ]	51.54 <sup>+1.04</sup> <sub>-0.70</sub>		27.09 <sup>+0.46</sup> <sub>-0.37</sub>	55.28 <sup>+0.25</sup> <sub>-0.37</sub>		25.18 <sup>+0.09</sup> <sub>-0.09</sub>
Apsidal and nodal motion related parameters						
$P_{\text{apse}}$ [year]	28.56 <sup>+0.12</sup> <sub>-0.15</sub>		199.8 <sup>+0.8</sup> <sub>-0.7</sub>	309 <sup>+3</sup> <sub>-4</sub>		1204 <sup>+3</sup> <sub>-4</sub>
$P_{\text{apse}}^{\text{dyn}}$ [year]	13.34 <sup>+0.05</sup> <sub>-0.06</sub>		22.21 <sup>+0.06</sup> <sub>-0.07</sub>	131.4 <sup>+0.9</sup> <sub>-0.7</sub>		190 <sup>+2</sup> <sub>-2</sub>
$P_{\text{node}}^{\text{dyn}}$ [year]		24.99 <sup>+0.10</sup> <sub>-0.08</sub>			225 <sup>+3</sup> <sub>-3</sub>	
$\Delta\omega_{3b}$ [arcsec/cycle]	1329 <sup>+7</sup> <sub>-6</sub>		4249 <sup>+16</sup> <sub>-16</sub>	441 <sup>+6</sup> <sub>-4</sub>		2863 <sup>+10</sup> <sub>-7</sub>
$\Delta\omega_{\text{GR}}$ [arcsec/cycle]	0.447 <sup>+0.020</sup> <sub>-0.014</sub>		0.111 <sup>+0.005</sup> <sub>-0.004</sub>	0.399 <sup>+0.003</sup> <sub>-0.004</sub>		0.0553 <sup>+0.0005</sup> <sub>-0.0006</sub>
$\Delta\omega_{\text{tide}}$ [arcsec/cycle]	0.026 <sup>+0.005</sup> <sub>-0.004</sub>		...	0.050 <sup>+0.001</sup> <sub>-0.002</sub>		...
stellar parameters						
	Aa	Ab	B	Aa	Ab	B
Relative quantities						
fractional radius [ $R/a$ ]	0.0274 <sup>+0.0008</sup> <sub>-0.0007</sub>	0.0266 <sup>+0.0010</sup> <sub>-0.0008</sub>	0.00944 <sup>+0.00022</sup> <sub>-0.00024</sub>	0.0315 <sup>+0.0002</sup> <sub>-0.0002</sub>	0.0188 <sup>+0.0002</sup> <sub>-0.0002</sub>	0.00190 <sup>+0.00004</sup> <sub>-0.00004</sub>
temperature relative to ( $T_{\text{eff}}$ ) <sub>Aa</sub>	1	0.9786 <sup>+0.0069</sup> <sub>-0.0075</sub>	1.3303 <sup>+0.0175</sup> <sub>-0.0159</sub>	1	0.8877 <sup>+0.0077</sup> <sub>-0.0042</sub>	0.8824 <sup>+0.0036</sup> <sub>-0.0035</sub>
fractional flux [in <i>Kepler</i> -band]	0.0203 <sup>+0.0012</sup> <sub>-0.0012</sub>	0.0174 <sup>+0.0010</sup> <sub>-0.0009</sub>	0.9623 <sup>+0.0017</sup> <sub>-0.0020</sub>	0.6875 <sup>+0.0098</sup> <sub>-0.0093</sub>	0.1588 <sup>+0.0048</sup> <sub>-0.0050</sub>	0.1532 <sup>+0.0073</sup> <sub>-0.0061</sub>
fractional flux [in <i>TESS</i> -band]	–	–	–	0.4995 <sup>+0.01791</sup> <sub>-0.0165</sub>	0.1227 <sup>+0.0016</sup> <sub>-0.0016</sub>	0.1084 <sup>+0.0048</sup> <sub>-0.0050</sub>
Physical Quantities						
$m$ [ $M_\odot$ ]	0.588 <sup>+0.038</sup> <sub>-0.026</sub>	0.571 <sup>+0.038</sup> <sub>-0.028</sub>	1.003 <sup>+0.081</sup> <sub>-0.055</sub>	1.774 <sup>+0.024</sup> <sub>-0.029</sub>	1.303 <sup>+0.018</sup> <sub>-0.016</sub>	1.285 <sup>+0.025</sup> <sub>-0.029</sub>
$R$ [ $R_\odot$ ]	0.588 <sup>+0.031</sup> <sub>-0.025</sub>	0.571 <sup>+0.034</sup> <sub>-0.027</sub>	1.980 <sup>+0.087</sup> <sub>-0.077</sub>	2.198 <sup>+0.017</sup> <sub>-0.017</sub>	1.310 <sup>+0.022</sup> <sub>-0.020</sub>	1.281 <sup>+0.034</sup> <sub>-0.037</sub>
$T_{\text{eff}}$ [K]	4134 <sup>+45</sup> <sub>-49</sub>	4041 <sup>+44</sup> <sub>-41</sub>	5495 <sup>+42</sup> <sub>-45</sub>	7062 <sup>+53</sup> <sub>-88</sub>	6260 <sup>+59</sup> <sub>-47</sub>	6228 <sup>+47</sup> <sub>-64</sub>
$L_{\text{bol}}$ [ $L_\odot$ ]	0.091 <sup>+0.013</sup> <sub>-0.010</sub>	0.079 <sup>+0.011</sup> <sub>-0.010</sub>	3.234 <sup>+0.240</sup> <sub>-0.279</sub>	10.822 <sup>+0.353</sup> <sub>-0.626</sub>	2.384 <sup>+0.103</sup> <sub>-0.132</sub>	2.225 <sup>+0.157</sup> <sub>-0.201</sub>
$M_{\text{bol}}$	7.38 <sup>+0.12</sup> <sub>-0.14</sub>	7.53 <sup>+0.15</sup> <sub>-0.14</sub>	3.50 <sup>+0.10</sup> <sub>-0.08</sub>	2.18 <sup>+0.06</sup> <sub>-0.03</sub>	3.83 <sup>+0.06</sup> <sub>-0.05</sub>	3.90 <sup>+0.10</sup> <sub>-0.07</sub>
$M_V$	8.27 <sup>+0.15</sup> <sub>-0.14</sub>	8.50 <sup>+0.16</sup> <sub>-0.12</sub>	3.62 <sup>+0.11</sup> <sub>-0.08</sub>	2.10 <sup>+0.07</sup> <sub>-0.03</sub>	3.80 <sup>+0.07</sup> <sub>-0.05</sub>	3.88 <sup>+0.11</sup> <sub>-0.08</sub>
$\log g$ [dex]	4.668 <sup>+0.018</sup> <sub>-0.017</sub>	4.679 <sup>+0.022</sup> <sub>-0.021</sub>	3.846 <sup>+0.016</sup> <sub>-0.014</sub>	4.000 <sup>+0.007</sup> <sub>-0.006</sub>	4.317 <sup>+0.009</sup> <sub>-0.009</sub>	4.331 <sup>+0.016</sup> <sub>-0.015</sub>
Global system parameters						
$\log(\text{age})$ [dex]		9.934 <sup>+0.075</sup> <sub>-0.107</sub>			9.016 <sup>+0.028</sup> <sub>-0.038</sub>	
$[M/H]$ [dex]		-0.230 <sup>+0.148</sup> <sub>-0.094</sub>			0.372 <sup>+0.039</sup> <sub>-0.107</sub>	
$E(B - V)$ [mag]		0.088 <sup>+0.015</sup> <sub>-0.012</sub>			0.351 <sup>+0.014</sup> <sub>-0.026</sub>	
extra light $\ell_4$ [in <i>TESS</i> -band]		...			0.270 <sup>+0.019</sup> <sub>-0.046</sub>	
$(M_V)_{\text{tot}}$		3.59 <sup>+0.11</sup> <sub>-0.08</sub>			1.73 <sup>+0.07</sup> <sub>-0.03</sub>	
distance [pc]		2443 <sup>+119</sup> <sub>-109</sub>			1374 <sup>+16</sup> <sub>-14</sub>	

**Table 3.** The same as in Table 2 but for KICs 5731312 and 8023317.

	KIC 5731312			KIC 8023317		
	orbital elements					
	Aa–Ab		A–B	Aa–Ab		A–B
$t_0$ [BJD - 2400000]	54953.0			54953.0		
$P$ [days]	7.946521 <sup>+0.000011</sup> <sub>-0.000010</sub>		917.00 <sup>+0.98</sup> <sub>-0.92</sub>	16.57544 <sup>+0.00021</sup> <sub>-0.00020</sub>		605.4 <sup>+2.3</sup> <sub>-2.2</sub>
$a$ [ $R_\odot$ ]	18.20 <sup>+0.10</sup> <sub>-0.09</sub>		448.0 <sup>+2.5</sup> <sub>-2.1</sub>	32.63 <sup>+0.45</sup> <sub>-0.42</sub>		368.1 <sup>+5.5</sup> <sub>-4.4</sub>
$e$	0.45866 <sup>+0.00048</sup> <sub>-0.00033</sub>		0.5745 <sup>+0.0077</sup> <sub>-0.0079</sub>	0.27889 <sup>+0.00041</sup> <sub>-0.00068</sub>		0.252 <sup>+0.013</sup> <sub>-0.013</sub>
$\omega$ [deg]	206.82 <sup>+0.15</sup> <sub>-0.12</sub>		36.06 <sup>+1.38</sup> <sub>-1.59</sub>	152.90 <sup>+0.32</sup> <sub>-0.15</sub>		159.14 <sup>+2.91</sup> <sub>-2.66</sub>
$i$ [deg]	87.378 <sup>+0.153</sup> <sub>-0.107</sub>		67.649 <sup>+0.487</sup> <sub>-0.354</sub>	87.019 <sup>+0.045</sup> <sub>-0.046</sub>		71.836 <sup>+0.369</sup> <sub>-0.267</sub>
$\mathcal{T}_0^{\text{inf}}$ [BJD - 2400000]	54968.0942 <sup>+0.0002</sup> <sub>-0.0002</sub>		...	54979.7311 <sup>+0.0003</sup> <sub>-0.0003</sub>		–
$\tau$ [BJD - 2400000]	54967.5686 <sup>+0.0023</sup> <sub>-0.0017</sub>		54830.70 <sup>+1.70</sup> <sub>-1.97</sub>	54975.7719 <sup>+0.0135</sup> <sub>-0.0061</sub>		55023.12 <sup>+4.82</sup> <sub>-4.22</sub>
$\Omega$ [deg]	0.0		35.18 <sup>+0.41</sup> <sub>-0.43</sub>	0.0		-55.25 <sup>+0.86</sup> <sub>-0.81</sub>
$i_{\text{mut}}$ [deg]	39.41 <sup>+0.32</sup> <sub>-0.31</sub>		–	55.71 <sup>+0.79</sup> <sub>-0.82</sub>		–
$\omega^{\text{dyn}}$ [deg]	263.9 <sup>+0.5</sup> <sub>-0.6</sub>		281.1 <sup>+1.5</sup> <sub>-1.7</sub>	79.4 <sup>+0.4</sup> <sub>-0.3</sub>		255.9 <sup>+2.7</sup> <sub>-2.6</sub>
$i^{\text{dyn}}$ [deg]	27.20 <sup>+0.33</sup> <sub>-0.34</sub>		12.22 <sup>+0.37</sup> <sub>-0.37</sub>	33.38 <sup>+0.85</sup> <sub>-0.88</sub>		22.33 <sup>+0.52</sup> <sub>-0.53</sub>
$\Omega^{\text{dyn}}$ [deg]	118.9 <sup>+0.6</sup> <sub>-0.6</sub>		298.9 <sup>+0.6</sup> <sub>-0.6</sub>	257.9 <sup>+0.5</sup> <sub>-0.4</sub>		77.9 <sup>+0.5</sup> <sub>-0.4</sub>
$i_{\text{inv}}$ [deg]	73.22 <sup>+0.23</sup> <sub>-0.24</sub>		–	78.59 <sup>+0.28</sup> <sub>-0.21</sub>		–
$\Omega_{\text{inv}}$ [deg]	23.62 <sup>+0.39</sup> <sub>-0.39</sub>		–	-32.62 <sup>+0.90</sup> <sub>-0.84</sub>		–
mass ratio [ $q = m_{\text{sec}}/m_{\text{pri}}$ ]	0.665 <sup>+0.031</sup> <sub>-0.042</sub>		0.120 <sup>+0.004</sup> <sub>-0.004</sub>	0.303 <sup>+0.010</sup> <sub>-0.013</sub>		0.079 <sup>+0.003</sup> <sub>-0.003</sub>
$K_{\text{pri}}$ [ $\text{km s}^{-1}$ ]	52.05 <sup>+1.63</sup> <sub>-2.28</sub>		2.99 <sup>+0.48</sup> <sub>-0.08</sub>	23.99 <sup>+0.48</sup> <sub>-0.50</sub>		2.25 <sup>+0.07</sup> <sub>-0.07</sub>
$K_{\text{sec}}$ [ $\text{km s}^{-1}$ ]	78.48 <sup>+1.50</sup> <sub>-1.40</sub>		24.96 <sup>+0.20</sup> <sub>-0.21</sub>	79.45 <sup>+2.15</sup> <sub>-1.56</sub>		28.51 <sup>+0.34</sup> <sub>-0.46</sub>
Apsidal motion related parameters						
$P_{\text{apse}}$ [year]	-4787 <sup>+280</sup> <sub>-306</sub>		18193 <sup>+1368</sup> <sub>-1238</sub>	-653 <sup>+31</sup> <sub>-36</sub>		-6567 <sup>+676</sup> <sub>-929</sub>
$P_{\text{apse}}^{\text{dyn}}$ [year]	1298 <sup>+34</sup> <sub>-33</sub>		873 <sup>+18</sup> <sub>-18</sub>	-1707 <sup>+229</sup> <sub>-342</sub>		1103 <sup>+56</sup> <sub>-54</sub>
$P_{\text{node}}^{\text{dyn}}$ [year]	899 <sup>+18</sup> <sub>-18</sub>		–	884 <sup>+24</sup> <sub>-23</sub>		–
$\Delta\omega_{3b}$ [arcsec/cycle]	-7.1 <sup>+0.3</sup> <sub>-0.4</sub>		179 <sup>+13</sup> <sub>-13</sub>	-91 <sup>+5</sup> <sub>-5</sub>		-327 <sup>+41</sup> <sub>-38</sub>
$\Delta\omega_{\text{GR}}$ [arcsec/cycle]	0.736 <sup>+0.008</sup> <sub>-0.007</sub>		0.0395 <sup>+0.0005</sup> <sub>-0.0005</sub>	0.465 <sup>+0.013</sup> <sub>-0.012</sub>		0.044 <sup>+0.001</sup> <sub>-0.001</sub>
$\Delta\omega_{\text{tide}}$ [arcsec/cycle]	0.47 <sup>+0.02</sup> <sub>-0.02</sub>		...	0.516 <sup>+0.034</sup> <sub>-0.035</sub>		...
stellar parameters						
	Aa	Ab	B	Aa	Ab	B
Relative quantities						
fractional radius [ $R/a$ ]	0.0399 <sup>+0.0007</sup> <sub>-0.0005</sub>	0.0277 <sup>+0.0011</sup> <sub>-0.0015</sub>	0.000409 <sup>+0.000009</sup> <sub>-0.000009</sub>	0.0600 <sup>+0.0007</sup> <sub>-0.0007</sub>	0.0121 <sup>+0.0002</sup> <sub>-0.0002</sub>	0.000474 <sup>+0.000017</sup> <sub>-0.000015</sub>
temperature relative to ( $T_{\text{eff}}$ ) <sub>Aa</sub>	1	0.7272 <sup>+0.0189</sup> <sub>-0.0225</sub>	0.5733 <sup>+0.0058</sup> <sub>-0.0053</sub>	1	0.5402 <sup>+0.0056</sup> <sub>-0.0061</sub>	0.4393 <sup>+0.0056</sup> <sub>-0.0063</sub>
fractional flux [in <i>Kepler</i> -band]	0.8986 <sup>+0.0207</sup> <sub>-0.0202</sub>	0.0984 <sup>+0.0200</sup> <sub>-0.0208</sub>	0.0031 <sup>+0.0003</sup> <sub>-0.0003</sub>	0.9978 <sup>+0.0001</sup> <sub>-0.0002</sub>	0.0021 <sup>+0.0002</sup> <sub>-0.0001</sub>	0.0001 <sup>+0.00001</sup> <sub>-0.00001</sub>
fractional flux [in <i>TESS</i> -band]	0.8774 <sup>+0.0233</sup> <sub>-0.0220</sub>	0.1194 <sup>+0.0218</sup> <sub>-0.0233</sub>	0.0033 <sup>+0.0003</sup> <sub>-0.0003</sub>	0.8479 <sup>+0.0256</sup> <sub>-0.0177</sub>	0.0023 <sup>+0.0002</sup> <sub>-0.0002</sub>	0.0001 <sup>+0.00001</sup> <sub>-0.00001</sub>
fractional flux [in $r'$ -band]	0.9086 <sup>+0.0197</sup> <sub>-0.0193</sub>	0.0892 <sup>+0.0192</sup> <sub>-0.0198</sub>	0.0022 <sup>+0.0002</sup> <sub>-0.0002</sub>	...	...	...
Physical Quantities						
$m$ [ $M_\odot$ ]	0.773 <sup>+0.008</sup> <sub>-0.013</sub>	0.510 <sup>+0.022</sup> <sub>-0.026</sub>	0.153 <sup>+0.004</sup> <sub>-0.005</sub>	1.300 <sup>+0.071</sup> <sub>-0.058</sub>	0.392 <sup>+0.008</sup> <sub>-0.009</sub>	0.134 <sup>+0.006</sup> <sub>-0.006</sub>
$R$ [ $R_\odot$ ]	0.728 <sup>+0.009</sup> <sub>-0.009</sub>	0.505 <sup>+0.023</sup> <sub>-0.029</sub>	0.184 <sup>+0.004</sup> <sub>-0.004</sub>	1.963 <sup>+0.029</sup> <sub>-0.046</sub>	0.394 <sup>+0.008</sup> <sub>-0.010</sub>	0.174 <sup>+0.008</sup> <sub>-0.007</sub>
$T_{\text{eff}}$ [K]	5079 <sup>+47</sup> <sub>-56</sub>	3693 <sup>+68</sup> <sub>-91</sub>	2911 <sup>+28</sup> <sub>-26</sub>	5869 <sup>+66</sup> <sub>-73</sub>	3166 <sup>+45</sup> <sub>-42</sub>	2575 <sup>+35</sup> <sub>-36</sub>
$L_{\text{bol}}$ [ $L_\odot$ ]	0.316 <sup>+0.020</sup> <sub>-0.018</sub>	0.042 <sup>+0.008</sup> <sub>-0.008</sub>	0.0022 <sup>+0.0002</sup> <sub>-0.0002</sub>	4.084 <sup>+0.196</sup> <sub>-0.215</sub>	0.014 <sup>+0.001</sup> <sub>-0.001</sub>	0.0012 <sup>+0.0001</sup> <sub>-0.0001</sub>
$M_{\text{bol}}$	6.02 <sup>+0.06</sup> <sub>-0.07</sub>	8.20 <sup>+0.23</sup> <sub>-0.18</sub>	11.43 <sup>+0.08</sup> <sub>-0.08</sub>	3.24 <sup>+0.06</sup> <sub>-0.05</sub>	9.41 <sup>+0.06</sup> <sub>-0.06</sub>	12.07 <sup>+0.11</sup> <sub>-0.12</sub>
$M_V$	6.27 <sup>+0.09</sup> <sub>-0.08</sub>	9.56 <sup>+0.36</sup> <sub>-0.26</sub>	14.68 <sup>+0.19</sup> <sub>-0.19</sub>	3.27 <sup>+0.07</sup> <sub>-0.06</sub>	11.91 <sup>+0.18</sup> <sub>-0.20</sub>	16.72 <sup>+0.15</sup> <sub>-0.17</sub>
$\log g$ [dex]	4.599 <sup>+0.007</sup> <sub>-0.006</sub>	4.739 <sup>+0.027</sup> <sub>-0.021</sub>	5.095 <sup>+0.007</sup> <sub>-0.007</sub>	3.967 <sup>+0.013</sup> <sub>-0.011</sub>	4.839 <sup>+0.013</sup> <sub>-0.009</sub>	5.077 <sup>+0.021</sup> <sub>-0.020</sub>
Global system parameters						
$\log(\text{age})$ [dex]	9.775 <sup>+0.043</sup> <sub>-0.046</sub>			9.639 <sup>+0.036</sup> <sub>-0.064</sub>		
$[M/H]$ [dex]	-0.122 <sup>+0.027</sup> <sub>-0.040</sub>			0.330 <sup>+0.064</sup> <sub>-0.150</sub>		
$E(B - V)$ [mag]	0.038 <sup>+0.009</sup> <sub>-0.011</sub>			0.080 <sup>+0.026</sup> <sub>-0.019</sub>		
extra light $\ell_4$ [in <i>TESS</i> -band]	...			0.150 <sup>+0.018</sup> <sub>-0.026</sub>		
$(M_V)_{\text{tot}}$	6.22 <sup>+0.08</sup> <sub>-0.07</sub>			3.27 <sup>+0.07</sup> <sub>-0.06</sub>		
distance [pc]	353 <sup>+6</sup> <sub>-7</sub>			814 <sup>+13</sup> <sub>-22</sub>		

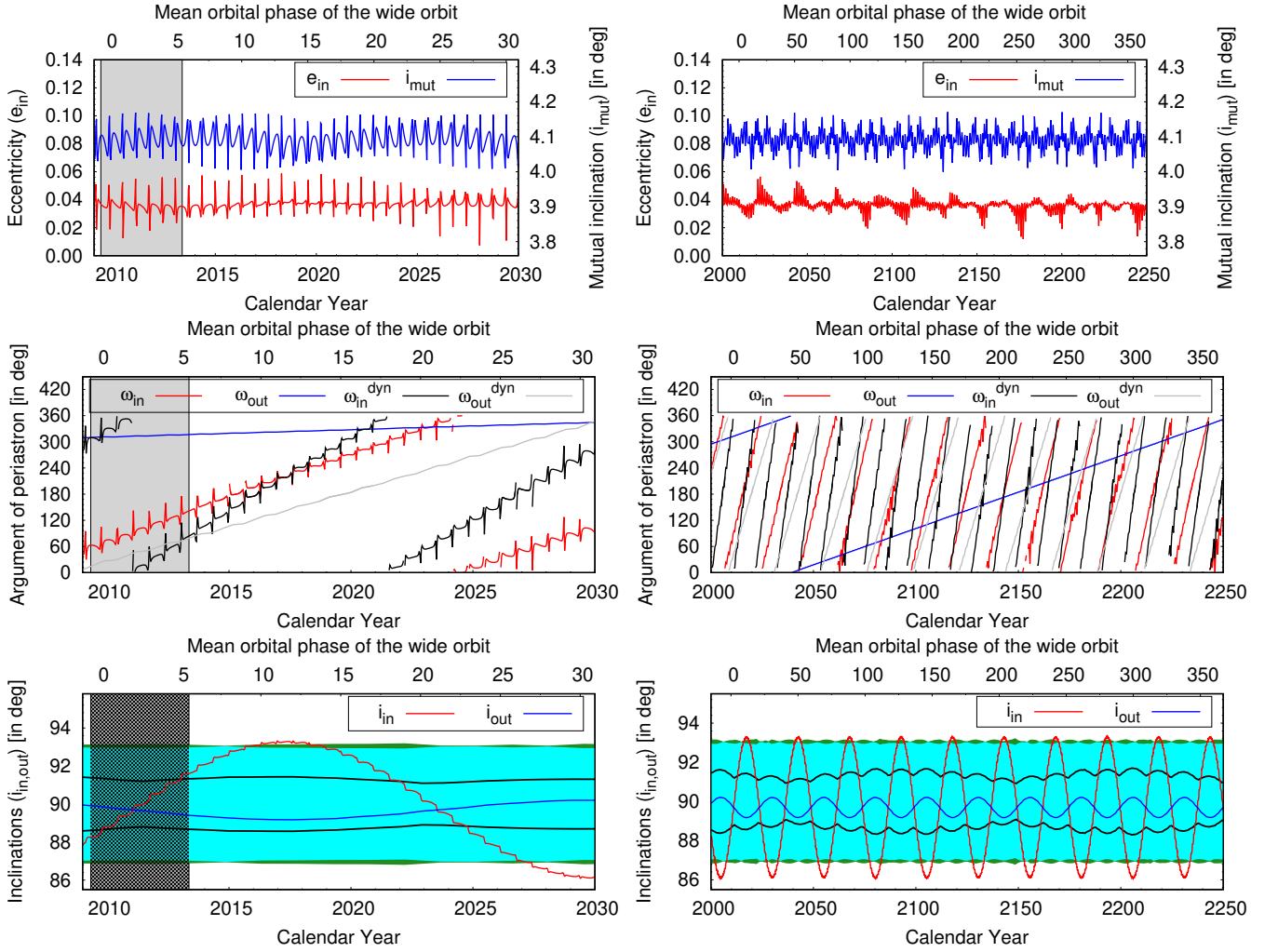


**Figure 7.** Variations of some of the osculating orbital elements in the triple system KIC 6964043. The left panels represent short timescale variations from 2009 to 2030, while the right panels show 250 years. The vertical shaded area in the left panels denote the time domain of the original *Kepler* mission. Note, that the medium-period perturbation effects, especially the bumps around the periastron passages of the third component, are also nicely visible on the left panels. *Upper panels:* Variations of the inner eccentricity ( $e_{in}$ ) and the mutual inclination ( $i_{mut}$ ). *Middle panels:* The variations of the observable and dynamical arguments of periastrons of the inner and outer orbits ( $\omega_{in,out}$  and  $\omega_{in,out}^{dyn}$ , respectively). *Lower panels:* Variations of the observable inclinations of the inner and outer orbital planes ( $i_{in}$ ,  $i_{out}$ , respectively). The green area represents the domain where at least one of the inner EB’s eclipses should be observed, while the cyan area stands for the inclination domain where both eclipses can be observed. Moreover, the horizontal black lines stand for the upper and lower outer inclination ( $i_{out}$ ) limits of the domain where outer, third-body eclipses might occur. See text for further details.

the apsidal motion of the inner binary in the observational frame of reference, which can be detected directly through the anticorrelated primary and secondary ETV curves (Fig. 6), has a theoretical period of  $P_{apse} = 28.59 \pm 0.02$  yr, in accord with both the numerical integrations and the observed ETV curves.

The bottom panels of Fig. 7 display the inclination angle variations of both the inner and outer orbits. The precession

(though it was taken into account for calculating the theoretical observable apsidal motion periods –  $P_{apse}$ , tabulated in Tables 2 and 3) and therefore, for the negative sign of  $\Delta\Omega^{dyn}$ , one can infer, that the observable apsidal advance rate should be lower than the dynamical one.

period is about 25 years. (The theoretical value is  $P_{node} = 25.0 \pm 0.1$  yr.) In these panels we also denote with cyan (or green) regions of the inclination-angle domain where both (or at least one) eclipses of the inner binary can be observed. The borders of these regions are calculated from the equation

$$|\cos i_{in}| = \frac{R_{Aa} + R_{Ab}}{a_{in}} \frac{1 \pm |e_{in} \sin \omega_{in}|}{1 - e_{in}^2}, \quad (2)$$

where, on the right hand side, the positive sign gives the inclination-angle limit for a single eclipse (i.e., the green area), while the negative sign gives the limit where both eclipses should occur (the cyan area). As one can see, during the first part of the *Kepler*-observations the inner inclination became closer and closer to  $90^\circ$ , and the inner orbit was seen exactly edge-on from the Earth around 2011.5. Therefore,

during the second part of the *Kepler* measurements the orbital plane was viewed under a continuously decreasing angle. This is in nice agreement with the first increasing, then constant (total eclipses) and, finally, decreasing eclipse depths (Fig. 1) that were seen. Moreover, one can also see in the lower left panel of Fig. 7, that during the Sector 14 and 15 *TESS*-observations ( $\approx 2019.6$ ), the inner binary was at the very edge of the eclipsing regime. Strictly speaking, the inner eclipses were present, however, their amplitudes were two orders of magnitude smaller than the scatter of the *TESS* lightcurve of this very faint ( $T = 15.0$  mag) source. And, indeed, no third-body eclipse was seen during the two sectors of *TESS* observations, therefore, the eclipsing nature of this system remained hidden from *TESS*. In contrast to this, during the scheduled Sector 54 and 55 observations ( $\approx 2022.6$ ) the inner binary will again be very close to its next edge-on position ( $i_{\text{in}} \approx 90^\circ.7$ ) offering much better conditions to observe the shallow regular eclipses.

In the same panels we also denote, with thin black lines, the inclination limits of the outer inclination domain for the possibility of third-body eclipses. These are defined as follows:

$$|\cos i_{\text{out}}| = \frac{R_B + R_{\text{Ab}} + \frac{a_{\text{in}}}{1+q_{\text{out}}} (1 + \tan^2 i_{\text{in}} \cos^2 \Delta\Omega)^{-1/2}}{a_{\text{out}}} \times \frac{1 + |e_{\text{out}} \sin \omega_{\text{out}}|}{1 - e_{\text{out}}^2}. \quad (3)$$

(We will discuss this expression in Appendix A.) As one can see, the system continuously remains in the domain of the third-body eclipses.

In addition we assess the long-term future evolution of KIC 6964043. On longer timescales of a few 100 Myr (Fig. 8), KIC 6964043 displays evolution of the eccentricity of the outer orbit due to the octupole term. The outer eccentricity slowly increases from the initial value of  $\approx 0.48$  to  $\approx 0.50$  at 765 Myr. At this point, the system formally crosses into the dynamically unstable regime. Given the current proximity to the stability limit, it is not surprising that the system's hierarchy may break down. As the secular theory that *TRES* is based on is no longer valid at this point, we stop the simulation. Based on Toonen et al. (2022) we expect the system to remain in the dynamically unstable regime as an unstable but bound triple for on average  $10^4$  crossing times, about 5 kyr. The most likely outcome of such an interaction is the dissolution of the system into a binary and single star, or the collision of two of the stars reducing the system from a triple into a binary. A summary of the evolution is shown in Fig. 9.

## 5.2 KIC 5653126

This triple contains the most massive stars in our sample, and it has the second highest inner and outer mass ratios ( $q_{\text{in}} = 0.736 \pm 0.006$ ;  $q_{\text{out}} = 0.418 \pm 0.004$ ). The most massive component is the early F-type primary of the inner pair ( $m_{\text{Aa}} = 1.77 \pm 0.03 M_\odot$ ;  $R_{\text{Aa}} = 2.20 \pm 0.02 R_\odot$ ;  $T_{\text{eff,Aa}} = 7060 \pm 80$  K), while its binary companion and the tertiary star are very similar late F-type stars ( $m_{\text{Ab}} = 1.30 \pm 0.02 M_\odot$ ;  $R_{\text{Ab}} = 1.31 \pm 0.02 R_\odot$ ;  $T_{\text{eff,Ab}} = 6260 \pm 60$  K and  $m_{\text{B}} = 1.29 \pm 0.03 M_\odot$ ;  $R_{\text{B}} = 1.28 \pm 0.04 R_\odot$ ;  $T_{\text{eff,B}} = 6230 \pm 60$  K). The age of the system is found to be  $\tau = 1.0 \pm 0.1$  Gyr. Our analysis yields a distance of  $d = 1375 \pm 15$  pc, which agrees with the trigonometric Gaia EDR3 distance to within  $3\sigma$ .

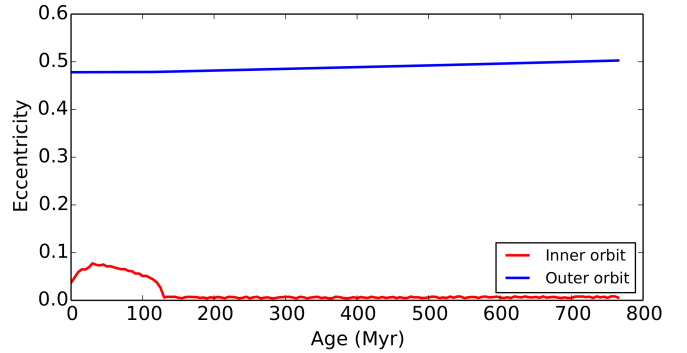


**Figure 8.** Evolution of the system eccentricities in KIC 6964043.

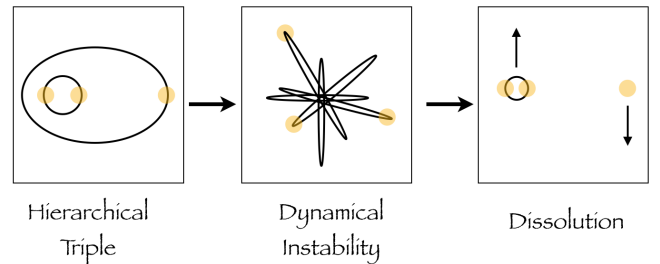


**Figure 9.** Schematic evolution of the triple star system KIC 6964043.

Turning to the orbital parameters, both the inner and outer orbits are moderately eccentric ( $e_{\text{in}} = 0.294 \pm 0.002$  and  $e_{\text{out}} = 0.179 \pm 0.001$ ). The mutual inclination of the orbital planes was found to be  $i_{\text{mut}} = 12^\circ.3 \pm 0^\circ.2$ , but at that epoch both orbits had very similar observable inclination angles. At the beginning of the *Kepler* observations, the inclination angles were  $i_{\text{in}} = 87^\circ.13 \pm 0^\circ.02$  and  $i_{\text{out}} = 87^\circ.6 \pm 0^\circ.5$  for the inner and outer orbital planes, respectively. Note that, despite the absence of third-body eclipses, which would strongly constrain the outer inclination angle as well as the mutual inclination, we were able to find these quantities with remarkable accuracies of some tenths of a degree (which is even better than the accuracies obtained for the same parameters in the case of some *TESS* observed triply eclipsing triples – see, e.g., Borkovits et al. 2022). This is a consequence of the fact that the variation of the inner inclination angle and, hence, the depths and durations of the inner eclipses are extremely sensitive to these parameters. (Note, for the former system, KIC 6964043, where both the eclipse depth variations and third body eclipses were detected continuously over a 3-year-long timescale, we were able to obtain even higher accuracies, some hundredths of a degree, for these parameters.)

At this point, we comment on the presence or absence of third-body eclipses. In contrast to the triply eclipsing triple KIC 69640433, in the case of this, and the other two systems we will discuss, in the absence of third-body eclipses, the lightcurves do not carry any information on the radii and effective temperatures of the tertiary components, because their only direct effects on the lightcurves are the dilution of the regular eclipses by their extra flux contamination. Thus, the third star's radius and temperature are largely dependent on the *PARSEC* isochrones. The latter, however, are con-

strained by the third star’s mass and mass ratios, which can be inferred quite accurately from the photodynamical analysis. This is especially true of the effects of the third-body perturbations which drive apsidal motion, leading to ETVs, and orbital plane precession (whose consequences were discussed in the preceding paragraph). Thus, the fact that the dynamically inferred third star masses led to fully consistent MDN solutions, in our view, again verifies the use of PARSEC isochrones as proxies either for the masses (in the absence of RV data in the case of regular EBs) or radii and other fundamental stellar parameters (in the absence of third-body eclipses).

Turning now to the above mentioned perturbations, in Fig. 10 we display the variations of some orbital elements over 30 and  $\approx 1300$  year-long intervals. In contrast to KIC 6964043, besides the characteristic medium ( $P_{\text{out}}$ ) timescale perturbations (upper left panel), now some longer timescale periodic variations can be identified both in the inner eccentricity and the mutual inclination. The amplitudes of these clearly exceed those of the medium period effects, though the relative variations in both orbital elements remain at the few percents level. As one can see,  $e_{\text{in}}$  and  $i_{\text{mut}}$  vary in an anticorrelated manner, and the characteristic period of these cycles is about half of the dynamical apsidal motion period. These findings are in good agreement with the theories of the quadrupole-order long-period perturbations in the low mutual inclination regime (see, e.g., Mazeh & Shaham 1979; Söderhjelm 1982; Borkovits et al. 2007). Moreover, another even longer period variation in the eccentricity can also be noticed, which we attribute to the octupole-order perturbations (e.g. Naoz et al. 2013). These variations, however, again remain small, and our longer, one million year numerical integration displays the same picture.

The variations of the observationally more relevant orbital elements, again, are shown in the middle (apsidal motion) and bottom (orbital precession) panels. The behaviour of the different arguments of periastron are similar to those of KIC 6964043, but the periods are somewhat longer, in accordance with the longer characteristic timescale of  $P_{\text{out}}^2/P_{\text{in}}$ . The calculated (theoretical) observable apsidal motion periods are  $P_{\text{apse,in}} = 309 \pm 4$  yr and  $P_{\text{apse,out}} = 1204 \pm 4$  yr for the inner and outer orbits, respectively. Besides the longer timescales, another minor difference in the behaviour of the rotations of the lines of the apsides relative to the previous system is that the dynamical apsidal motion no longer remains strictly linear, but a low amplitude cyclic variation (with a period similar to that of the eccentricity variation period) is also superposed on the linear trend. For such a low mutual inclination, however, the amplitude of this extra cyclic term, from an observational point of view, remains negligible.

In the bottom panels, the variations of the observable inclination angles, and the domains within which eclipses are possible are plotted. The precession period is calculated to be  $P_{\text{node}} = 225 \pm 3$  yr. During one cycle, the inner binary exhibits eclipses only in two, separated,  $\approx 40$  yr-long intervals. The current eclipsing session will terminate at the very end of 2031. What is more interesting, is that there are short intervals when third-body eclipses are also possible. The last such interval of outer eclipses occurred circa the 1970s. In order to check whether third body eclipses had actually occurred during that period, we back-integrated our best solution (i.e. the set of input parameters which yielded the lowest net  $\chi^2$

value) to 1950, and found two third-body events during 12-14 January 1976 and 11-15 September 1978. The same integration has revealed that the next third-body eclipse is expected only in the year 2143. As one can see in the lower right panel of Fig. 10, these third-body eclipses may occur when the inner binary is the farthest from its eclipsing binary state. At the current time only one such triple star system is known with certainty, and it currently shows third-body eclipses without inner binary eclipses. This is KIC 2835289, a 0.86-day-period ellipsoidal variable, orbited by a third star with a period of  $P_{\text{out}} = 755$  d, from which two third-body eclipses were observed with *Kepler* (Conroy et al. 2014, 2015), and a further one with *TESS*. Moreover, Borkovits et al. (2020a) found that TIC 167692429, which currently is an EB with remarkable eclipse depth variations, has also produced third-body eclipses in the recent past, *before* the beginning of its recent eclipsing session. And, the last of those events was actually identified with great likelihood in the archival SuperWASP observations of that triple.

As with KIC 6964043, we address the long-term future evolution of KIC 5653126 by making use of the *TRES* code. The long-term future of KIC 5653126 is different that of the previous system as in the case of KIC 5653126 the stars are massive enough to evolve off the MS in a Hubble time (see Fig. 11). As the primary of the inner binary, which is the most massive star in this triple ascends the first giant branch and expands rapidly, the system changes due to three reasons; (1) tidal torques amplify leading to the near circularisation of the inner binary (Fig. 12). The inclination freezes out at about 30 degrees, after increasing steadily from the current inclination of about 12 degrees. (2) the primary star loses  $0.004 M_{\odot}$  of envelope material due to its stellar winds. As a result there is a slight increase in the outer semi-major axis from  $675.8 R_{\odot}$  to  $676.42 R_{\odot}$ . There is also a widening effect from the wind mass loss on the inner orbit, however the dominant effect is a slight shrinkage of the semi-major axis from  $69.77 R_{\odot}$  to  $69.46 R_{\odot}$  due to stellar tides. (3) Lastly, and most importantly, at 1910 Myr, the primary star fills its Roche lobe.

Given the evolutionary state of the donor star and its deep convective envelope, the ensuing mass transfer phase proceeds in an unstable way, quickly leading to a common-envelope (CE) phase (for a review, see Ivanova et al. 2013). During this phase the secondary star orbits around the core of the primary star inside its envelope. Friction causes the secondary’s orbit to decay leading to the merger of the secondary with the core of the star, or a tight binary if the envelope can be ejected. Adopting the classical energy-based CE-prescription (i.e. the  $\alpha$ -model; Paczynski 1976; Webbink 1984; Livio & Soker 1988; de Kool 1990), the CE-phase leads to a merger of the two stars in the inner binary. This holds for both the classical values of the CE-efficiency ( $\alpha \approx 1$ ) as well as the observationally derived reduced efficiencies ( $\alpha \approx 0.25$ ; Zorotovic et al. 2010; Toonen & Nelemans 2013; Camacho et al. 2014; Zorotovic et al. 2022). The resulting merger product is a giant-like object with a compact helium-rich core of  $0.32 M_{\odot}$  and a massive hydrogen-rich envelope of  $2.75 M_{\odot}$  assuming a conservative merger.

As this object evolves further, it will initiate core helium burning followed by helium-shell burning as it ascends the asymptotic giant branch (AGB). During this phase, when the merger remnant is still orbited by the initial tertiary star, it fills its Roche lobe again. This second CE-phase does not lead

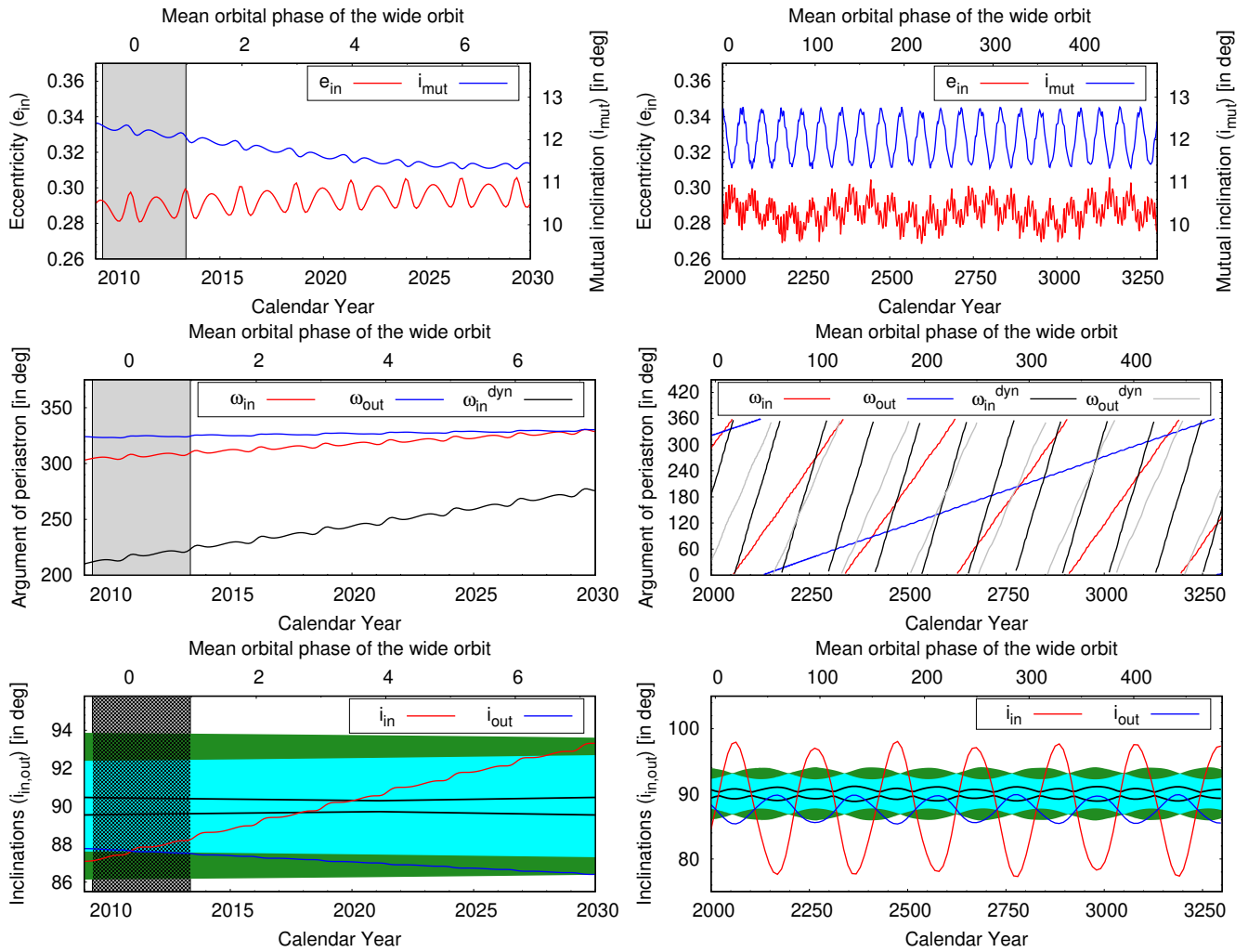


**Figure 10.** Variations of the same orbital elements as in Fig. 7 above, but for KIC 5653126. Note, that the right panels here and also for the other two systems represent an interval of 1300 years. See text for details.

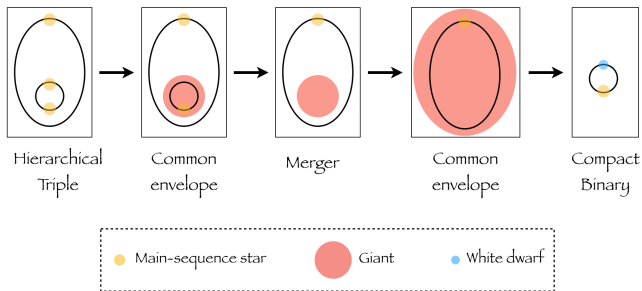


**Figure 11.** Schematic evolution of the triple star system KIC 5653126.

to a merger, as the pre-CE orbit is much wider than for the first CE-phase. After the second CE-phase, the system consists of a  $0.65 M_{\odot}$  white dwarf (i.e., the old core of the AGB-star) and a  $1.29 M_{\odot}$  main-sequence companion. The orbit of the post-CE system depends critically on the CE-efficiency i.e. the efficiency with which the orbital energy is converted to unbind the envelope. In both cases of inefficient ( $\alpha = 1$ )

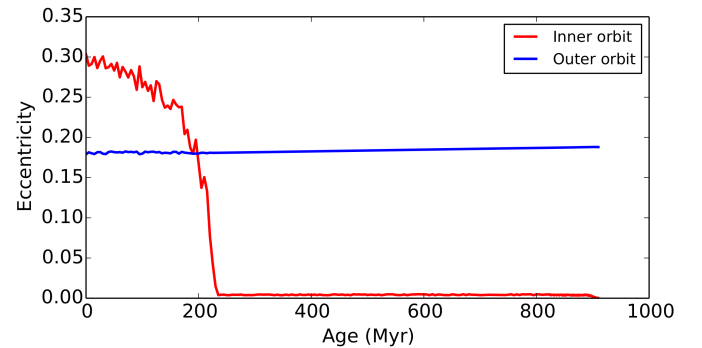


**Figure 12.** Evolution of the system eccentricities in KIC 5653126.

and efficient ( $\alpha = 0.25$ ) CE-evolution, the system experience an ultimate mass transfer event, with the white dwarf as the accretor star, and the donor star either on the main-sequence or giant branch, respectively. In both cases the system ends its life as a single white dwarf of mass  $0.8 - 0.9 M_{\odot}$ . Even

though, the systems started out its life as a triple star system, we expect it will end its life as a single star.

### 5.3 KIC 5731312

Now we turn to the two dynamically more interesting, high mutual inclination systems. KIC 5731312 is the least massive triple in our sample. The inner binary is formed by a K and an M-type dwarf ( $m_{Aa} = 0.77 \pm 0.01 M_{\odot}$ ;  $R_{Aa} = 0.73 \pm 0.01 R_{\odot}$ ;  $T_{\text{eff},Aa} = 5080 \pm 60 \text{ K}$  and  $m_{Ab} = 0.51 \pm 0.02 M_{\odot}$ ;  $R_{Ab} = 0.51 \pm 0.03 R_{\odot}$ ;  $T_{\text{eff},Ab} = 3690 \pm 30 \text{ K}$ , respectively), while the distant, third component is a very low mass, cool, late M star ( $m_B = 0.15 \pm 0.01 M_{\odot}$ ;  $R_B = 0.18 \pm 0.01 R_{\odot}$ ;  $T_{\text{eff},B} = 2910 \pm 30 \text{ K}$ ). Thus, the mass ratios are far from unity ( $q_{\text{in}} = 0.665 \pm 0.040$ ;  $q_{\text{out}} = 0.120 \pm 0.004$ ) and, in such a way, they differ substantially from the mass ratios of the flat triples investigated above. This fact, together with the inclined tertiary orbit, certainly imply a different formation scenario. The system is found to be quite old ( $\tau = 5.9 \pm 0.6 \text{ Gyr}$ ). Its photodynamically obtained distance ( $d = 353 \pm 7 \text{ pc}$ ) is in excellent agreement with the Gaia EDR3 distance.

As mentioned in Sect. 2 this triple is by far the least tight one in our sample ( $P_{\text{out}}/P_{\text{in}} \approx 122$ ). Moreover, the outer mass ratio is also very low. As a consequence, one can observe remarkable, readily detectable ETVs in this system largely due to the high inner and outer eccentricities ( $e_{\text{in}} = 0.4587 \pm 0.0005$  and  $e_{\text{out}} = 0.575 \pm 0.008$ ). In an opposite, i.e. nearly circular, case the presence of the distant tertiary probably would have remained unnoticed even via an ETV analysis based on the highly accurate timing data that were obtained from *Kepler* observations. While the semi-major axes of the two orbits are found to be  $a_{\text{in}} = 18.2 \pm 0.1 R_{\odot}$  and  $a_{\text{out}} = 448 \pm 2 R_{\odot}$ , respectively, at the times of apastron passage of the inner orbit, and periastron passage of the outer orbit, the orbital separations are  $r_{\text{in}}^{\text{apo}} \approx 26.5 R_{\odot}$  and  $r_{\text{out}}^{\text{peri}} \approx 190.6 R_{\odot}$ . Hence, the ratio of the equivalent periods becomes  $P_{\text{out}}^{\text{peri}}/P_{\text{in}}^{\text{apo}} \approx 19.2$ , temporarily resulting in a very tight triple system.

The mutual inclination of the two orbits is found to be  $i_{\text{mut}} = 39^{\circ}.4 \pm 0^{\circ}.3$ , i.e., the former findings of Borkovits et al. (2015, 2016), which were based only on an analytic analysis of the ETV curves, is nicely confirmed. This mutual inclination value is very close to the famous mutual inclination limit ( $i_{\text{mut}}^{\text{ZKL}} = 39^{\circ}.23$ , and its retrograde counterpart) of the original, quadrupole, asymptotic ZKL theory, which separates the low- and high mutual inclination regimes of the phase space (see the short summary in the Introduction). However, as discussed next, the configuration of the present system is far from appropriate to be fit in the framework of the original ZKL theory. Due to the large outer eccentricity and small inner mass ratio, the octupole-order perturbations may become significant, and hence the evolution of the orbital elements should be modeled within the framework of the eccentric ZKL formalism (see e.g. Naoz 2016).

First we introduce again the short-term characteristics of these perturbations in some of the orbital elements, as well as their direct observational consequences. In order to do this, similar to the previous two triples, we display decades and centuries long variations of a few orbital elements obtained from a 1 Myr-long numerical integration in the various panels of Fig. 13. Now the eccentricity cycles of the inner binary, and the corresponding variations of the mutual inclination with a

period of  $P_{\text{ZKL}} \approx 690 \text{ yr}$  and full amplitudes of  $\Delta e_{\text{in}} \approx 0.28$  and  $\Delta i_{\text{mut}} \approx 10^{\circ}$  are clearly visible in the upper panels. The characteristics of these variations do not change significantly during the entire 1-million-year integration, however, a slow sinusoidal variation in the amplitudes of  $\approx 10\%$  on an  $\approx$  ten-thousand year timescale is also apparent, probably due to the octupole terms.

As one can see in the middle left panel, the inner EB exhibits retrograde apsidal motion in the observational frame over the current several decades. This results because a negative contribution arises from the nodal regression which temporarily overpowers the effect of the prograde apsidal advance in the dynamical frame of reference. However, as the middle right panel shows, this is only part of a longer-term oscillatory (i.e., libration) cycle. The dynamical apsidal motion of both the inner and outer orbits remain continuously prograde, however their non-linear nature, i.e., the presence of a significant librating motion in addition to the usual circular apsidal motion is readily visible in the middle right panel. Their period is about 1300-1400 yr, i.e., twice of that of the eccentricity cycles (which, again, is in perfect agreement with the theory of the secular perturbations). Note, however, that these values do not agree with the theoretical apsidal motion periods tabulated in Table 3. The reason is that these latter periods were calculated from the instantaneous apsidal motion rates (also listed in the tables) simply by linear interpolation and, hence, do not give accurate results for highly non-linear apsidal motions.

The variations in the visible inclination angles are shown in the bottom panels of Fig. 13. The nodal precession cycle of this triple has a period of  $P_{\text{node}} \approx 1400 \text{ yr}$ . During such a cycle the inner pair of stars exhibits eclipses only for two short, 80-100 year-long intervals. The current eclipsing session began around the 1950's, and the EB was seen edge-on at the beginning of the 1990's. During the prime *Kepler* mission, both kinds of eclipses were observable. Then, however, the eclipse closer to apastron would no longer have been observable since  $\sim 2016.5$ , which is in accord with the 2019 and 2021 *TESS* measurements. The remaining, solo eclipses will also disappear in about 2029.0, and the eclipses will return only in the XXIX-th century. Finally, as one can see, between circa 2300 and 2600 there might be a chance for third-body eclipses to appear. In order to check this possibility, we numerically generated the system's lightcurve for a section of this interval, and found two very shallow (with depth of  $\sim 0.3\%$ ) third-body eclipses at the epoch 2453.63.

The long-term future of KIC 5731312 is reminiscent of that of KIC 6964043 (see Fig. 9). On long timescales, here of the order of more than a few Gyr, we find an extra modulation in the eccentricity of the outer orbit due to the octupole term (Fig. 14). The eccentricity first decreases from the original value of  $\approx 0.57$  to 0.55, after which it starts increasing. When the outer eccentricity reaches a value of  $\approx 0.81$  at 3.96 Gyr, the system crosses the stability limit, in analogy of KIC 6964043. Given the stellar masses of KIC 5731312, the stars are still on the MS when this happens, and will remain so within a Hubble time. The evolution during the dynamically unstable phase is therefore a pure dynamical (gravitational) problem. After many crossing times ( $10^4$  crossing time is about 0.75 kyr), the system most likely dissolves into a bound binary and a single star ejecting the low-mass tertiary star from the system.

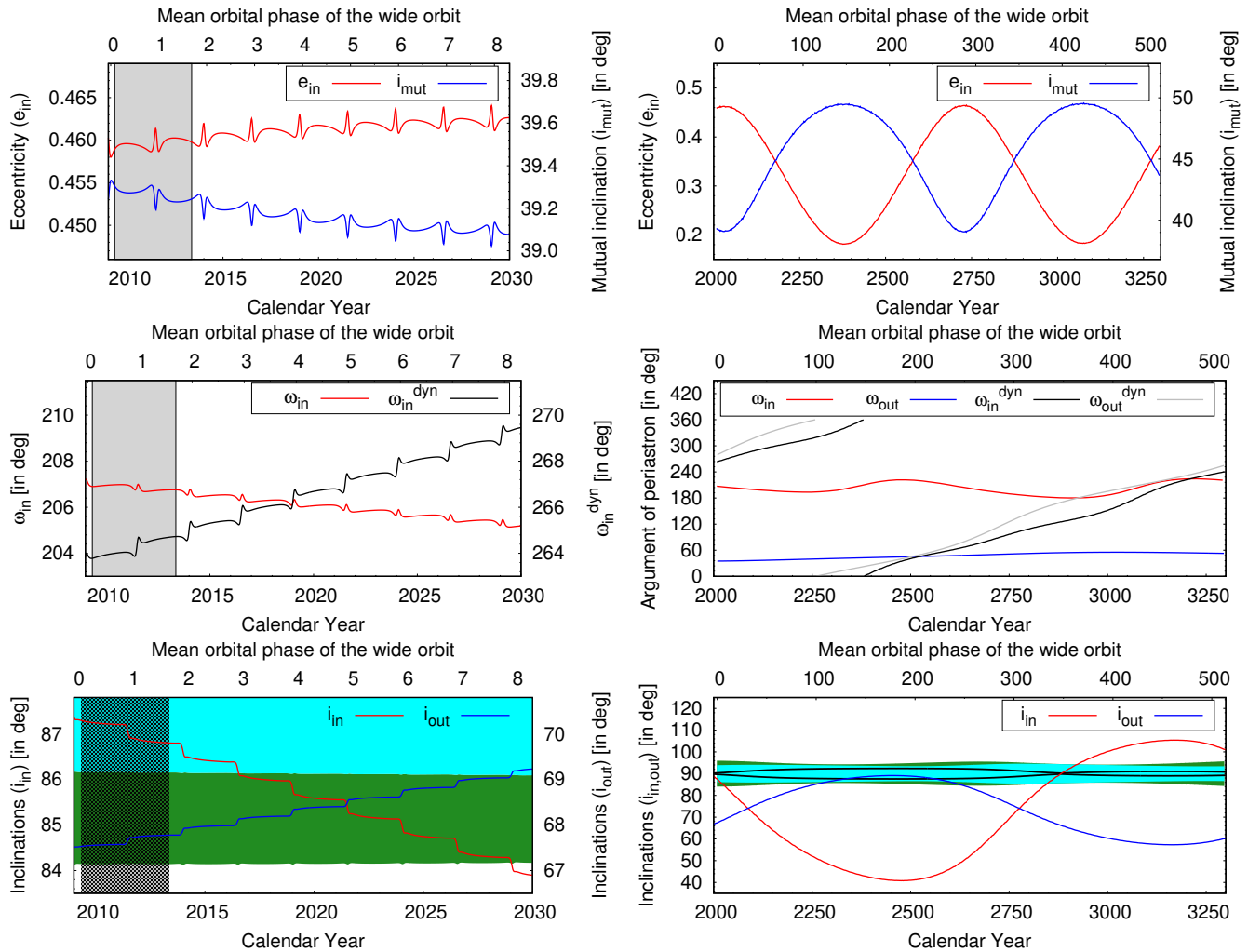


**Figure 13.** Variations of the same orbital elements as in Fig. 7 above, but for KIC 5731312. See text for details.

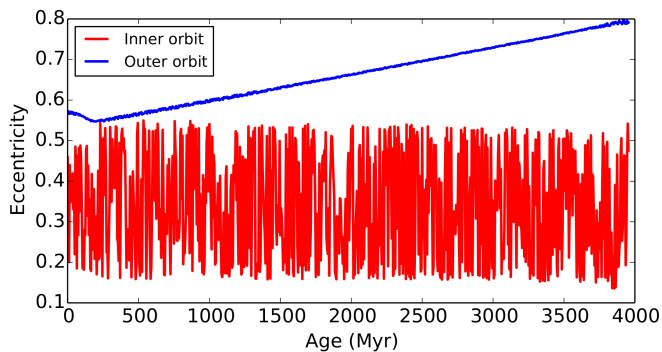


**Figure 14.** Evolution of the system eccentricities in KIC 5731312.

#### 5.4 KIC 8023317

This triple has the most extreme inner and outer mass ratios in our sample ( $q_{\text{in}} = 0.303 \pm 0.013$ ;  $q_{\text{out}} = 0.079 \pm 0.003$ ). The main stellar component is one of the EB stars, and is a slightly evolved G-type star ( $m_{\text{Aa}} = 1.30 \pm 0.07 M_{\odot}$ ;  $R_{\text{Aa}} =$

$1.96 \pm 0.05 R_{\odot}$ ;  $T_{\text{eff,Aa}} = 5870 \pm 70 \text{ K}$ ). Its binary companion is a low mass M-type red dwarf ( $m_{\text{Ab}} = 0.39 \pm 0.01 M_{\odot}$ ;  $R_{\text{Ab}} = 0.39 \pm 0.01 R_{\odot}$ ;  $T_{\text{eff,Ab}} = 3165 \pm 45 \text{ K}$ ). The tertiary is another even lower mass M star with  $m_{\text{B}} = 0.13 \pm 0.01 M_{\odot}$ ,  $R_{\text{B}} = 0.17 \pm 0.01 R_{\odot}$ , and  $T_{\text{eff,B}} = 2575 \pm 35 \text{ K}$ . The latter star has the lowest mass among all dozen in our full sample. The age of the triple is found to be  $\tau = 4.3 \pm 0.5 \text{ Gyr}$ . The photodynamically obtained distance is  $d = 814 \pm 20 \text{ pc}$ , which is larger than the Gaia EDR3 inferred distance by about  $3\text{-}\sigma$ .

The mutual inclination is found to be  $i_{\text{mut}} = 55.7 \pm 0.8^{\circ}$ , which is even higher by  $\sim 6^{\circ}$  than the former result of Borkovits et al. (2015, 2016). Thus, according to our knowledge, this system has the second highest mutual inclination after Algol amongst all triple star systems with accurately known mutual inclinations.

The ZKL cycles in the inner eccentricity and the mutual inclination are, again, clearly visible (see upper panels of Fig. 15) and look quite similar to those same features of the previous system, KIC 5731312. One quantitative difference, however, is that the ZKL cycle period is shorter, being  $P_{\text{ZKL}} \approx 360 \text{ yr}$ , in accordance with the shorter  $P_{\text{out}}^2/P_{\text{in}}$  timescale. The ranges of the variations of both parameters are

very close to that of KIC 5731312, but the phase is almost opposite. While KIC 5731312 currently is close to its maximum eccentricity and, hence, minimum mutual inclination phase, KIC 8023317 is close to its smallest inner eccentricity, and largest mutual inclination.

There is, however, an important qualitative difference in the behavior of the apsidal lines of the inner orbits between the present and the previous system. While in the case of KIC 5731312, the dynamical apsidal line circulates, in the case of KIC 8023317 it librates around  $\omega_{\text{in}}^{\text{dyn}} = 90^\circ$ , with a half-amplitude of  $\approx 27^\circ$ . The period of this libration is the same as that of the inner eccentricity cycles. Though prior numerical (e.g. Ford et al. 2000) and theoretical works (Naoz 2016) have shown that the periods of apsidal librations and circulations may alter each other, in the present situation the libration remained unchanged throughout our 1 Myr-long numerical integration. Regarding the observable apsidal motion of the inner pair, it is again clearly retrograde, as can be seen nicely in the middle panels of Fig. 15.

Finally, we consider the variations of the inclination angles in the bottom panels of Fig. 15. The precession period is about  $P_{\text{node}} \approx 650$  yr. The current eclipsing session of the inner pair started around 2000.0, and central eclipses will occur around 2023.7. The eclipses will then completely disappear around 2052.7, and will return only near the beginning of 2088. Moreover, similar to the other three triples studied in this work, third-body eclipses are also possible during given sections of a precession cycle. In contrast to the previous systems, however, in the case of KIC 8023317, the outer inclination crosses both the lower and upper borders of the possible third-body eclipse regions (and hence, the outer orbit may also be seen edge-on two times during a precession cycle). The next session of possible third-body eclipses will begin around 2354 and last until 2404.

The long-term evolution of KIC 8023317 is similar to that of KIC 5653126 (see Fig. 11). The primary star is massive enough to evolve off the main-sequence at 4.7 Gyr and fill its Roche lobe as it ascends the first giant branch at 5.3 Gyr. At this point the primary star has lost a small amount of mass due to its stellar wind, i.e.,  $0.004 M_\odot$ , such that the outer semimajor axis has increased by 0.2%. The inner orbit did not widen, in fact the inner semimajor axis was reduced from the original  $32.6 R_\odot$  to  $24.5 R_\odot$  due to tidal friction in combination with ZKL cycles (Kiseleva et al. 1998). Furthermore, the inner orbit has circularized by the time of the onset of the mass transfer phase and the inclination freezes out at about 41 degrees. With the extreme mass ratio of the inner binary, the mass transfer leads to a common-envelope phase and a subsequent merger of the two stars in the inner binary. The merger remnant is a giant-like object with a helium core of  $0.24 M_\odot$  and a relatively thick envelope of at most  $1.44 M_\odot$ . In analogue with KIC 5653126, the merger remnant will fill its Roche lobe as an AGB star, initiate a second CE-phase. A compact binary is formed with a  $0.52 M_\odot$  white dwarf component and a  $0.13 M_\odot$  main-sequence companion. In the case of an efficient CE-phase, the post-CE semimajor axis is about  $8 R_\odot$ . In the inefficient case it is  $\sim 1 R_\odot$ , which is compact enough such that magnetic braking and gravitational wave emission can reduce the orbit to form a cataclysmic variable in a Hubble time.

## 5.5 Implications of the results for different multiple star formation processes

As indicated above, there appears to be an anti-correlation between the mutual inclination and tertiary mass. Our two highly misaligned triples, KIC 5731312 with  $i_{\text{mut}} = 39^\circ$  and KIC 8023317 with  $i_{\text{mut}} = 56^\circ$ , both contain low-mass M5/6V tertiaries with  $m_{\text{B}} = 0.13\text{--}0.15 M_\odot$ . Meanwhile, our two relatively aligned triples have more comparable component masses. To determine if this trend is statistically significant, we expand our sample to include all of our previously analyzed triples with reliably measured mutual inclinations and outer mass ratios  $q_{\text{out}} = m_{\text{B}}/(m_{\text{Aa}}+m_{\text{Ab}})$ . From the Borkovits et al. (2016) sample of 62 compact *Kepler* triples with measured mutual inclinations, we update the four systems presented in this study with the current, more accurate photodynamical results. We also update KIC 7955301 with  $i_{\text{mut}} = 6.2^\circ$  and  $q_{\text{out}} = 0.71$  according to our upcoming photodynamical analysis (Gaulme et al., in prep). We exclude KIC 3345675 and KIC 7593110, which have large mutual inclination uncertainties that exceed  $\delta i_{\text{mut}} > 10^\circ$ . We also ignore the only retrograde triple, KIC 7670617 with  $i_{\text{mut}} = 147^\circ$ , which likely formed differently than the remaining 59 KIC prograde triples spanning  $0^\circ < i_{\text{mut}} < 56^\circ$ . We also add the 12 recently discovered *TESS* triples, most of which are nearly coplanar triply eclipsing systems (Borkovits et al. 2020a,b, 2022; Mitnyan et al. 2020; Rappaport et al. 2022). Nonetheless, TIC 042565581 is slightly misaligned with  $i_{\text{mut}} = 5.5^\circ$  and  $q_{\text{out}} = 0.65$  while TIC 167692429, (the only one currently non-eclipsing *TESS* triple) is moderately misaligned with  $i_{\text{mut}} = 27^\circ$  and  $q_{\text{out}} = 0.34$ .

A Spearman rank correlation test demonstrates that the mutual inclinations and outer mass ratios of our selected 71 compact triples are anti-correlated with a coefficient of  $\rho_{\text{S}} = -0.40$  and statistical significance of  $p_{\text{S}} = 0.0006$  ( $3.5\sigma$ ). In Fig. 16, we plot the distributions of  $q_{\text{out}}$  for three subsamples: (1) the 29 nearly coplanar triply eclipsing systems with  $i_{\text{mut}} < 4^\circ$  that are subject to different selection effects than the non-triply eclipsing systems; (2) the 20 somewhat misaligned triples with  $4^\circ \leq i_{\text{mut}} < 25^\circ$ ; and (3) the 22 highly misaligned triples with  $25^\circ \leq i_{\text{mut}} < 56^\circ$ . The nearly coplanar triples are concentrated across  $q_{\text{out}} = 0.33\text{--}1.00$ , but there are a few systems below  $q_{\text{out}} < 0.33$  and above  $q_{\text{out}} > 1.00$ . Similarly, all but one of the 20 somewhat misaligned triples span  $q_{\text{out}} = 0.33\text{--}1.00$ . The single outlier with  $q_{\text{out}} = 3.0$  and  $i_{\text{mut}} = 8^\circ$  is KIC 5897826, which is barely a triply eclipsing system (Carter et al. 2011). Meanwhile, more than half of the highly misaligned triples have small mass ratios  $q_{\text{out}} < 0.33$ . The single outlier with  $i_{\text{mut}} = 54^\circ$  and  $q_{\text{out}} = 1.8$  is KIC 4055092, which has one of the widest tertiaries with  $a_{\text{out}} = 11$  AU and therefore likely formed differently from the more compact triples in our sample<sup>13</sup>. An Anderson-Darling test demonstrates that the somewhat misaligned and highly misaligned triples have different  $q_{\text{out}}$  distributions at the  $p_{\text{AD}} = 8 \times 10^{-6}$  ( $4.3\sigma$ ) significance level. Moreover, if we limit our sample to the 40 triples with  $4^\circ \leq i_{\text{mut}} < 56^\circ$  and  $q_{\text{out}} \leq 1.0$ , then a Spearman rank test yields an even stronger de-

<sup>13</sup> Note, however, that the Borkovits et al. (2016) ETV solution for KIC 4055092 should be considered only with considerable caution, as it gives an outer period of  $P_{\text{out}} \approx 31.6$  yr which is  $\sim 8$ -times longer than the duration of the analysed *Kepler* dataset.

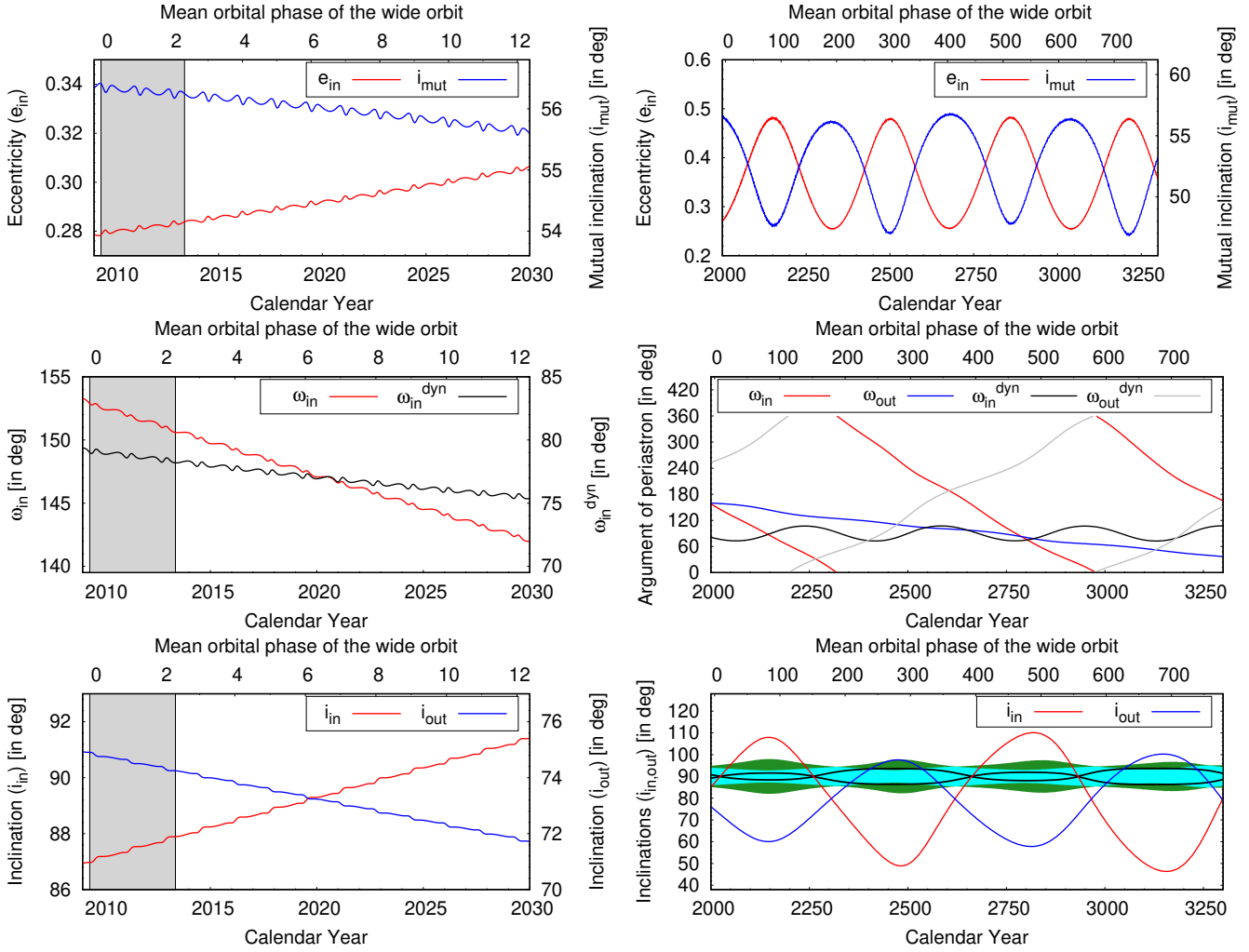


**Figure 15.** Variations of the same orbital elements as in Fig. 7 above, but for KIC 8023317. See text for details.

gree of anti-correlation with  $\rho_S = -0.66$  and  $p_S = 4 \times 10^{-6}$  ( $4.5\sigma$ ). The anti-correlation between the mutual inclinations and outer mass ratios for this subset of 40 compact triples is clearly visible in Fig. 17.

Compact triples with  $a_{\text{out}} \lesssim 10$  au likely formed either through two successive episodes of disk fragmentation or disk-mediated capture of the outer tertiary (Tobin et al. 2016; Bate 2018; Tokovinin & Moe 2020; Offner et al. 2022). In both scenarios, the tertiary tends to be initially less massive than the inner binary, but the triple subsequently accretes from the surrounding protostellar disk. For an isolated protobinary that accretes from a circumbinary disk, the low-mass secondary sweeps out a larger orbit and thus accretes most of the infalling material, effectively driving the binary mass ratio  $q = M_2/M_1$  toward larger values (Bate & Bonnell 1997; Farris et al. 2014; Young & Clarke 2015). Close binaries exhibit a large excess of twins with  $q > 0.95$  (Tokovinin 2000; Moe & Di Stefano 2017; El-Badry et al. 2019; Tokovinin & Moe 2020), consistent with the predictions of the hydrodynamical simulations of circumbinary disk accretion. Similarly, a low-mass tertiary in a compact triple will accrete most of

the mass from the circumbinary disk, thereby increasing the outer mass ratio  $q_{\text{out}}$  (Tokovinin & Moe 2020).

For a protobinary with small to moderate eccentricity, circumbinary disk accretion also tends to align the binary orbit to the plane of the disk (Papaloizou & Terquem 1995; Lubow & Ogilvie 2000; Lodato & Facchini 2013; Foucart & Lai 2014; Martin et al. 2020). Close pre-MS binaries undergo tidal circularization (Meibom & Mathieu 2005; Moe & Kratter 2018; Zanazzi & Wu 2021). Indeed, pre-MS binaries with  $P < 30$  days have small to moderate eccentricities and nearly coplanar circumbinary disks as expected Czekala et al. (2019). A significant majority of the inner binaries in our sample of compact triples also have small to moderate eccentricities and short periods, and so we expect the inner binary and circumbinary disk to have aligned prior to the formation or disk-capture of the tertiary. A notable exception includes KIC 5731312 investigated in this study, which has an inner binary with a relatively large eccentricity  $e_{\text{in}} = 0.46$  given its short period of  $P_{\text{in}} = 7.95$  days. Nonetheless, KIC 5731312 also has a highly inclined tertiary with  $i_{\text{mut}} = 39.4^\circ$ , precisely matching the critical von Zeipel-Kozai-Lidov angle (see Section 5.3), and suggesting this particular triple

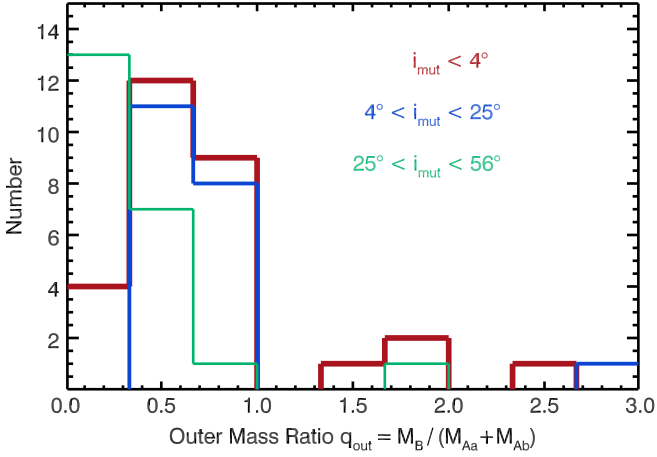


**Figure 16.** The distributions of outer mass ratios for the 29 nearly coplanar triply eclipsing systems with  $i_{\text{mut}} < 4^\circ$  (thick red), the 20 moderately misaligned triples with  $4^\circ \leq i_{\text{mut}} < 25^\circ$  (blue), and the 22 highly misaligned triples with  $25^\circ \leq i_{\text{mut}} < 56^\circ$  (thin green). More coplanar triples tend to have more massive outer tertiaries, suggesting that compact triples accreted from surrounding protostellar disks that simultaneously aligned the orbits while leading to preferential mass accretion onto the outer tertiaries.

dynamically evolved via ZKL cycles coupled to tidal friction (Kiseleva et al. 1998; Fabrycky & Tremaine 2007; Naoz & Fabrycky 2014). For the rest of our systems, once the tertiary forms in the outer disk via disk fragmentation (born nearly coplanar) or is captured by the disk, subsequent inclination evolution of the tertiary depends on the mass of the disk (Martin et al. 2016). For massive disks, the tertiary accretes much of the mass and angular momentum from the disk, thereby dissipating into a coplanar configuration. Meanwhile, for low-mass disks with negligible accretion onto the tertiary, Martin et al. (2016) demonstrated that the tertiary can remain at large mutual inclinations or even be pumped to large inclinations via secular oscillations.

The combination of the tertiary accreting most of the mass and angular momentum from the surrounding disk explains the observed anti-correlation between  $q_{\text{out}}$  and  $i_{\text{mut}}$ . Accretion from a massive disk will substantially increase  $q_{\text{out}}$  while dissipating the triple toward coplanarity. Moreover, compact triples that formed via two episodes of disk fragmentation should be especially coplanar, perhaps explaining the excess of triply eclipsing systems with  $i_{\text{mut}} < 4^\circ$  relative to moderately misaligned triples, albeit an observational selection bias could also play a role. Meanwhile, a tertiary that is captured by a low-mass disk late in the formation of the system will accrete only marginal additional mass and its inclination with respect to the inner binary will change only slightly. Hence the observed population of low-mass tertiaries tend to have large mutual inclinations.

## 6 CONCLUSIONS

In this paper we have carried out complex photodynamical analyses of four compact, tight, hierarchical triple stellar sys-

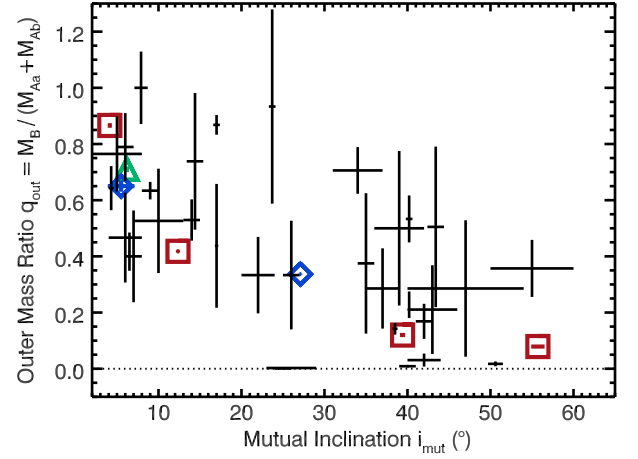


**Figure 17.** Outer mass ratios versus mutual inclinations for the 40 compact triples with  $4^\circ \leq i_{\text{mut}} < 56^\circ$  and  $q_{\text{out}} \leq 1.0$ . We highlight the 4 KIC triples presented in this study (red boxes), the two misaligned TIC triples (blue diamonds), and the Gaulme et al. preliminary result for KIC 7955301 (green triangle). The outer mass ratios systematically decrease with mutual inclination at the  $4.5\sigma$  level. A more massive tertiary likely accreted from a massive circumtriple protostellar disk that aligned both the inner and outer orbits with the disk.

tems. These systems were observed quasi-continuously with high photometric precision by the *Kepler* spacecraft during its four-year-long prime mission, and then were more recently revisited with the *TESS* space telescope. All four triples consist of currently eclipsing, eccentric inner binaries which, due to strong third-body interactions and the non-alignment of the inner and outer orbits, produce rapid and large amplitude eclipse timing and depth variations. These serve as ideal targets for precise, in-depth dynamical analyses. Moreover, one of the four targets, KIC 6964043, also exhibits third-body eclipses, thereby allowing further refinements of the system parameters.

On the other hand, unfortunately, due the faintness of the systems no RV measurements are available for any of them. Thus, we used an analysis of the composite system SED in combination with astrophysical-model dependent PARSEC isochrones as proxies for the determination of the individual stellar masses and, indirectly, radii. In such a manner, we were able to obtain fundamental stellar parameters with accuracies of about 2 – 8%. This relatively lower accuracy in these physical stellar parameters, however, does not affect our main purpose of mapping the full 3-dimensional configurations of the triples and their dynamics with unprecedentedly high precision. This results from the fact that the geometry and dynamics of the systems are mainly determined by such relative dimensionless quantities as the mass ratios and the orbital positions of the bodies relative to each other. Thus, we were able to determine the orbital elements, both in the observational and the dynamical frames of references, for all systems and subsystems with precisions of better than 1%. Here we mainly highlight the precise determinations not only of the mutual inclination angles, but also of the current positions of the dynamical lines of apsides, and dynamical nodes.

These are direct important key parameters in the equations of secular perturbation theory and, hence, in addition to the mutual inclination of the orbits and the ratios of the masses and separations (periods), they substantially influence the future dynamical evolution of the systems. Thus, knowing these parameters, we were able to model realistically the future dynamical, and corresponding astrophysical, evolution of the four triple systems.

Two of the four triples, KICs 6964043 and 5653126 were found to be practically flat. In these systems our short-term numerical integrations have shown only minor orbital variations in the forthcoming 1 million years, despite the fact that KIC 6964043 is an extremely tight triple system. On the other hand, integrating the secular dynamical evolution of these systems over longer timescales, we find that KIC 6964043 is expected to become dynamically unstable and most likely dissolve within the next 1 Gyr. In contrast to this scenario, KIC 5653126 will pass through two common envelope phases and also stellar merger(s) before it will end its life most likely as a single white dwarf.

The other two systems, KICs 5731312 and 8023317 were demonstrated to belong to the high mutual inclination regime, at least in the sense of the original ZKL theory. To the best of our knowledge, KIC 8023317 has the second highest accurately known mutual inclination angle among the known hierarchical triple stellar systems. (The highest mutual inclination system is Algol, where the outer orbit is nearly perpendicular to the inner one; Lestrade et al. 1993; Csizmadia et al. 2009; Zavala et al. 2010.) According to our short-term numerical integrations, both inclined KIC triple systems exhibit characteristic, quasi-sinusoidal variations in their inner eccentricities and mutual inclinations ( $e$ -cycles of the ZKL-theorem) on some hundred year-long timescales, with amplitudes of 10–30% of the entire physically meaningful range of these parameters. Moreover, while the dynamical lines of apsides of the inner pair in KIC 5731312 circulates (though this circulation has superposed on it some librations), KIC 8023317 exhibits clear libration, at least during the forthcoming one million years. On the other hand, the observable apsidal motion in both of these highly mutually inclined systems is retrograde, which make these EBs more exotic. Similar to the previous, almost flat systems, the final fates of these triples are driven again by the masses of their components. Our secular dynamical evolution studies predict that the low-mass triple KIC 5731312 will also become unstable on a Gyr timescale, and most probably, the less massive tertiary will be ejected from the system. Finally, the evolution of the more massive triple KIC 8023317 is expected to resemble that of KIC 5653126 with the difference in this case being that the most probable final remnant may be a cataclysmic variable instead of a single white dwarf.

Due to the non-alignment of the inner and outer orbits, all four targets exhibit rapid orbital precession and hence, eclipse depth variations. As a consequence, none of the four inner binaries remain eclipsing during their complete precession cycle. In this regard the nearly flat system, KIC 6964043 is the least affected, as its inner pair will display eclipses over the vast majority of its precession cycle. In the case of the other three systems, they will exhibit regular, inner eclipses only during short portions of their  $\sim 200 - 1400$  yr-long precession cycles. Naturally, this implies that there may be numerous similar tight compact systems which are currently in

non-eclipsing phases, but which can be discovered as EBs in the near or far future.

What is more interesting is that our photodynamical results predict that all four systems may well exhibit third-body eclipses during some shorter or longer phases of their complete precession cycles. In this regard KIC 6964043 is exceptional in the sense that it continuously displays third-body eclipses. We further note that this system is similar to the vast majority of the presently known triply eclipsing triple systems, which were found to be practically flat and, hence, they continuously exhibit regular inner as well as third-body eclipses. One might therefore think that finding third-body eclipses in EBs is just an observational selection effect, since EBs are naturally more intensively observed and followed than non-eclipsing stars. By this reasoning, there would be a much smaller chance to discover serendipitously third-body eclipses in the case of a target that exhibits neither regular eclipses nor some other kind of characteristic light variations which would make it worthy of frequent observations. It turns out that finding third-body eclipses in EBs is indeed a selection effect, but not simply because EBs tend to be better studied. In Rappaport et al. (2022) we discussed the fact that substantially more triply eclipsing triples were found in a visual survey of  $\sim 10^6$  preselected EBs than in  $\sim 10^7$  random stars, all taken from the *TESS* full frame images. The selection effects involved include the facts that: (i) the more compact triple systems that we are studying (i.e., with  $P_{\text{out}} \lesssim 1000$  days) are expected to be nearly flat (see Sect. 5.5); (ii) the shorter the outer period in a triple system (i.e., the more compact), the wider the outer inclination domain where third-body eclipses may occur; and (iii) once an eclipsing binary has been found, it is already somewhat preferentially aligned so as to increase the eclipse probability of an outer triple star. Therefore, in such a manner, the enhancement of the third-body eclipsers amongst the EBs (forming *triply* eclipsing triples) may be an indirect consequence of the formation mechanism(s) of most compact triples, i.e., one that produces practically flat systems.

Our results show that there might be a fair number of episodically appearing third-body eclipser systems amongst inclined compact triple systems.<sup>14</sup> The cases of KIC 2835289 and TIC 167692429 were already mentioned above (Sect. 5.2). We note, furthermore, that we have also found a few more solo third-body eclipse-like events in the *TESS* observations of other currently non-eclipsing targets, and one such event was especially noteworthy for being detected in the lightcurve of a former eclipsing binary, V699 Cygni<sup>15</sup>. Further investigations of these events are in progress.

Finally we discuss briefly the possible connection of our findings with the different formation scenarios of multiple systems. What is quite evident at first sight, is that the mass ratios are markedly different for the flat and the inclined systems, which may imply different formation scenarios.

<sup>14</sup> This situation partially resembles the findings of Martin & Triaud (2015) who claimed that most of the inclined circumbinary planets orbiting EBs should produce transits for shorter or longer times during their orbital precession cycles.

<sup>15</sup> Shortly before the submission of this manuscript the discovery of a likely third-body eclipse in the former, but no-longer eclipsing binary V699 Cygni was also reported independently by Zasche et al. (2022)

## ACKNOWLEDGMENTS

TB acknowledges the support of the PRODEX Experiment Agreement No. 4000137122 between the ELTE Eötvös Loránd University and the European Space Agency (ESA-D/SCI-LE-2021-0025), and the support of the city of Szombathely.

ST acknowledges support from the Netherlands Research Council NWO (VENI 639.041.645 and VIDI 203.061 grants).

The operation of the BRC80 robotic telescope of Baja Astronomical Observatory has been supported by the project “Transient Astrophysical Objects” GINOP 2.3.2-15-2016-00033 of the National Research, Development and Innovation Office (NKFIH), Hungary, funded by the European Union.

This paper includes data collected by the *TESS* mission. Funding for the *TESS* mission is provided by the NASA Science Mission directorate. Some of the data presented in this paper were obtained from the Mikulski Archive for Space Telescopes (MAST). STScI is operated by the Association of Universities for Research in Astronomy, Inc., under NASA contract NAS5-26555. Support for MAST for non-HST data is provided by the NASA Office of Space Science via grant NNX09AF08G and by other grants and contracts.

This work has made use of data from the European Space Agency (ESA) mission *Gaia*<sup>16</sup>, processed by the *Gaia* Data Processing and Analysis Consortium (DPAC)<sup>17</sup>. Funding for the DPAC has been provided by national institutions, in particular the institutions participating in the *Gaia* Multilateral Agreement.

This publication makes use of data products from the Wide-field Infrared Survey Explorer, which is a joint project of the University of California, Los Angeles, and the Jet Propulsion Laboratory/California Institute of Technology, funded by the National Aeronautics and Space Administration.

This publication makes use of data products from the Two Micron All Sky Survey, which is a joint project of the University of Massachusetts and the Infrared Processing and Analysis Center/California Institute of Technology, funded by the National Aeronautics and Space Administration and the National Science Foundation.

We used the Simbad service operated by the Centre des Données Stellaires (Strasbourg, France) and the ESO Science Archive Facility services (data obtained under request number 396301).

This research made use of Lightkurve, a Python package for Kepler and TESS data analysis (Lightkurve collaboration 2018).

This research made use of Astropy,<sup>18</sup> a community-developed core Python package for Astronomy (Astropy Collaboration 2013, 2018).

This research made use of astroquery: An Astronomical Web-querying Package in Python (Ginsburg et al. 2018).

## DATA AVAILABILITY

The *TESS* data underlying this article were accessed from MAST (Barbara A. Mikulski Archive for Space Telescopes) Portal (<https://mast.stsci.edu/portal/Mashup/Clients/Mast/Portal.html>). The ASAS-SN archival photometric data were accessed from <https://asas-sn.osu.edu/>. The ATLAS archival photometric data were accessed from <https://fallingstar-data.com/forcedphot/queue/>. A part of the data were derived from sources in public domain as given in the respective footnotes. The derived data generated in this research and the code used for the photodynamical analysis will be shared on reasonable request to the corresponding author.

## REFERENCES

- Abdul-Masih, M., Prša, A., Conroy, K. et al. 2016, *AJ*, 151, 101  
 Astropy Collaboration, Robitaille, T. P., Tollerud, E. J., Greenfield, P., et al. 2013, *A&A*, 558, A33  
 Astropy Collaboration, Price-Whelan, A. M., Sipőcz, B. M., Güther, H. M., et al. 2018, *AJ*, 156, 123  
 Auvergne, M. et al., 2009, *A&A*, 506, 411  
 Bailer-Jones, C. A. L., Rybizki, J., Foesneau, M., Demleitner, M., Andrae, R., 2021, *AJ*, 161, 147  
 Bate, M. R., 2018, *MNRAS*, 475, 5618  
 Bate, M. R., Bonnell, I. A., 1997, *MNRAS*, 285, 33  
 Borkovits, T., 2022, *Galaxies*, 10, 9  
 Borkovits, T., Forgács-Dajka, E., Regály, Zs., 2007, *A&A*, 473, 191  
 Borkovits, T., Derekas, A., Kiss, L. L., et al., 2013, *MNRAS*, 428, 1656  
 Borkovits, T., Rappaport, S., Hajdu, T., Sztakovics, J., 2015, *MNRAS*, 448, 946  
 Borkovits, T., Hajdu, T., Sztakovics, J., et al. 2016, *MNRAS*, 455, 413  
 Borkovits, T., Albrecht, S., Rappaport, S., et al. 2018, *MNRAS*, 478, 513  
 Borkovits, T., Rappaport, S., Kaye, T., et al. 2019a, *MNRAS*, 483, 1934  
 Borkovits, T., Sperauskas, J., Tokovinin, A., Latham, D. W., Csányi, I., Hajdu, T., Molnár, L., 2019b, *MNRAS*, 487, 4631  
 Borkovits, T., Rappaport, S., Hajdu, T., et al. 2020a, *MNRAS*, 493, 5005  
 Borkovits, T., Rappaport, S., Tan, T.G., et al. 2020b, *MNRAS*, 496, 4624  
 Borkovits, T., Rappaport, S., Maxted, P. F. L., et al. 2021, *MNRAS*, 503, 3759  
 Borkovits, T., Mitnyan, T., Rappaport, S. A., et al. 2022, *MNRAS*, 510, 1352  
 Borucki, W. J., Koch, D., Basri, G. et al. 2010, *Science*, 327, 977  
 Bressan, A., Marigo, P., Girardi, L. et al. 2012, *MNRAS*, 427, 127  
 Camacho, J., Torres, S., García-Berro, E., Zorotovic, M., Schreiber, M.R., Rebassa-Mansergas, A., Nebot Gómez-Morán, A., & Gänsicke, B.T 2014, *A&A*, 566, A86  
 Carter, J.A., et al., 2011, *Science*, 331, 562  
 Castelli, F., & Kurucz, R. L., 2004, arXiv:astro-ph/0405087  
 Conroy, K. E., Prša, A., Stassun, K. G., Orosz, J. A., Fabrycky, D. C., & Welsh, W. F. 2014, *AJ*, 147, 45  
 Conroy, K. E., Prša, A., Stassun, K. G. 2015, In *Living Together: Planets, Host Stars and Binaries*; Rucinski, S. M., Torres, G., Zejda, M., Eds.; ASP Conf. Ser., 496, 99.  
 Csizmadia, Sz., Borkovits, T., Paragi, Zs. et al. 2009, *ApJ*, 705, 436  
 Csizmadia, Sz., Smith, A. M. S., Cabrera, J., Klagyivik, P., Chaushv, A., Lam, K. W. F., 2021, *A&A*, submitted, arXiv:2108.11822

<sup>16</sup> <https://www.cosmos.esa.int/gaia>

<sup>17</sup> <https://www.cosmos.esa.int/web/gaia/dpac/consortium>

<sup>18</sup> <http://www.astropy.org>

- Cutri, R.M., Wright, E.L., Conrow, T., et al. 2013, wise.rept, 1C.  
 Czekala I., Chiang, E., Andrews, S. M. et al., 2019, ApJ, 883, 22  
 de Kool, M. 1990, ApJ, 358, 189  
 El-Badry, K., Rix, H.-W., Tian, H., Duchêne, G., Moe, M., 2019, MNRAS, 489, 5822  
 Fabrycky, D., Tremaine, S., 2007, ApJ, 669, 1298  
 Farris, B. D., Duffell, P., MacFadyen, A. I., Haiman, Z., 2014, ApJ, 783, 134  
 Ford, E. B., Kozinsky, B., Rasio, F. A. 2000, ApJ, 535, 385  
 Ford, E. B., 2005, AJ, 129, 1706  
 Foucart, F., Lai, D., 2014, MNRAS, 445, 1731  
 Gaia Collaboration, Brown, A. G. A., Vallenari, A., Prusti, T. et al. 2021, A&A, 649, A1  
 Gimenez, A., Garcia-Pelayo, J. M., 1983, Ap&SS, 92, 203  
 Ginsburg, A., Sipőcz, B. M., Brasseur, C. E., et al. 2019, AJ, 157, 98  
 Greiss, S., Steeghs, D., Gänsicke, B. T. et al. 2012, AJ, 144, 24  
 Harrington, R. S. 1968, AJ, 73, 190  
 Henden, A. A. 2019, JAAVSO, 47, 130  
 Henden, A. A., Levine, S., Terrell, D., Welch, D. 2015, American Astronomical Society, AAS Meeting #225, id.336.16  
 Ito, T., Ohtsuka, K. 2019, Monogr. Environ. Earth Planets, 7, 1  
 Ivanova, N., Justham, S., Chen, X., et al. 2013, A&ARv, 21, 59, arXiv(1209.4302)  
 Jordi, C., Gebran, M., Carrasco, J. M. et al. 2010, A&A, 523, A48  
 Kirk, B., Conroy, K. Prša, A. et al. 2016, AJ, 151, 68  
 Kiseleva, L. G., Eggleton, P. P., Mikkola, S., 1998, MNRAS, 300, 292  
 KlingleSmith, D. A., Sobieski, S., 1970, AJ, 75, 175  
 Kozai, Y. 1962, AJ, 67, 591  
 Lestrade, J.-F., Phillips, R. B., Hodges, M. W., Preston, R. A. 1993, ApJ, 410, 808  
 Lidov, M. L. 1962, Planetary and Space Science, 9, 719  
 Lightkurve Collaboration, Cardoso, J. V. d. M., Hedges, C., Gully-Santiago, M., et al. 2018, Astrophysics Source Code Library, record ascl:1812.013  
 Livio, M., & Soker, N. 1988, ApJ, 329, 764  
 Lodato, G., Facchini, S., 2013, MNRAS, 433, 2157  
 Lubow, S. H., Ogilvie, G. I., 2000, ApJ, 538, 326  
 Lucy, L.B. 1967, Zeitschrift für Astrophysik, 65, 89  
 Mardling, R. A., Aarseth, S. J. 2001, MNRAS, 321, 398  
 Martin, D. V., Triaud, A. H. M. J., 2015, MNRAS, 449, 781  
 Martin, R. G., Lubow, S. H., Nixon, Ch., Armitage, Ph. J., 2016, MNRAS, 458, 4345  
 Martin, R. G., Zhu, Zh., Armitage, Ph. J., 2020, ApJ, 898, L26  
 Mazeh, T., Shaham, J. 1979, A&A, 77, 145  
 Meibom, S., Mathieu, R. D., 2005, ApJ, 620, 970  
 Mitnyan, T., Borkovits, T., Rappaport, S., Pál, A., Maxted, P. F. L., 2020, MNRAS, 498, 6034  
 Moe, M., Di Stefano, R., 2017, ApJS, 230, 15  
 Moe, M., Kratter, K. M., 2018, ApJ, 854, 44  
 Naoz, S., 2016, ARA&A, 54, 441  
 Naoz, S., Fabrycky, D. C., 2014, ApJ, 793, 137  
 Naoz, S., Farr, W. M., Lithwick, Y., Rasio, F. A., Teyssandier, J., 2013, MNRAS, 431, 2155  
 Offner, S. S. R., Moe, M., Kratter, K. M., Sadavoy, S. I., Jensen, E. L. N., Tobin, John J., 2022, arXiv:2203.10066  
 Paegert, M. et al, 2021, arXiv:2108.04778  
 Papaloizou, J. C. B., Terquem, C., 1995, MNRAS, 274, 987  
 Pál, A., 2012, MNRAS, 421, 1825  
 Paczynski, B. 1976, in Structure and Evolution of Close Binary Systems, eds. P. Eggleton, S. Mitton, & J. Whelan.  
 Prša, A., & Zwitter, T., 2005, ApJ, 628, 426  
 Rappaport, S., Deck, K., Levine, A., et al. 2013, ApJ, 768, 33  
 Rappaport, S., Borkovits, T., Gagliano, R. et al. 2022, MNRAS, submitted  
 Ricker, G.R., Winn, J.N., Vanderspek, R., et al. 2015, JATIS, 1, 014003  
 Skrutskie, M.F., Cutri, R.M., Stiening, R., et al. 2006, AJ, 131, 1163  
 Söderhjelm, S. 1975, A&A, 42, 229  
 Söderhjelm, S. 1982, A&A, 107, 54  
 Tobin, J. J. et al., 2016, Nature, 538, 483  
 Toonen, S., & Nelemans, G. 2013, A&A, 557, A87  
 Toonen, S., Hamers, A., Portegies Zwart, S., 2016, Comput. Astrophys., 3, 6  
 Toonen, S., Portegies Zwart, S., Hamers, A. S., Bandopadhyay, D. 2020, A&A, 640, A16  
 Toonen, S.; Boekholt, T. C. N.; Portegies Zwart, S. 2022, A&A, 661, A61  
 Tokovinin, A. A., 2000, A&A, 360, 997  
 Tokovinin, A., 2014, AJ, 147, 87  
 Tokovinin, A., 2018, AJ, 155, 160  
 Tokovinin, A., 2021, Universe, 7, 352  
 Tokovinin, A., Moe, M., 2020, MNRAS, 491, 5158  
 Webbink, R. 1984, ApJ, 277, 355  
 Young, M. D., Clarke, C. J., 2015, MNRAS, 452, 3085  
 von Zeipel, H. 1910, Astron. Nachr., 183, 345  
 Zasche, P., Henzl, Z., Masek, M., 2022, A&A, in press, arXiv:2205.03934  
 Zanazzi, J. J., Wu, Y., 2021, AJ, 161, 263  
 Zavala, R. T., Hummel, C. A., Boboltz, D. A. et al. 2010, ApJ, 715, L44  
 Zorotovic, M., Schreiber, M.R., Gänsicke, B.T., & Nebot Gómez-Morán, A. 2010, A&A, 520, A86  
 Zorotovic, M., & Schreiber, M.R. 2022, submitted to MNRAS; arXiv: 2204.13715

## APPENDIX A: DETERMINATION OF THE LIMITS OF THE INCLINATION DOMAIN WHERE THIRD-BODY ECLIPSES MIGHT OCCUR

In order to find reasonable estimations for the inclination limits of the occurrence of third-body eclipses, we follow the same formalism as was used formerly in Appendix A of Borkovits et al. (2013). There, we have shown that using the formalism of Jacobian position vectors, the spatial distances of the centers of the three stars can be calculated as

$$\vec{d}_{AaAb} = \vec{\rho}_1 \quad (A1)$$

$$\vec{d}_{AaB} = \vec{\rho}_2 + \frac{q_1}{1+q_1} \vec{\rho}_1 \quad (A2)$$

$$\vec{d}_{AbB} = \vec{\rho}_2 - \frac{1}{1+q_1} \vec{\rho}_1, \quad (A3)$$

respectively.<sup>19</sup> Let's use an observational frame of reference in which the origin is the center of mass of the inner binary, 'X-Y' is the tangential plane of the sky, and the 'Z' axis is directed away from the observer. Then the Cartesian coordinates of the first two Jacobians can be written as

$$x = \rho[\cos u \cos \Omega - \sin u \sin \Omega \cos i], \quad (A4)$$

$$y = \rho[\cos u \sin \Omega + \sin u \cos \Omega \cos i], \quad (A5)$$

$$z = \rho \sin u \sin i, \quad (A6)$$

<sup>19</sup> In order to save space in this Appendix, we hereafter use indices 1,2, instead of in,out to distinguish parameters referring to the inner and outer orbits, respectively.

where  $u$  denotes the longitude of second/third body (to which the first/second Jacobian points) along the given orbit, measured from the ascending node. (In the eccentric case  $u = v + \omega$ , where  $v$  stands for the true anomaly.) Then, the sky-projected distances can readily be obtained as

$$d_{\text{AaAb}}^{xy} = \rho_1 \sqrt{1 - \sin^2 i_1 \sin^2 u_1}, \quad (\text{A7})$$

$$d_{\text{AbB}}^{xy} = \rho_2 \left[ 1 - \sin^2 i_2 \sin^2 u_2 - 2 \frac{1}{1 - q_1} (\lambda - \sin i_1 \sin u_1 \sin i_2 \sin u_2) + \left( \frac{1}{1 + q_1} \frac{\rho_2}{\rho_1} \right)^2 (1 - \sin^2 i_1 \sin^2 u_1) \right]^{1/2} \quad (\text{A8})$$

where  $\lambda$  denotes the direction cosine between the two Jacobian vectors. Note, the expression referring to distance  $d_{\text{AaB}}^{xy}$  is not shown, however, one can obtain it very easily by replacing  $-1/(1+q_1)$  with  $q_1/(1+q_1)$ . It is clear that eclipses may occur when the sky-projected distances of any of the two bodies become less than the sum of their radii. For regular two body eclipses then Eq. (A7) leads readily to the usual condition of  $R_1 + R_2 \geq a |\cos i|$ , which is, however, strictly valid only for circular orbits. It also directly follows that at times of mid-eclipse,  $u_1 = \pm\pi/2$ . In eccentric, not exactly edge-on cases, however, the smallest distance may occur somewhat earlier or later than the conjunction occurs. The departure is, however, in almost all cases, small, and therefore, negligible (Gimenez & Garcia-Pelayo 1983). Thus, when we calculated and utilized the condition given by Eq. (2) for the inner eclipses, we were working with the conjunction points (i.e.,  $u_1 = \pm\pi/2$ ).

The case of third-body eclipses is much more complex, and no robust, exact condition(s) can be given. Thus, we adopted the following assumptions. Again, one can expect third-body eclipses around the conjunctions of the outer orbit. Hence, we arbitrarily set  $u_2 = \pm\pi/2$ . At these times, the projection of the second Jacobian vector onto the plane of the sky becomes

$$\vec{\rho}_2^{xy} = \rho_2 \cos i_2 (\mp \sin \Omega_2; \pm \cos \Omega_2; 0). \quad (\text{A9})$$

Then, we look for that value of  $u_1$ , at which the sky-projected vector of the first Jacobian ( $\vec{\rho}_1^{xy}$ ) is parallel to the former  $\vec{\rho}_2^{xy}$ , which may allow us to find the minimum sky-projected distance between the two bodies. The two vectors become parallel when their cross product yields zero. From this condition, and assuming that  $\cos i_2 \neq 0$ , one can easily calculate that

$$\sin^2 u_1 = \frac{\cos^2 \Delta\Omega}{1 - \sin^2 i_1 \sin^2 \Delta\Omega}. \quad (\text{A10})$$

Thus, one can readily find that the length of the sky-projected vector  $\vec{\rho}_1^{xy}$  becomes

$$\begin{aligned} \rho_1^{xy} &= \rho_1 \sqrt{1 - \sin^2 i_1 \sin^2 u_1} \\ &= \rho_1 \sqrt{\frac{\cos^2 i_1}{1 - \sin^2 i_1 \sin^2 \Delta\Omega}}. \end{aligned} \quad (\text{A11})$$

Then, as this vector is parallel to the sky-projected vector of

the second Jacobian, one can write directly that

$$\begin{aligned} d_{\text{AbB}}^{xy} &= \rho_2 |\cos i_2| \pm \frac{1}{1 + q_1} \rho_1 |\cos i_1| \sqrt{\frac{1}{1 - \sin^2 i_1 \sin^2 \Delta\Omega}} \\ &= \rho_2 |\cos i_2| \pm \frac{1}{1 + q_1} \rho_1 \sqrt{\frac{\cos^2 i_1}{\cos^2 i_1 + \sin^2 i_1 \cos^2 \Delta\Omega}} \\ &= \rho_2 |\cos i_2| \pm \frac{1}{1 + q_1} \rho_1 \sqrt{\frac{1}{1 + \tan^2 i_1 \cos^2 \Delta\Omega}}. \end{aligned} \quad (\text{A12})$$

From this last form of the expression one can easily obtain Eq. (3), where we also made a further simplification, replacing  $\rho_1$  with  $a_1$  on the right hand side of the equation.

## APPENDIX B: TABLES OF DETERMINED TIMES OF MINIMA FOR ALL THE FOUR SYSTEMS

In this appendix, we tabulate the individual mid-minima times of the primary and secondary eclipses, including *Kepler*, *TESS*, and ground-based observed ones, for the inner EBs of the four triples considered in this study (Tables B1-B4).

The complete Appendix B is available supplementary material to the journal, and also in the present arXiv version.

**Table B1.** Binary Mid Eclipse Times for KIC 6964043

BJD −2 400 000	Cycle no.	std. dev. (d)	BJD −2 400 000	Cycle no.	std. dev. (d)	BJD −2 400 000	Cycle no.	std. dev. (d)	BJD −2 400 000	Cycle no.	std. dev. (d)
55190.173588	0.0	0.000688	55495.729755	28.5	0.000505	55796.037501	56.5	0.000497	56112.482348	86.0	0.000672
55195.460530	0.5	0.000538	55501.102486	29.0	0.000536	55801.369553	57.0	0.000446	56117.968120	86.5	0.001017
55200.886326	1.0	0.000801	55506.447625	29.5	0.000968	55806.764662	57.5	0.000393	56133.913187	88.0	0.000587
55206.172452	1.5	0.000961	55511.820059	30.0	0.000861	55812.101279	58.0	0.000409	56139.407798	88.5	0.000847
55211.601150	2.0	0.000762	55517.160827	30.5	0.000711	55822.865967	59.0	0.001426	56144.627374	89.0	0.000677
55222.317438	3.0	0.001062	55522.536941	31.0	0.000633	55828.367561	59.5	0.000570	56150.125700	89.5	0.000971
55227.602391	3.5	0.000799	55527.877431	31.5	0.000478	55839.081236	60.5	0.000504	56155.340121	90.0	0.000732
55238.318601	4.5	0.000860	55533.256203	32.0	0.000498	55849.818469	61.0	0.000421	56160.839199	90.5	0.000876
55243.743685	5.0	0.000709	55538.593485	32.5	0.000475	55859.818469	61.5	0.000388	56166.054369	91.0	0.000773
55249.038230	5.5	0.000625	55549.311845	33.5	0.000531	55855.108304	62.0	0.000468	56171.555981	91.5	0.000516
55254.459530	6.0	0.001183	55570.764524	35.5	0.000438	55860.550658	62.5	0.000667	56176.771913	92.0	0.000721
55259.747089	6.5	0.000986	55576.159985	36.0	0.000452	55876.550659	64.0	0.000525	56182.270350	92.5	0.000706
55265.170662	7.0	0.000728	55581.552540	36.5	0.000568	55881.997269	64.5	0.000952	56187.482710	93.0	0.000766
55270.466723	7.5	0.000901	55586.935079	37.0	0.000443	55887.267179	65.0	0.000511	56192.985929	93.5	0.000837
55281.174261	8.5	0.001023	55592.366837	37.5	0.000638	55892.716930	65.5	0.000433	56198.196368	94.0	0.000747
55286.600988	9.0	0.001019	55597.676834	38.0	0.000492	55897.980067	66.0	0.000485	56203.702472	94.5	0.001134
55291.891233	9.5	0.001037	55603.078800	38.5	0.000459	55908.695388	67.0	0.000676	56208.911051	95.0	0.000690
55297.325465	10.0	0.000912	55608.431983	39.0	0.000517	55914.146946	67.5	0.000578	56214.415334	95.5	0.001477
55302.608118	10.5	0.000573	55613.819266	39.5	0.000514	55919.411396	68.0	0.000457	56219.627442	96.0	0.000992
55313.329315	11.5	0.000951	55619.165008	40.0	0.000423	55924.865240	68.5	0.000612	56225.132630	96.5	0.000603
55318.767221	12.0	0.000690	55624.552763	40.5	0.000641	55930.120478	69.0	0.000488	56230.344551	97.0	0.000501
55324.047906	12.5	0.000922	55629.889603	41.0	0.000592	55935.578562	69.5	0.000839	56235.848362	97.5	0.000688
55329.494681	13.0	0.000680	55635.278777	41.5	0.000496	55940.836280	70.0	0.000587	56241.060220	98.0	0.000805
55334.787302	13.5	0.000661	55646.079263	42.5	0.001026	55946.298236	70.5	0.000539	56251.772460	99.0	0.001024
55345.506170	14.5	0.000999	55651.325473	43.0	0.000501	55957.010179	71.5	0.000538	56257.279768	99.5	0.000939
55351.013111	15.0	0.000645	55656.720776	43.5	0.000500	55962.264805	72.0	0.000495	56262.494709	100.0	0.000807
55356.358888	15.5	0.000594	55662.040660	44.0	0.000405	55967.726462	72.5	0.000475	56267.995214	100.5	0.000896
55361.760234	16.0	0.000642	55667.440537	44.5	0.000550	55972.979333	73.0	0.000497	56273.223127	101.0	0.000942
55367.087933	16.5	0.000552	55672.754895	45.0	0.000611	55978.439783	73.5	0.000692	56278.718490	101.5	0.000656
55372.506219	17.0	0.000588	55683.469003	46.0	0.000394	55983.693744	74.0	0.000532	56283.949424	102.0	0.000835
55377.825983	17.5	0.000392	55688.871939	46.5	0.000706	55989.154588	74.5	0.000553	56289.446880	102.5	0.000905
55383.234593	18.0	0.000584	55694.183544	47.0	0.000348	55999.871173	75.5	0.000480	56294.698965	103.0	0.002269
55388.557970	18.5	0.000563	55699.587626	47.5	0.000510	56005.126585	76.0	0.000682	56300.244529	103.5	0.000617
55393.953470	19.0	0.000537	55704.898793	48.0	0.000607	56010.587115	76.5	0.000490	56305.467755	104.0	0.001790
55399.283659	19.5	0.000537	55710.302091	48.5	0.000752	56015.844256	77.0	0.000756	56321.764224	105.5	0.001067
55404.672129	20.0	0.000553	55715.614288	49.0	0.000633	56021.303286	77.5	0.000600	56326.965378	106.0	0.001313
55415.386026	21.0	0.000488	55721.022439	49.5	0.000926	56026.563994	78.0	0.000575	56337.699957	107.0	0.001383
55420.722963	21.5	0.000613	55726.327539	50.0	0.000414	56032.020760	78.5	0.001174	56348.428551	108.0	0.001215
55426.100890	22.0	0.000472	55731.734106	50.5	0.000528	56037.290799	79.0	0.000592	56353.951312	108.5	0.001430
55436.813775	23.0	0.000491	55737.045699	51.0	0.000394	56042.742439	79.5	0.000545	56364.669588	109.5	0.000918
55442.159044	23.5	0.000851	55742.449747	51.5	0.000611	56048.481243	80.5	0.000471	56375.390259	110.5	0.000913
55447.527523	24.0	0.001023	55747.763260	52.0	0.000479	56058.772697	81.0	0.000639	56380.578115	111.0	0.000901
55452.872094	24.5	0.000811	55753.167304	52.5	0.000346	56065.313580	81.5	0.000577	56386.110902	111.5	0.001041
55458.244107	25.0	0.000598	55758.479819	53.0	0.000386	56069.534880	82.0	0.000663	56396.827476	112.5	0.001104
55463.585359	25.5	0.000440	55763.884715	53.5	0.000520	56075.563994	82.5	0.000945	56402.001462	113.0	0.000929
55468.956843	26.0	0.000574	55769.198047	54.0	0.000442	56080.283777	83.0	0.000710	56407.547455	113.5	0.0003209
55474.299841	26.5	0.000818	55774.600402	54.5	0.000437	56085.786810	83.5	0.000593	56412.719525	114.0	0.000981
55479.670071	27.0	0.000719	55779.917753	55.0	0.000488	56091.030676	84.0	0.001283	56423.431712	115.0	0.001415
55485.016731	27.5	0.000656	55785.315934	55.5	0.000453	56096.519692	84.5	0.000957			
55490.387630	28.0	0.000607	55790.642026	56.0	0.000557	56107.246770	85.5	0.000691			

*Notes.* Integer and half-integer cycle numbers refer to primary and secondary eclipses, respectively.

**Table B2.** Binary Mid Eclipse Times for KIC 5653126

BJD −2 400 000	Cycle no.	std. dev. (d)	BJD −2 400 000	Cycle no.	std. dev. (d)	BJD −2 400 000	Cycle no.	std. dev. (d)	BJD −2 400 000	Cycle no.	std. dev. (d)
54985.880280	0.0	0.001008	55601.819600	16.0	0.000606	55924.515186	24.5	0.000873	56232.501154	32.5	0.000407
55024.378351	1.0	0.000919	55616.792529	16.5	0.001050	55948.315731	25.0	0.000611	56256.101135	33.0	0.000512
55062.864010	2.0	0.000987	55655.301329	17.5	0.001073	55962.989074	25.5	0.000831	56270.996996	33.5	0.000535
55101.342264	3.0	0.000757	55678.740626	18.0	0.000473	55986.817581	26.0	0.000585	56294.580181	34.0	0.000649
55139.814286	4.0	0.000768	55693.781426	18.5	0.001091	56001.469564	26.5	0.000736	56309.469386	34.5	0.000546
55178.279810	5.0	0.001009	55717.229270	19.0	0.000452	56025.309280	27.0	0.000494	56333.095304	35.0	0.000538
55255.190783	7.0	0.000505	55732.241098	19.5	0.000946	56039.959497	27.5	0.000633	56347.910705	35.5	0.000421
55293.653366	8.0	0.000773	55755.739637	20.0	0.000627	56063.793230	28.0	0.000680	56371.655943	36.0	0.000631
55332.139298	9.0	0.000720	55794.256460	21.0	0.000628	56102.261335	29.0	0.001786	56386.331661	36.5	0.000380
55370.669436	10.0	0.000685	55809.139507	21.5	0.000915	56116.966702	29.5	0.000533	56410.251600	37.0	0.000559
55409.241435	11.0	0.000620	55832.775348	22.0	0.000647	56140.730905	30.0	0.000483	56895.507479	96.5	0.001907
55447.836369	12.0	0.000839	55847.593106	22.5	0.000714	56155.479722	30.5	0.000489	58720.043332	97.0	0.000359
55486.412344	13.0	0.000539	55871.292892	23.0	0.000296	56179.187227	31.0	0.000550	58733.938821	97.5	0.001338
55524.926705	14.0	0.000669	55886.050315	23.5	0.001052	56193.992289	31.5	0.000461	59426.660574	115.5	0.000410
55578.251428	15.5	0.001871	55909.807881	24.0	0.000502	56217.642274	32.0	0.000453			

*Notes.* Integer and half-integer cycle numbers refer to primary and secondary eclipses, respectively. Most of the eclipses (cycle nos. 0.0 to 37.0) were observed by the *Kepler* spacecraft. The last 4 times of minima were determined from the *TESS* observations.

Table B3. Binary Mid Eclipse Times for KIC 5731312

BJD -2 400 000	Cycle no.	std. dev. (d)	BJD -2 400 000	Cycle no.	std. dev. (d)	BJD -2 400 000	Cycle no.	std. dev. (d)	BJD -2 400 000	Cycle no.	std. dev. (d)
54966.175075	-0.5	0.000764	55333.628289	46.0	0.000015	55707.103506	93.0	0.000406	56088.531453	141.0	0.000024
54968.092761	0.0	0.000010	55339.658250	46.5	0.000203	55713.140117	93.5	0.000163	56094.569256	141.5	0.000246
54974.122050	0.5	0.000159	55341.574723	47.0	0.000009	55715.049151	94.0	0.000144	56096.477872	142.0	0.000032
54976.039127	1.0	0.000011	55347.604496	47.5	0.000183	55721.088077	94.5	0.000125	56102.515246	142.5	0.000216
54982.068903	1.5	0.000209	55349.521137	48.0	0.000015	55722.995113	95.0	0.000094	56104.424325	143.0	0.000277
54983.985463	2.0	0.000010	55355.550880	48.5	0.000180	55729.035866	95.5	0.000165	56110.461418	143.5	0.000249
54990.015264	2.5	0.000161	55357.467537	49.0	0.000008	55730.941608	96.0	0.000013	56112.370760	144.0	0.000270
54991.931847	3.0	0.000013	55363.497299	49.5	0.000109	55736.983159	96.5	0.000165	56118.408837	144.5	0.000406
54997.961705	3.5	0.000540	55365.413917	50.0	0.000023	55738.889104	97.0	0.000028	56120.317231	145.0	0.000025
55005.908035	4.0	0.000126	55373.360400	51.0	0.000011	55744.929443	97.5	0.000188	56134.301656	146.5	0.000408
55007.824646	4.5	0.000025	55379.389844	51.5	0.000141	55746.837036	98.0	0.000019	56136.209982	147.0	0.000246
55013.854918	5.0	0.000273	55381.306792	52.0	0.000020	55752.873788	98.5	0.000345	56142.247624	147.5	0.000466
55021.801620	5.5	0.007533	55387.336423	52.5	0.000239	55754.785199	99.0	0.000017	56144.156486	148.0	0.000273
55023.717443	6.0	0.000044	55389.253239	53.0	0.000029	55760.818335	99.5	0.000179	56150.194516	148.5	0.000224
55029.747824	6.5	0.000206	55395.282538	53.5	0.000187	55762.732813	100.0	0.000027	56152.103133	149.0	0.000033
55031.663898	7.0	0.000009	55397.199631	54.0	0.000012	55768.762676	100.5	0.000294	56158.140284	149.5	0.000224
55037.694218	7.5	0.000460	55403.229213	54.5	0.000162	55776.707519	101.0	0.000187	56160.049328	150.0	0.000033
55039.610323	8.0	0.000009	55405.146081	55.0	0.000017	55778.625921	101.5	0.000036	56166.089922	150.5	0.000218
55045.641197	8.5	0.000200	55411.175125	55.5	0.000177	55784.653615	102.0	0.000248	56167.995737	151.0	0.000166
55047.556735	9.0	0.000119	55413.092493	56.0	0.000025	55786.571836	102.5	0.000022	56174.032976	151.5	0.000406
55053.587571	9.5	0.000221	55419.121650	56.5	0.000155	55792.598831	103.0	0.000451	56175.942240	152.0	0.000105
55055.503124	10.0	0.000457	55421.038916	57.0	0.000016	55794.517621	103.5	0.000195	56181.979363	152.5	0.000332
55061.533981	10.5	0.000112	55427.067802	57.5	0.000216	55800.546393	104.0	0.000241	56183.888641	153.0	0.000024
55069.480237	11.0	0.000243	55428.985335	58.0	0.000018	55808.493170	104.5	0.000315	56189.925969	153.5	0.000533
55071.395971	11.5	0.000022	55435.014009	58.5	0.000425	55810.409207	105.0	0.000021	56191.835061	154.0	0.000049
55077.426517	12.0	0.007966	55436.931662	59.0	0.000016	55816.439608	105.5	0.000206	56197.871736	154.5	0.000313
55079.342482	12.5	0.000026	55442.960559	59.5	0.000350	55818.355067	106.0	0.000016	56199.781524	155.0	0.000036
55085.373394	13.0	0.000164	55444.878146	60.0	0.000010	55824.385890	106.5	0.000171	56207.727951	155.5	0.000266
55087.288850	13.5	0.000598	55450.908660	60.5	0.000187	55826.301094	107.0	0.000013	56213.764372	156.0	0.000184
55093.319711	14.0	0.000218	55452.824531	61.0	0.000356	55828.333141	107.5	0.000383	56215.674350	156.5	0.000148
55095.235304	14.5	0.000139	55458.853540	61.5	0.000541	55834.247096	108.0	0.000333	56221.710617	157.0	0.000579
55101.266198	15.0	0.000256	55460.770949	62.0	0.000018	55840.280563	108.5	0.000318	56223.620809	157.5	0.000033
55103.181739	15.5	0.000016	55466.799626	62.5	0.000264	55842.193305	109.0	0.000052	56229.657510	158.0	0.000228
55109.212758	16.0	0.000274	55468.717395	63.0	0.000011	55848.226221	109.5	0.000337	56231.567421	158.5	0.000091
55111.128177	16.5	0.000158	55474.746069	63.5	0.000251	55850.139471	110.0	0.000029	56239.513593	159.0	0.000022
55117.159292	17.0	0.000216	55476.663736	64.0	0.000019	55856.174065	110.5	0.000287	56245.550641	159.5	0.000309
55119.074613	17.5	0.000016	55482.692261	64.5	0.000151	55858.085681	111.0	0.000254	56253.496328	160.0	0.000612
55125.105809	18.0	0.000175	55484.610170	65.0	0.000011	55864.120557	111.5	0.000205	56255.406420	160.5	0.000018
55127.021056	18.5	0.000090	55490.638475	65.5	0.000177	55872.067321	112.0	0.000161	56261.443196	161.0	0.000342
55133.052014	19.0	0.000150	55492.556593	66.0	0.000023	55873.978294	112.5	0.000024	56263.352962	161.5	0.000023
55134.967491	19.5	0.000019	55498.584800	66.5	0.000107	55880.014242	113.0	0.000188	56269.389212	162.0	0.000559
55140.998089	20.0	0.000122	55500.503001	67.0	0.000015	55881.924550	113.5	0.000020	56271.299378	162.5	0.000031
55142.913891	20.5	0.000010	55506.531027	67.5	0.000187	55889.959977	114.0	0.000384	56277.334994	163.0	0.000493
55148.944450	21.0	0.000218	55508.449363	68.0	0.000016	55898.870913	114.5	0.000015	56279.245843	163.5	0.000021
55150.860349	21.5	0.000014	55514.477090	68.5	0.000184	55895.906594	115.0	0.000428	56285.282095	164.0	0.000309
55156.891079	22.0	0.000476	55516.395763	69.0	0.000059	55897.817329	115.5	0.000032	56287.192268	164.5	0.000043
55158.806794	22.5	0.000073	55522.423206	69.5	0.000366	55905.763674	116.0	0.000019	56295.138601	165.0	0.000046
55164.837494	23.0	0.000169	55524.342128	70.0	0.000021	55911.800220	116.5	0.000484	56301.174530	165.5	0.000198
55166.753201	23.5	0.000650	55530.370030	70.5	0.000226	55913.710071	117.0	0.000023	56303.085053	166.0	0.000357
55172.784071	24.0	0.000172	55532.288492	71.0	0.000068	55919.746814	117.5	0.000254	56309.120862	166.5	0.000331
55174.699652	24.5	0.000017	55538.316200	71.5	0.001541	55921.656462	118.0	0.000069	56325.014869	167.0	0.000215
55180.730393	25.0	0.000828	55540.234957	72.0	0.000013	55927.693120	118.5	0.000269	56326.924190	167.5	0.000031
55188.677403	25.5	0.001428	55546.262841	72.5	0.000237	55929.602879	119.0	0.000985	56332.959752	168.0	0.000869
55190.592567	26.0	0.000014	55548.181352	73.0	0.000019	55935.639834	119.5	0.000384	56334.870731	168.5	0.000024
55196.623579	26.5	0.000365	55550.101220	73.5	0.000264	55937.549249	120.0	0.000019	56340.906265	169.0	0.000344
55198.539015	27.0	0.000013	55552.020390	74.0	0.000105	55943.586154	120.5	0.000424	56342.817103	169.5	0.000498
55204.569878	27.5	0.000672	55558.047381	74.5	0.000217	55945.495649	121.0	0.000015	56348.852519	170.0	0.000405
55206.485398	28.0	0.000012	55559.966819	75.0	0.000012	55953.442100	121.5	0.000063	56350.763564	170.5	0.000030
55212.516022	28.5	0.000114	55565.993701	75.5	0.000803	55961.388436	122.0	0.000249	56356.799018	171.0	0.000299
55214.431877	29.0	0.000500	55567.913096	76.0	0.000016	55967.426352	122.5	0.000344	56364.745086	171.5	0.000334
55220.462131	29.5	0.000183	55569.939728	76.5	0.000169	55969.334845	123.0	0.000017	56366.656424	172.0	0.000300
55222.378315	30.0	0.000011	55601.886558	77.0	0.005672	55975.371437	123.5	0.000368	56372.691072	172.5	0.000629
55228.408542	30.5	0.000220	55603.805734	77.5	0.000009	55977.281365	124.0	0.000014	56374.602784	173.0	0.000011
55236.355244	31.0	0.000116	55609.832308	78.0	0.000192	55983.318477	124.5	0.000854	56380.637708	173.5	0.000240
55238.271157	31.5	0.000304	55611.752134	78.5	0.000537	55985.227795	125.0	0.000018	56382.549227	174.0	0.000023
55244.301614	32.0	0.000138	55617.778659	79.0	0.000465	55991.265481	125.5	0.000314	56388.584601	174.5	0.000455
55246.217527	32.5	0.000124	55619.698344	79.5	0.000035	55993.174277	126.0	0.000026	56390.495616	175.0	0.000040
55252.247660	33.0	0.000150	55625.725513	80.0	0.009792	55999.211256	126.5	0.000419	56398.441961	175.5	0.000020
55254.163981	33.5	0.000011	55627.644583	80.5	0.000020	56001.120707	127.0	0.000023	56404.476857	176.0	0.000275
55260.194203	34.0	0.000210	55633.670959	81.0	0.000139	56007.158095	127.5	0.000242	56406.388372	176.5	0.000014
55262.110499	34.5	0.000018	55641.617754	81.5	0.000482	56009.067095	128.0	0.000079	56412.423649	177.0	0.000237
55268.140794	35.0	0.009811	55643.536983	82.0	0.000017	56017.013518	128.5	0.000013	56414.334813	177.5	0.000015
55270.056859	35.5	0.000016	55649.564014	82.5	0.015367	56023.050882	129.0	0.000179	56420.369227	178.0	0.000304
55278.003269	36.0	0.000021	55651.483076	83.0	0.000017	56024.959968	129.5	0.000047	56422.281258	178.5	0.000030
55284.033439	36.5	0.000115									

**Table B4.** Binary Mid Eclipse Times for KIC 8023317

BJD −2 400 000	Cycle no.	std. dev. (d)	BJD −2 400 000	Cycle no.	std. dev. (d)	BJD −2 400 000	Cycle no.	std. dev. (d)	BJD −2 400 000	Cycle no.	std. dev. (d)
54957.481039	-1.5	0.003882	55322.222343	20.5	0.001913	55703.530522	43.5	0.003163	56068.272800	65.5	0.002545
54963.158283	-1.0	0.002084	55327.891045	21.0	0.000374	55709.208576	44.0	0.000152	56073.945577	66.0	0.000335
54979.735521	0.0	0.000667	55338.803137	21.5	0.003081	55720.109439	44.5	0.005567	56084.849998	66.5	0.002950
54990.646340	0.5	0.002306	55344.469324	22.0	0.00296	55725.789237	45.0	0.000153	56090.525492	67.0	0.000403
54996.312001	1.0	0.000751	55355.382042	22.5	0.004062	55736.691345	45.5	0.003046	56118.010828	68.5	0.003700
55007.226717	1.5	0.002444	55361.047751	23.0	0.000435	55742.369592	46.0	0.000195	56134.584409	69.5	0.002488
55012.889006	2.0	0.000632	55377.626530	24.0	0.000303	55753.273202	46.5	0.003360	56140.265744	70.0	0.000353
55023.805337	2.5	0.002539	55388.537765	24.5	0.004921	55758.949237	47.0	0.000192	56151.162291	70.5	0.002339
55029.465882	3.0	0.000580	55394.205565	25.0	0.000313	55775.528335	48.0	0.000181	56156.845581	71.0	0.000440
55040.386336	3.5	0.002063	55405.115258	25.5	0.004043	55786.428708	48.5	0.005962	56167.740271	71.5	0.020530
55046.044017	4.0	0.000559	55410.784624	26.0	0.000313	55792.107196	49.0	0.000158	56173.424274	72.0	0.000405
55056.961520	4.5	0.005357	55421.695571	26.5	0.001658	55808.685892	50.0	0.000161	56184.320573	72.5	0.003389
55062.624482	5.0	0.000456	55427.364175	27.0	0.000282	55819.585934	50.5	0.004095	56190.002597	73.0	0.000444
55073.535058	5.5	0.001753	55438.275599	27.5	0.002804	55825.264396	51.0	0.000192	56200.921955	73.5	0.026363
55079.202423	6.0	0.000258	55443.943368	28.0	0.000278	55836.168155	51.5	0.003206	56206.581385	74.0	0.001063
55090.113963	6.5	0.003792	55454.848437	28.5	0.002016	55841.842568	52.0	0.000205	56217.488623	74.5	0.004251
55095.786785	7.0	0.000426	55460.523121	29.0	0.000260	55852.743217	52.5	0.002779	56223.155198	75.0	0.000425
55106.689719	7.5	0.002709	55471.431640	29.5	0.002633	55858.421038	53.0	0.000161	56234.063821	75.5	0.014746
55112.367385	8.0	0.000534	55477.103342	30.0	0.000330	55869.325089	53.5	0.003970	56239.731504	76.0	0.000712
55123.266507	8.5	0.002415	55488.008317	30.5	0.001156	55874.999472	54.0	0.000227	56256.309637	77.0	0.000735
55128.947101	9.0	0.000418	55504.588103	31.5	0.002551	55885.904695	54.5	0.002017	56267.221811	77.5	0.014309
55139.849036	9.5	0.002429	55510.263108	32.0	0.000239	55891.577273	55.0	0.000210	56272.888721	78.0	0.000606
55145.527153	10.0	0.000438	55521.163567	32.5	0.002804	55902.488453	55.5	0.004037	56283.789721	78.5	0.002393
55162.106056	11.0	0.000355	55526.843208	33.0	0.000242	55908.155799	56.0	0.000245	56289.469261	79.0	0.000913
55173.013238	11.5	0.002594	55537.741007	33.5	0.002578	55919.065074	56.5	0.002868	56306.052051	80.0	0.001044
55178.684850	12.0	0.000413	55543.423250	34.0	0.000308	55924.734286	57.0	0.000199	56322.631580	81.0	0.000807
55189.595226	12.5	0.004625	55570.904480	35.5	0.005396	55941.312915	58.0	0.000181	56339.212519	82.0	0.000724
55195.263418	13.0	0.000438	55576.580449	36.0	0.000265	55952.225777	58.5	0.006010	56355.792119	83.0	0.000654
55211.842421	14.0	0.000383	55587.485614	36.5	0.002632	55957.891016	59.0	0.000343	56366.682411	83.5	0.004419
55222.745060	14.5	0.003732	55593.157418	37.0	0.000287	55968.802452	59.5	0.003377	56372.371163	84.0	0.000999
55228.420428	15.0	0.000442	55604.062571	37.5	0.001942	55974.470044	60.0	0.000232	56388.950337	85.0	0.000752
55239.330302	15.5	0.002764	55609.734119	38.0	0.000215	55985.380551	60.5	0.005272	56399.846617	85.5	0.003054
55244.998533	16.0	0.000331	55620.648239	38.5	0.003179	55991.049106	61.0	0.000317	56405.528614	86.0	0.000884
55255.907944	16.5	0.004017	55626.309496	39.0	0.000181	56001.957595	61.5	0.003586	56422.108527	87.0	0.000893
55261.577101	17.0	0.000433	55642.887215	40.0	0.000154	56007.627930	62.0	0.000315	58693.430893	224.0	0.004442
55272.483288	17.5	0.004255	55653.801692	40.5	0.003299	56018.535295	62.5	0.005302	58710.011053	225.0	0.013546
55278.155506	18.0	0.000407	55659.466322	41.0	0.000151	56024.206950	63.0	0.000303	59406.320603	267.0	0.011177
55289.067358	18.5	0.002984	55670.377522	41.5	0.006269	56035.117721	63.5	0.003322	59422.914616	268.0	0.013971
55294.733814	19.0	0.000283	55676.046305	42.0	0.000144	56040.786267	64.0	0.000426	59439.478298	269.0	0.015880
55305.643953	19.5	0.003086	55686.954996	42.5	0.002951	56051.692989	64.5	0.008381			
55311.312393	20.0	0.000428	55692.627680	43.0	0.000148	56057.366071	65.0	0.000409			

*Notes.* Integer and half-integer cycle numbers refer to primary and secondary eclipses, respectively. Most of the eclipses (cycle nos. −1.5 to 87.0) were observed by the *Kepler* spacecraft. The last 5 times of minima were determined from the *TESS* observations.

Table B5. Binary Mid Eclipse Times for KIC 6964043

BJD −2 400 000	Cycle no.	std. dev. (d)	BJD −2 400 000	Cycle no.	std. dev. (d)	BJD −2 400 000	Cycle no.	std. dev. (d)
55190.173588	0.0	0.000688	55603.078800	38.5	0.000459	56005.126585	76.0	0.000682
55195.460530	0.5	0.000538	55608.431983	39.0	0.000517	56010.587115	76.5	0.000490
55200.886326	1.0	0.000801	55613.819266	39.5	0.000514	56015.844256	77.0	0.000756
55206.172452	1.5	0.000961	55619.165008	40.0	0.000423	56021.303286	77.5	0.000600
55211.601150	2.0	0.000762	55624.552763	40.5	0.000641	56026.563994	78.0	0.000575
55222.317438	3.0	0.001062	55629.889603	41.0	0.000592	56032.020670	78.5	0.001174
55227.602391	3.5	0.000799	55635.278777	41.5	0.000496	56037.290799	79.0	0.000592
55238.318601	4.5	0.000860	55640.079263	42.5	0.001026	56042.742439	79.5	0.000545
55243.743685	5.0	0.000709	55651.325473	43.0	0.000501	56053.481243	80.5	0.000471
55249.038230	5.5	0.000625	55656.720776	43.5	0.000500	56058.772697	81.0	0.000639
55254.459530	6.0	0.001183	55662.040660	44.0	0.000405	56064.313580	81.5	0.000577
55259.747089	6.5	0.000986	55667.440537	44.5	0.000550	56069.534880	82.0	0.000663
55265.170662	7.0	0.000728	55672.754895	45.0	0.000611	56075.056447	82.5	0.000945
55270.466723	7.5	0.000901	55683.469003	46.0	0.000394	56080.283777	83.0	0.000710
55281.174261	8.5	0.001023	55688.871939	46.5	0.000706	56085.786810	83.5	0.000593
55286.606988	9.0	0.001019	55694.183544	47.0	0.000348	56091.030676	84.0	0.001283
55291.891233	9.5	0.001037	55699.587626	47.5	0.000510	56096.519692	84.5	0.000957
55297.325645	10.0	0.000912	55704.898973	48.0	0.000607	56107.246770	85.5	0.000691
55302.608118	10.5	0.000573	55710.302091	48.5	0.000752	56112.482348	86.0	0.000672
55313.329315	11.5	0.000951	55715.614288	49.0	0.000633	56117.968120	86.5	0.001017
55318.767221	12.0	0.000690	55721.022439	49.5	0.000926	56133.913187	88.0	0.000587
55324.047906	12.5	0.000922	55726.327539	50.0	0.000414	56139.407798	88.5	0.000847
55329.494681	13.0	0.000680	55731.734106	50.5	0.000528	56144.627374	89.0	0.000677
55334.787302	13.5	0.000661	55737.045969	51.0	0.000394	56150.125700	89.5	0.000971
55345.606170	14.5	0.000999	55742.449747	51.5	0.000561	56155.340121	90.0	0.000732
55351.013111	15.0	0.000645	55747.763620	52.0	0.000479	56160.839199	90.5	0.000876
55356.358888	15.5	0.000594	55753.167304	52.5	0.000346	56166.054369	91.0	0.000773
55361.760234	16.0	0.000642	55758.479819	53.0	0.000386	56171.555981	91.5	0.000516
55367.087933	16.5	0.000552	55763.884715	53.5	0.000520	56176.771913	92.0	0.000721
55372.506219	17.0	0.000588	55769.198047	54.0	0.000442	56182.270350	92.5	0.000706
55377.825983	17.5	0.000392	55774.600402	54.5	0.000437	56187.482710	93.0	0.000766
55383.234593	18.0	0.000584	55779.917753	55.0	0.000488	56192.985929	93.5	0.000837
55388.557970	18.5	0.000563	55785.315934	55.5	0.000453	56198.196368	94.0	0.000747
55393.953470	19.0	0.000537	55790.642026	56.0	0.000557	56203.702472	94.5	0.001134
55399.283659	19.5	0.000537	55796.037501	56.5	0.000497	56208.911051	95.0	0.000690
55404.672129	20.0	0.000553	55801.369553	57.0	0.000446	56214.415334	95.5	0.001477
55415.386026	21.0	0.000488	55806.764662	57.5	0.000393	56219.627442	96.0	0.000992
55420.722963	21.5	0.000613	55812.101279	58.0	0.000409	56225.132630	96.5	0.000603
55426.100800	22.0	0.000472	55822.865967	59.0	0.001426	56230.344551	97.0	0.000501
55436.813775	23.0	0.000491	55828.367561	59.5	0.000570	56235.848362	97.5	0.000688
55442.155904	23.5	0.000851	55839.081236	60.5	0.000504	56241.060220	98.0	0.000805
55447.527523	24.0	0.001023	55844.365770	61.0	0.000421	56251.772460	99.0	0.001024
55452.872094	24.5	0.000811	55849.818469	61.5	0.000388	56257.279768	99.5	0.000939
55458.244107	25.0	0.000598	55855.108304	62.0	0.000468	56262.494709	100.0	0.000807
55463.585359	25.5	0.000440	55860.506558	62.5	0.000667	56267.995214	100.5	0.000896
55468.956843	26.0	0.000574	55876.550659	64.0	0.000525	56273.223127	101.0	0.000942
55474.299841	26.5	0.000818	55881.997269	64.5	0.000952	56278.718490	101.5	0.000656
55479.670071	27.0	0.000719	55887.267179	65.0	0.000511	56283.949424	102.0	0.000835
55485.016731	27.5	0.000656	55892.716930	65.5	0.000433	56289.446880	102.5	0.000905
55490.387630	28.0	0.000607	55897.980067	66.0	0.000485	56294.698965	103.0	0.002269
55495.729755	28.5	0.000505	55908.695388	67.0	0.000676	56300.244529	103.5	0.000617
55501.102486	29.0	0.000536	55914.146946	67.5	0.000578	56305.467755	104.0	0.001790
55506.447625	29.5	0.000968	55919.411396	68.0	0.000457	56321.764224	105.5	0.001067
55511.820059	30.0	0.000861	55924.865240	68.5	0.000612	56326.965378	106.0	0.001313
55517.160827	30.5	0.000711	55930.120478	69.0	0.000488	56337.699957	107.0	0.001383
55522.536941	31.0	0.000633	55935.578562	69.5	0.000839	56348.428551	108.0	0.001215
55527.877431	31.5	0.000478	55940.836280	70.0	0.000587	56353.951312	108.5	0.001430
55533.256203	32.0	0.000498	55946.298236	70.5	0.000539	56364.669588	109.5	0.000918
55538.593485	32.5	0.000475	55957.010179	71.5	0.000538	56375.390259	110.5	0.000913
55549.311845	33.5	0.000531	55962.264805	72.0	0.000495	56380.578115	111.0	0.000901
55570.764524	35.5	0.000438	55967.726462	72.5	0.000475	56386.110902	111.5	0.001041
55576.159985	36.0	0.000452	55972.979333	73.0	0.000497	56396.827476	112.5	0.001104
55581.552540	36.5	0.000568	55978.439783	73.5	0.000692	56402.001462	113.0	0.000929
55586.935079	37.0	0.000443	55983.693744	74.0	0.000532	56407.547455	113.5	0.003209
55592.366837	37.5	0.000638	55989.154588	74.5	0.000553	56412.719525	114.0	0.000981
55597.676834	38.0	0.000492	55999.871173	75.5	0.000480	56423.431712	115.0	0.001415

Notes. Integer and half-integer cycle numbers refer to primary and secondary eclipses, respectively.